Modeling Present and Future Physical Coastal Vulnerability to Climate Change: North Shore, Prince Edward Island

by

Katelyn MacDonald

A thesis
presented to the University of Waterloo
in fulfillment of the
thesis requirement for the degree of
Master of Science
in
Geography

Waterloo, Ontario, Canada, 2014

AUTHOR'S DECLARATION

I hereby declare that I am the sole author of this thesis. This is a true copy of the thesis, including any required final revisions, as accepted by my examiners.

I understand that my thesis may be made electronically available to the public.

ABSTRACT

The IPCC has identified small islands and coastal zones among regions most vulnerable to climate change. The geomorphological characteristics of Prince Edward Island (PEI), such as highly erodible sandstone bedrock and low elevation, contribute to a high degree of physical vulnerability to climate change. The province is highly susceptible to physical impacts of climate change including relative sea-level rise and increased rates of coastline retreat. In order to assess the physical coastal vulnerability of the ParCA study area of the North Shore, PEI, a model employing Geographic Information Systems (GIS), multi-criteria evaluation (MCE), and time step analysis is formulated. The physical vulnerability of the North Shore for the year 2010 was quantified in terms of wind-wave exposure condition, morphological resiliency, and permanent and episodic flood risk. These results are employed as model inputs to predict the shoreline for the subsequent time steps (2050, 2100), which are again analyzed to estimate future physical coastal vulnerability. Such an approach allows for updated predictions in intent to improve accuracy when compared to linear extrapolation. Finally, areas of highest priority for adaptation measures are quantified for each time step. This physical vulnerability analysis together with community-based and socioeconomic coastal vulnerability analyses will portray the comprehensive vulnerability of the North Shore to current and future effects of climate change.

ACKNOWLEDGEMENTS

I would like to thank my two supervisors for their knowledge and dedication to my work. Dr. Danika van Proosdij has pushed me to accomplish my goals through believing in my abilities. Dr. van Proosdij has taught me more in the past two years than I thought possible. Her positive attitude has allowed me to surpass moments where I thought I could not finish this work. Thank you to Dr. Dan Scott for his continued guidance and support in the completion of this thesis. Dr. Scott 's expertise and prestige in the field of climate change has inspired me to persevere.

Thank you to Dr. Adam Fenech and Dr. Peter Johnson for volunteering their time to be on my thesis committee. A further thank you is due to Dr. Fenech for allowing me to use the LiDAR elevation data that was so integral to this work.

Thank you very much to those who have been researching climate change and PEI long before I started, and provided me with all of their wisdom: Don Jardine for providing me with reports that I may not have otherwise gotten a hold of, Paul Giroux for not only supplying me with invaluable knowledge of PEI National Park but for also setting up my stay in the Parks Canada cabin, and to Randy Angus for sharing his wealth of knowledge and for taking our ParCA group on an incredibly comprehensive tour of the North Shore study area.

I would also like to thank Greg Baker and Barbara Perott of Saint Mary's University for their GIS, GPS, and cartographic help.

Thank you to the members of the ParCA team and the staff and faculty of the Department of Geography at UW. It has been a pleasure to work with each and every person.

Finally I would like to thank my friends and family, especially my parents, who have always stuck by my side. Most importantly of all I would like to thank my partner Mark Hunter for not only helping me in the field and with the completion of this methodology, but also for believing in me.

TABLE OF CONTENTS

LIST OF FIGURES

LIST OF TABLES

LIST OF ACRONYMS

AR4	Forth Assessment Report
AR5	Fifth Assessment Report
CD	Chart Datum
CGVD28	Canadian Geodetic Vertical Datum of 1928
CHS	Canadian Hydrographic Service
CVA	Coastal Vulnerability Assessment
CVI	Coastal Vulnerability Index
DEM	Digital Elevation Model
GIS	Geographic Information Systems
GPS	Global Positioning System
IPCC	Intergovernmental Panel on Climate Change
LiDAR	Light Detection and Ranging
MCE	Multicriteria Evaluation
MR	Morphological Resiliency
ParCA	Partnership for Canada-Caribbean Climate Change Adaptation
PEI	Prince Edward Island
REI	Relative Wave Energy Index
RWE	Representative Wave Energy
SLGO	St. Lawrence Global Observatory
SLR	Sea-Level Rise
VSC	Volumetric Sediment Change
WEMo	Wave Exposure Model
WG1	Working Group One

1. Introduction

1.1. Study Context

The Intergovernmental Panel on Climate Change (IPCC) Fifth Assessment Report (AR5) (2013) states there is unequivocal evidence the Earth has experienced warming since the 1950s that is unprecedented for the current instrumental record. This warming is largely attributed to an increase of CO_2 atmospheric concentrations. This change in climate has lead to an increase in oceanic temperatures, a decrease in ice sheet and glacial coverage, and has contributed to the rise of global mean sea-levels. The effects of climate change are interconnected in a positive feedback. As global CO_2 atmospherics emissions continue, the effects of climate change will continue to intensify.

The Intergovernmental Panel on Climate Change (IPCC) Fifth Assessment Report indicates that the global oceans have stored the largest amount of heat energy from climate change, leading to global (eustatic) sea-level change. The factors contributing greatest to the change in eustatic sea-levels are oceanic thermal expansion and the addition of melt water previously stored on land as glaciers and ice sheets. Global sea-levels have risen at a rate of 3.2 milimeters annually from the years 1993 to 2010. However, the magnitude of relative sea-levels depends on local glacier gravitational field characteristics as well as glacial isostatic adjustment (IPCC, 2013).

The North Shore of Prince Edward Island (PEI) is experiencing relative sea-level rise at a rate of 29 centimeters per century, calculated from tide gauge data recorded since 1900 (Shaw, 2001). Relative sea-level rise in the area is attributed to global mean sea-level rising as well as crustal subsidence through glacial isostatic adjustment (Shaw, 2001). According to Richards & Daigle (2011), a total increase in relative sea-level could reach 1.08 meters by 2100 in the area. Thus, portions of the North Shore are at risk to permanent inundation through sea-level rise. Furthermore, the study area is further at risk to climate change induced hazards including the potential increase of episodic storm surge intensity as well as coastal erosion.

The North Shore is experiencing a high incidence of shoreline retreat largely due to sea-level rise inundation (Webster, 2012) and a corresponding increase size of waves reaching inshore as relative sea-levels increase. Mean erosion rates between the years 2000-2010 range from 0.08 to 0.46 meters annually, with the greatest erosion occurring in the Malpeque littoral cell at 19.94

meters annually. This is a substantial increase in the annual rate of erosion, as between the years 1968 and 2010 the coastal change rates ranged from -0.04 to 0.34 meters annually, with the Cavendish littoral cell experiencing accretion (Webster, 2012). Although there are extensive sand beaches, the North Shore is limited in sediment supply (Forbes *et al.,* 2004). It is assumed that these rates of erosion will increase across the study area as climate change induced hazards continue to effect the area.

The definition of vulnerability developed in this research states that it is the degree of risk which the geophysical coastal systems experience adverse impacts of climate change hazards as well as the coastal systems resiliency to the hazard. The North Shore is also particularly vulnerable to erosion due to permanent sea-level rise and episodic storm surge. The region is situated on the Gulf of St. Lawrence, a large body of water which produces strong fetches and powerful waves (Shaw, 2001). Furthermore, the island is comprised of highly erodible Pennsylvanian-Permian sandstone and shale (Mathew, Davidson-Arnott, & Ollerhead, 2010). Observations have indicated an increase in strong storm activity in the region with accompanying stronger storm surges (Shaw, 2001).

The North Shore is highly vulnerable to climate change induced hazards due to a history of increased rates of coastal erosion, the vulnerability of the coast due to its biophysical state, and an observed increase in storm activity. This vulnerability will increase over time as the effects of climate change progress, including permanent sea-level rise inundation and episodic storm surge flooding. These effects will directly affect both the natural and built environments. Sea-level rise inundation and episodic storm surge flooding has already altered local ecosystems, reduced shoreline stability, and incurred large costs in the repair of human infrastructure (Richards & Daigle, 2011). Thus, it is necessary to quantify this vulnerability in order to assess present and future exposure-sensitivities as well as plan climate change mitigation and adaptation strategies.

A physical Coastal Vulnerability Assessment (CVA) is a tool used to quantify the relative susceptibility of the physical coast to a range of hazards, and comparatively discern the areas of greatest risk. Criteria indicators are used to spatially represent hazards the coast experiences or to depict susceptible biophysical conditions; the literature cites the most frequently used criteria as coastal geomorphology, shoreline change, mean wave height, sea-level rise, mean tidal range,

and slope (Dwarakish et al., 2009; Gaki-Papanastassiou et al., 2010; Gornitz *et al.*, 1994; Kumar *et al.*, 2010; Kumar & Kunte, 2012; Le Cozannet *et al.,* 2013; Pendleton, Thieler, & Jeffress, 2005; Pendleton, Thieler, & Williams, 2010; Thieler & Hammar-Klose, 2000; Shaw et al., 1998; Yin *et al.*, 2012). The values representing the criteria are ranked in terms of lowest to highest vulnerability, usually within a GIS where the data can be spatially represented. Each criteria is summed together to produce an overall vulnerability assessment.

The physical CVA produced in this work utilize the criteria of exposure condition, morphological resiliency, and permanent and episodic flood risk to assess coastal vulnerability. The initial factor which governs the magnitude and direction of change in a coastal system is the exposure condition, or the potential amount of stress acted upon the coastline. The level of morphological resiliency of the coastal system also determines the degree of coastal change, as it is the ability of the system to return to a state of equilibrium following a stress event. As the exposure condition and morphological resiliency quantifications did not capture the vulnerability of the study area shoreline to storm surge and sea-level rise flooding, a separate vulnerability criteria to assess flood risk was included. The CVA was conducted for three time steps (2010, 2050, and 2100) in order to evaluate the change in vulnerability the North Shore will experience as a result of increasing climate change hazards. Between each time step, the coastline position was modeled in order to accurately represent this change through time; this has not been incorporated in previous CVAs within the literature.

The results of the CVA will identify specific locations of highest vulnerability to climate change along the North Shore. It will aid in the assessment of potential mitigation and adaptation strategies as well as prioritize areas which are in need of immediate time and resources to prevent damage to natural and human environments.

1.2. Research Goals

The fundamental goal of this research is to evaluate the physical coastal vulnerability of the North Shore to climate change for years 2010, 2050, and 2100 using a Coastal Vulnerability Assessment (CVA). The following objectives achieved this goal:

- Quantified three criteria indicators ranked from lowest (1) to highest (5) vulnerability for three time steps:
    - Assessed the exposure condition using the Wave Exposure Model and GIS
    - Determined morphological resiliency using numerical and GIS modeling
    - Used GIS to identify coastal vulnerability to sea-level and storm surge flooding
- Evaluated, assessed, and compared the relative physical vulnerability of the coastal system to climate change using three criteria indicators in a CVA for the years 2010, 2050, and 2100
- Utilized findings of assessment to determine areas of highest priority for adaptation measures in terms of tourism and fisheries

1.3. Thesis Structure

This thesis is comprised of six chapters. The first chapter introduces the research problem as well as the objectives utilized to address the problem. The second chapter provides additional context and information pertaining to the research problem in the form of a literature review; this chapter reviews physical Coastal Vulnerability Assessments (CVA) from their advent and compares the methodologies used in each. The third chapter describes the study area of the North Shore as well as an in-depth analysis of the different regions in which it is comprised of. Chapter four outlines the methodology used to quantify the physical coastal vulnerability of the study area. The fifth chapter provides the results of the physical CVA as well as a discussion of the implications of these findings. Finally, the sixth chapter reviews study limitations, recommendations for future work, and provides a summary of the research.

2. Physical Coastal System Vulnerability, a Literature Review

2.1. Introduction

Coastal vulnerability assessments (CVAs) are tasked with identifying areas at risk to the hazards of climate change. These evaluations must simplify complex and dynamic coastal systems. They rely on assumptions to determine the degree and location of future hazards and the extend of the resulting impact on the system. There are inherent uncertainties, limitations and errors with a CVA. Thus, the use of a CVA to determine future adaptation and mitigation options must be used in conjunction with historical and expert knowledge, and the full recognition of these limitations. Even with these drawbacks, the CVA provides an invaluable method for determining coastal vulnerability.

This literature review is intended to provide an overview of the methods used to assess physical coastal vulnerability and to provide background information important to this assessment. The review is divided in to three sections. The first section provides definitions of key factors involved in the physical CVA in order to clarify terms that may have multiple meanings across the literature. The second outlines variables causing vulnerability to the system. Lastly, the third section summarizes physical CVAs through the literature and discusses issues inherent in these assessments.

2.2. Key Definitions

2.2.1. Vulnerability

This research aims to assess the vulnerability of the North Shore of PEI coast to future impacts of climate change. The term *vulnerability* has a range of definitions within the literature which are especially divergent between climate change and natural hazard research communities (Romieu *et al.,* 2010). Furthermore, the terms *risk, hazard,* and *vulnerability* are at times used interchangeably within the literature. Thus, a clear understanding of the term *vulnerability* in the context of this study is necessary.

The Intergovernmental Panel on Climate Change (IPCC) Fourth Assessment Report (AR4) (Adger *et al.,* 2007) define *vulnerability* as:

> *"...the degree to which geophysical, biological and socio-economic systems are susceptible to, and unable to cope with, adverse impacts of climate change."*

While this definition is critical in the assessment of climate change impacts, it does not focus on the physical impacts of climate change. Thus, the definition of *vulnerability* in the context of this study will be focused on the physical impacts of climate change on the coastal system.

Gornitz (1991) developed the first assessment of physical coastal vulnerability, and defines *coastal vulnerability* as:

> *"the liability of the shore to respond adversely to a hazard"*

and a *coastal hazard* as:

> *"a natural phenomenon that exposes the littoral zone to risk of damage or other adverse effects."*

Thus *vulnerability* is a function of a *hazard* and the degree to which the shore responds to the *hazard*, which can be termed the *exposure* of the coast.

Douglas (2007) succinctly summarizes *vulnerability* in terms of *hazard* and *risk:*

> *"An evaluation of the risk to an exposed element from a hazardous event requires a consideration of the element's vulnerability, which expresses its propensity to suffer damage."*

Thus, *vulnerability* of the coast is an evaluation of the *risk* of impact from climate change *hazard.* The IPCC AR4 definition of *risk* is taken from the risk management standard ISO/IEC Guide 73 (Halsnæs *et al.,* 2007):

> *"The combination of the probability of an event and its consequences"*

Resiliency is defined by the IPCC AR4 (Adger *et al.,* 2007) as:

"the ability of a system to return to a predisturbed state without incurring any lasting fundamental change"

Integrating these above definitions together provides the definition of physical coastal *vulnerability* which will be used in this study:

"The degree of risk which the geophysical coastal system experiences adverse impacts of climate change hazards as well as the coastal systems resiliency to the hazard."

2.2.2. Coastal Zone Definitions

Nearshore, Foreshore, Backshore

The *coastal zone* is a dynamic area influenced by its proximity to the sea. It is comprised of three sections: the *nearshore, foreshore,* and *backshore* (Davidson-Arnott, 2010). The *nearshore* is the seaward-most zone and extends from the high-tide breaker line to the low-tide breaker line. The *foreshore* extends landward from the nearshore to include the portion of the coastal zone which is exposed at low-tide. The *backshore* is the upper zone of shore between the mean spring tide high-water line and the upper limit of coastal zone processes. The definitions of the coastal zone sections are depicted in **Figure 1**.

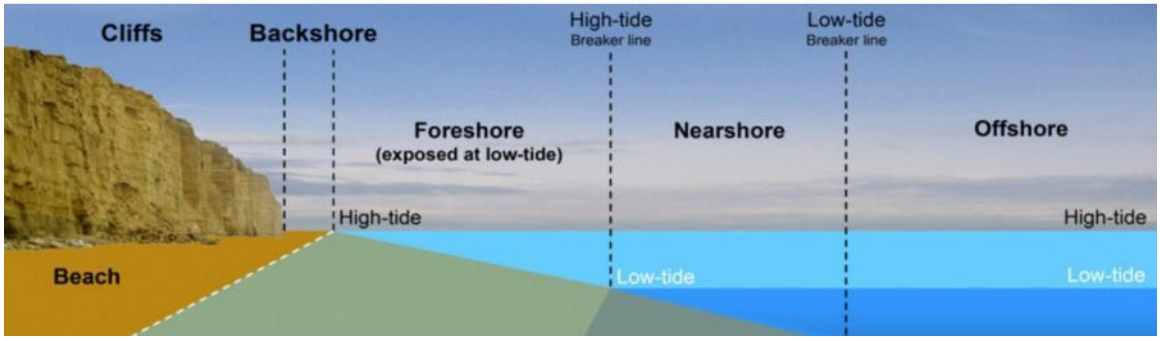

Figure 1: Boundaries of the coastal zone, from Pietersma-Perott & van Proosdij (2012)

Coastal Equilibrium

Coastlines are highly dynamic by nature. A variety of natural forces act on the coast including currents, tides, wave action, and aeolian processes. These forces act to erode, entrain, transport, and deposit sediment. The inputs and outputs of sediment shape the physical profile and structure of the coastline. *Coastal equilibrium* is the balance of sediment inputs and outputs of the coastal

system over a period of time. Coastline profiles are largely stable over time, however large increases in the magnitude of force acting on the system can push the coast out of equilibrium.

Briggs *et al.* (1997) defined three states of coastal equilibrium. The first, steady-state equilibrium, is described as a state where changes in energy occur for a short period of time and the coast is able to quickly recover back to its original state. Meta-stable equilibrium coastlines usually occur after a storm event, where large quantities of sediment are often relocated. A longer time period is necessary for the coast to recover after these events. Finally, dynamic equilibrium occurs when there is constant change in coastal equilibrium. It may occur due to large disruptive forces alter the coastlines natural equilibrium, such as sea-level change or climate change. A coastline can experience any number of these states of equilibrium at any point in time.

Storm Surge Return Period

The coastal zone is effected by tides as well as storm surge. Storm surge is defined as the difference between predicted astronomical tides and recorded water levels. For this research, the *return period* of a storm surge is used to assess the vulnerability of the coastal zone. Richards & Daigle (2011) define a *return period (T)* as the mean amount of storm surge occurrences which surpass a given threshold, for example a certain period of time. This predicted threshold is represented as 1/T. Each return period has an associated return-period sea level which varies spatially based on the tidal conditions and morphology of the coast. For example, each year has a 1% chance of a 100 year storm surge return period being exceeded, which could correlate to a sea-level of 1.4 meters (Richards & Daigle, 2011).

2.3. Vulnerability of Coastal Systems to Climate Change

The Intergovernmental Panel on Climate Change (IPCC) Fourth Assessment Report (AR4) has indicated key hotpots for coastal vulnerability to climate change (IPCC, 2007b). Coastal vulnerability within the study area include locations subject to multiple stresses (both anthropogenic and natural), areas with significant coastal populations, and coastal areas dependant on tourism. Increased levels of sea-level rise as well as increased frequency of extreme storm events will lead to amplified rates of coastal change across the study area

(Mathew, Davidson-Arnott, & Ollerhead, 2010; Shaw 2001). These vulnerabilities are evaluated in the research through the assessment of long-term flooding through climate change-induced sea-level rise and increased intensity of episodic flooding events through storm surge.

2.3.1. Sea-Level Change

Change in Eustatic Sea-Levels

Climate change, particularly the rise in average global temperatures, has been observed to alter global sea-levels. The IPCC Working Group One (WG1) of the AR4 (IPCC, 2007a) indicates the largest contributors to eustatic (global) sea-level rise are thermal expansion of oceanic waters and the input of freshwater from glacial and ice sheet melt. The increase in average oceanic temperature results in a significant volumetric increase; this warmer water will subsequently inundate coastal areas. Temperature observations of the ocean over the last half century have found warming in all basins, the largest being the Atlantic, Pacific, and Indian Ocean basins. WG1 assesses the steric (thermal) sea-level change calculated over seven studies as 1.5 ± 0.5 millimeters annually for the upper layer of the ocean and 1.6 ± 0.5 millimeters annually for the ocean below 700 meters. Warmer temperatures also increase the volume of water input into the global oceans from the melt of land based glaciers and ice sheets. As global temperatures continue to rise, there will be an acceleration in this melt and thus an increase in the water volume input (IPCC, 2007a).

Changes in oceanic salinity through the input of freshwater glacial and ice sheet melt have a positive feedback effect of increasing the rate of melt. Measurements of oceanic salinity have confirmed freshening of oceanic waters worldwide. This freshening along with thermal expansion directly results in changes to ocean circulation of cool and warm water masses through meridional transport; cooler water is more dense than warm water and thus sinks, causing warmer water to move atop colder water. This causes a “conveyor belt” transfer of cool and warm water globally. As salinity and temperature directly affect the density of water, their change will directly impact this global conveyor belt and alter global climates. This change in climate will cause the increased melt rate of glaciers and ice sheets, which directly contributes to continued global sea-level rise (IPCC, 2007a).

Estimations by the IPCC AR4 WG1 indicate average global rates of total sea-level rise from 1961 to 2003 at 1.8 ± 0.3 millimeters annually. This number has been quantified through the use of coupled atmosphere-ocean general circulation models (AOGCMs) and altimetry measurements. These estimates do not include contribution of anthropogenic factors, such as land use and land cover change, as changes in human behavior and its effect on global-sea level rise are unquantified and difficult to forecast (IPCC, 2007a).

The IPCC AR4 (IPCC, 2007a) projected a rise of global sea level for the year 2100 at 0.18-0.59 meters relative to 1980-1999 sea levels. Recent studies (Rahmstorf, 2007; Rignot & Kanagaratnam, 2006) estimate a doubling of the IPCC predicted estimate for the year 2100 at 1.4 meters globally. This range of predictions are attributable to deviations between regional and global mean rises in sea-level as well as the movement of Earth through glacial isostatic adjustment (IPCC, 2007a). The Intergovernmental Panel on Climate Change (IPCC) Fifth Assessment Report (AR5) states that global sea-levels have risen at a rate of 3.2 millimeters annually from the years 1993 to 2010 (IPCC, 2013).

Relative Sea-Level Change

Although the rising of eustatic sea-levels have been observed, the magnitude of sea-level change varies spatially. Local sea-level change will vary from global sea-level rise measurements. Relative (local) sea-level change amounts are dependent on eustatic change. Geographical factors also contribute to the magnitude of change, which include glacial isostatic adjustment and melt fingerprinting as depicted in **Figure 2**.

Glacial isostatic adjustment is the vertical movement of Earth's crust from the redistribution of ice sheets from the last glaciation period. This readjustment causes a rise or fall of the Earth's crust dependant on its proximity to the preexisting ice sheet. A rise of depressed crust on land masses occurs in conjunction with the deepening of ocean basins. Glacial isostatic adjustment causes variation in relative sea-level spatially (Whitehouse, 2009).

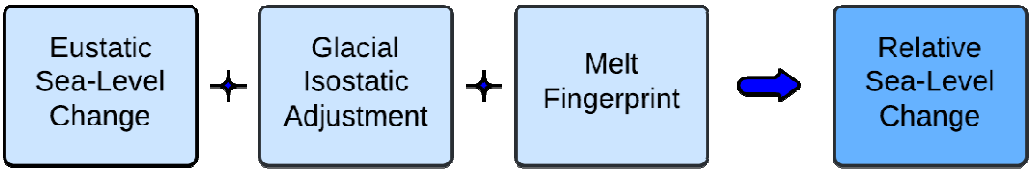

Figure 2: The combination of eustatic sea-level change, glacial isostatic adjustment, and melt fingerprinting results in local relative sea-level change

Melt fingerprinting of ice sheets is a relatively new concept and was first described by Woodworth *et al.* (1999). Ice sheets are extremely large in mass and create a gravitational pull on nearby water bodies, causing greater relative sea-levels nearer to the sheet. As melt through climate change occurs there is a redistribution of meltwater into the global oceans. In conjunction with this redistribution, the gravitational mass of the ice sheet is reduced. This causes sea-levels to increase further away from the ice sheet and decrease nearer to the sheet. Thus, relative sea-level change through the addition of meltwater may be greater or less than changes in global sea-levels based on proximity to the sheet (Mitrovica *et al.*, 2001; Mitrovica *et al.,* 2011).

Research provided by Bamber, Riva, Vermeersen, & LeBrocq (2009) suggests the collapse of the West Antarctica Ice Sheet due to climate change will raise global sea-levels by roughly five meters, however the IPCC AR5 states that this increase is highly unlikely (IPCC, 2013). Richards & Daigle (2011) states that the Northern Hemisphere will experience greater relative sea-level rise due to distance from the sheet. The effects of this sheet collapse will not be experienced until the next century (Richards & Daigle, 2011).

Coastal Vulnerability to Sea-Level Rise

The IPCC states with high confidence that sea-level rise is unavoidable due to climate change (IPCC, 2007a). The effects of sea-level rise are direct and indirect: directly, the coastal zone will be inundated and experience increased flood rates; indirectly, the zone will experience ecosystem damage, saltwater intrusion of freshwater sources, shoreline retreat and erosion, changes in sediment dynamics, and severe coastal infrastructure damage (Pethick, 2001; Gornitz et al.,1994;

Church et al., 2006). The severity which coastal zones will experience these consequences will vary spatially depending on local geomorphological and oceanic characteristics.

2.3.2. Storm Surge

Storm surge events are sudden changes in coastal water levels that differ from predicted astronomical tides (Forbes *et al.,* 2004). This elevation of sea-level is attributed to a decrease in atmospheric pressure and increase in wind speeds associated with strong storm events. The increase of water levels may lead to coastal flooding, especially during periods of high tides. Not only are natural and human environments negatively impacted by flooding, but wave action and winter ice ride-up may cause further destruction to inland areas not previously exposed. Coastline geomorphology change my result from storm events, including the readjustment of the nearshore profile, coastal erosion, and barrier island overwash and breach (Forbes *et al.,* 2004). Storm surge in Canada occurs typically during extra-tropical cyclones (Danard, Munro, & Murty, 2003). In the Gulf of St. Lawrence, storm surges of 1.5 meters occur each year (Parkes *et al*., 1997).

If storm events intensify with global climate change, increases of wind speed could result in larger surges (Danard, Munro, & Murty, 2003). Trenberth (2005) hypothesized a relationship between a rise in sea surface temperature and the amplification of hurricane intensity and frequency. Webster *et al*. (2005) found an increase in intensity of global extreme storm events during the period of 1970 to 2004. The study also reported a positive correlation between the frequency and duration of North Atlantic storms and a rise in sea surface temperatures.

The IPCC Fifth Assessment Report (AR5) draft has recently concluded that there is "low confidence" extratropical cyclones will change in intensity and it is "unlikely" the number of extratropical cyclones will be significantly changed due to anthropogenic climate change (IPCC, 2013). There is also a "lower confidence" that cyclones will make a polar shift in storm track and increase in frequency in higher latitudes (IPCC, 2013). Hurricane intensity and rainfall amounts may potentially increase, raising the number of class 4 and 5 storms (IPCC, 2013; Moser *et al.,* 2014). Walsh *et al.,* (2014) note that increase of duration, intensity, and frequency of North Atlantic hurricanes since the 1980s. Extreme storms produced off the North American north

eastern Atlantic coast, entitled Nor'easters, could potentially increase in intensity and make a polar shift in storm track (Horton *et al.,* 2014).

Storm surge heights may increase and become more severe with climate change. In regions where relative sea-levels are rising, deeper coastal waters will increase the height of a storm surge. For example, as water levels rise, current 50 centimeter storm surges may increase to one meter storm surges by 2050. Thus, although storm events may not intensify or increase in frequency with climate change, storm surges may continue to increase in severity.

Coastal Vulnerability to Storm Surge

Storm surge is regarded as the most destructive component of an extreme storm event. Flooding and wave action on inland coastal regions alter morphological structures, disrupt sensitive ecosystems, and damage human infrastructure. Coastal morphodynamics are altered during storm events as storm surge raise the elevation of wave attack further landward. Storm energy increases current velocities which increases shear stress on the nearshore, which in combination with high sediment transport rates causes rapid shoreline profile change (Forbes *et al.,* 2004).

The impacts of storm surge are a function of timing and the physical characteristics of the coastline. A positive surge during high tide could result in greater damage than compared to a positive surge during a time of low tide (Richards & Daigle, 2011). Furthermore, relaxation time between storm events allows the coastal system to return to the pre-existing state of equilibrium; if a storm event occurs before the coastal system is allowed to reach an equilibrium state after a previous event, impacts are compounded resulting in exponentially increased damage. The shoreline orientation and geomorphology will also determine the coasts response to a storm event (Forbes *et al.,* 2004; Richards & Daigle, 2011).

The geomorphological and ecological structure of the coast will affect how far flooding is able to proceed inland. A coast characterized by high elevation, low erodiblity sediment, and with thick vegetation will experience less flooding than a coast of lower elevation, highly erodible sediment, and no vegetation (Hinton, 2000). The conjunction of these factors will influence the vulnerability of the coast to storm surge.

Richards & Daigle (2011) indicate that storm surge in PEI can result in increased wave energy reaching the coast, leading to increased destruction of the natural and built environment. The maximum water level in the tide gauge record for the study area was observed in November 1988 at 2.14 meters with a surge of 1.28 meters (Forbes *et al.,* 2004). During months of sea ice, storm surge can cause ice ride up which further increases damages to the PEI coast. As relative sea-level rises along the North Shore, PEI coast, storm surge events will become more severe. Increased storm surge height coupled with a large percentage of highly erodible sandstone coastline leads to the PEI coast being highly vulnerable to storm surge in both the present and future.

2.3.3. Coastal Risk to Climate Change Hazards

As stated in Section 2.2.1, vulnerability in the context of this research is defined as the degree of risk which the geophysical coastal system experiences adverse impacts of climate change hazards as well as the coastal systems resiliency to the hazard. The climate change hazards of key interest to this research include sea-level rise and the increased intensity of storm events, respectively causing the risk of permanent and episodic inundation of the coast. Coastline transgression due to relative sea-level rise occurs at various rates spatially and is compounded during periods of extreme storminess (Forbes *et al.,* 2004). Together with the geomorphological characteristics of the coastline, secondary risks include the shift from coastal equilibrium and alongshore sediment transport, the exposure of inland areas to wave action, and an increase in the effect of a given storm surge due to higher seas. The hazards and risks due to climate change are depicted in **Figure 3**.

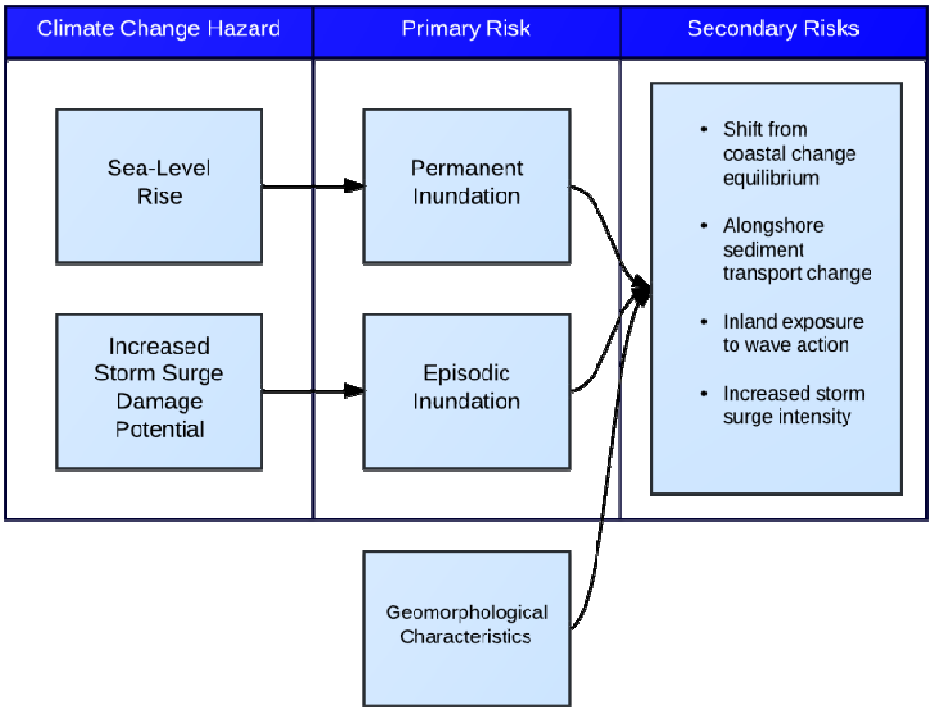

Figure 3: Physical coastal vulnerability in the context of hazard and risk

2.3.4. Adaptation Responses to Coastal Vulnerability

There are a range of adaptation options coastal communities can implement in order to reduce the adverse effects of sea-level flooding. There is no prescribed technique that can work in every situation – environmental and economic conditions vary spatially, and thus so do the options for adaptation and mitigation. Adaptation measures due to sea-level inundation and coastal erosion include deliberate retreat from the coast (Abel et al., 2011), hard infrastructure protection such as sea walls and berms, or soft structures such as flood-proofing or wetland buffer zones. The implementation of these adaptation measures may rely on change in local policy framework and land use plans, such as with integrative coastal zone management. Policy approaches in some instances are adaptation measures, such as when limiting future coastal population and infrastructure growth (IPCC, 2007b; U.S. EPA 2011).

2.4. Quantifying Coastal Vulnerability

Climate change will have lasting impacts on coastal systems globally. Assessing these future consequences is of importance to policy-makers in order to prepare mitigation and adaptation strategies. A Coastal Vulnerability Assessment (CVA) attempts to quantify the total hazards acting on a coastal region, and comparatively discern the areas of greatest risk. For this research, only physical CVAs were considered; although many CVAs include socioeconomic and cultural components, this was beyond the scope of the work. This section chronologically reviews physical CVAs in order to compare methods and variables used across the literature.

Multicriteria Evaluation (MCE) is an integral component of CVAs throughout the literature. A MCE scores the suitability of a spatial unit based on the summation of criteria values and a specified objective (Voogd, 1983; Zheng *et al.,* 2009). The process is used in spatial problems which require the consideration of a number of factors when determining the best alternative or result (Jankowski, 1995). Two common methods of MCE include Boolean Overlay and Weighted Linear Combination (WLC). The Boolean Overlay method assess all standardized criteria as equally weighted, and combine these criteria using logical operators (ie. AND, OR). The Weighted Linear Combination method weighs the standardized criteria in order to increase the importance of certain criteria in relation to others (Jiang & Eastman, 2000).

MCE provides a method of spatial evaluation for multiple options in order to allow educated decision making in a relatively straight forward and simple manner. Furthermore, weighing criteria allows for decision makers to compare trade-offs and uncertainties (Jankowski, 1995).There are problems associated with the use of MCE however. Jiang & Eastman (2000) warn that the use of Boolean MCE may not yield the same results as WLC MCE, thus the decision of what method to use may be dependent on the spatial location and the intended use. Furthermore, the work cautions that the method of standardization for criterion is not the same for every data set. In some situations, linear transformation in to a data range may be more suitable, where in others a distribution towards the minimum and maximum values may be best (Jiang & Eastman, 2000). With these limitations considered, MCE can aid decision making in a variety of situations.

2.4.1. Physical Coastal Vulnerability Assessments

Gornitz (1991) published the first physical coastal vulnerability assessment, quantifying the vulnerability of coasts worldwide to sea-level rise. Three processes were identified as major influencers of the coastal system: inundation, erosion, and saltwater intrusion. A vulnerable coastline was defined as being of low elevation, comprised of erodible substrate, experiencing historical erosion and subsidence, and receiving high amounts of wave and tide energy, as outlined in **Table 1**. To calculate the vulnerability of the coast, this method employed a Coastal Vulnerability Index (CVI) of seven variables including elevation, lithology, coastal geomorphology, relative sea level change, horizontal shoreline change, tidal ranges, and wave heights. The variables were first standardized into coastal risk classes, rating each from very low risk (1) to very high risk (5), are presented in Figure 4. These classes were then input in to a function to define a coastal segment's vulnerability within a GIS:

$$CVI = \left(\frac{1}{n}\sum_{i=1}^{n} a_i\right)^{\frac{1}{2}} \quad (1)$$

where a_i=variable and n=total number of variables present.

The vulnerability index was calculated in a GIS at 0.25° grid cells. The resulting CVI was divided in to four equal groups with the upper quarter receiving the class of "very high risk coastline".

Gornitz *et al.* (1994) expanded on this work through the addition of variables quantifying the coastal risk of extreme storm events; variables included annual tropical storm probability, annual hurricane probability, hurricane frequency-intensity index, mean forward velocity, annual mean number of extra-tropical cyclones, and mean hurricane surge. In order to represent each variable in terms of their associated risk to either erosion or inundation, each variable was grouped in to one of three factors using a principal factor analysis. These three factors were titled permanent inundation factor, episodic inundation factor, and erosion potential factor, with the permanent inundation factor receiving the greatest weighting of 50%. CVI was calculated in a GIS for the study area divided in to 0.25° grid cells.

Shaw *et al.* (1998) utilized the methodology of Gornitz (1991) and Gornitz *et al.* (1994) to assess the sensitivity of the Canadian coastlines to sea-level rise; the CVI was quantified using the seven variables suggested by Gornitz (1991). Thieler & Hammar-Klose (2000) also utilized the methodology found in Gornitz (1991), however this work omitted the lithology variable.

Pethick & Crooks (2000) partially diverge from the methods outlined in Gornitz (1991) by computing a CVI based on coastal form "relaxation time" following an extreme event. The vulnerability index was calculated using global data on the estimates of extreme event return intervals, and the consequent relaxation time, or the time a coastline will respond to perturbations from an extreme event. Coastal forms included in the calculation of the CVI included cliffs, beaches, sand dunes, mudflats, spits, salt marshes, estuaries, and shingle ridges.

Following methodologies similar to preceding works (Gornitz 1991; Gornitz *et al.,* 1994; Shaw *et al.,* 1998) and utilizing the same CVI variables as Thieler & Hammar-Klose (2000), Pendleton, Thieler, & Jeffress (2005), Dwarakish *et al.* (2009), and Gaki-Papanastassiou *et al.* (2010) assess the coastal vulnerability of the Golden Gate National Recreation Area in Northern California, Karnataka State, India, and the Argolikos Gulf of Greece, respectively. Kumar *et al.* (2010) follow these previous methods as well with their coastal vulnerability of the east coast of India, but also include a variable measuring tsunami wave run-up.

Pendleton, Thieler, & Williams (2010) followed previous methodologies, but incorporated an analysis of submerging and emerging coastlines. Furthermore, this work conducted a principal component analysis to discover that 99% of the CVI results were dependant on only four of the seven variables at larger spatial scales: geomorphology, coastal slope, sea-level change, and wave height.

Hanson *et al.* (2010) use an "outcome-driven deductive methodology" to assess geomorphological change of the East Anglican coast. The method utilizes Bayesian analyses and fuzzy logic to predict a most probable future coastal state while considering less possible outcomes. The method also utilizes fuzzy logic in order to rank the vulnerability of each criteria.

Table 1: CVA variable ranking from very low (1) to very high (5) 5, from Gornitz (1991)

Variable	Rank				
	Very Low 1	**Low 2**	**Moderate 3**	**High 4**	**Very High Risk 5**
Relief (m)	≥ 30.1	20.1 - 30.0	10.0 - 20.0	5.1 - 10.0	0 - 5.0
Rock type (relative resistance to erosion)	Plutonic Volcanic (lava) High-medium grade metamorphics	Low-grade metamor. Sandstone conglomerate (well-cemented)	Most sedimentary rocks	Coarse and/or poorly-sorted unconsolidated sediments	Fine unconsolidated sediment Volcanic ash
Landform	Rocky, cliffed Coasts Fiords Fiards	Medium cliffs Indented coasts	Low cliffs Glacial drift Salt marsh Coral reefs Mangrove	Beaches (pebble) Estuary Lagoon Alluvial plains	Barrier beaches Beaches (sand) Mudflats Deltas
Vertical movement (RSL change) (mm/yr)	≤ -1.1	-1 - 0.99	1.0 - 2.0	2.1 - 4.0	≥ 4.1
Shoreline displacement (m/yr)	≥ 2.1	1.0 -2.0	-1.0 - 1.0	-1.1 - -2.0	≤ -2.0
	Accretion	<----------	Stable	---------->	Erosion
Tidal range m (mean)	≤ 0.99	1.0 - 1.9	2.0 - 4.0	4.1 - 6.0	≥ 6.1
	Microtidal	<----------	Mesotidal	---------->	Macrotidal
Wave height m (max)	0 - 2.9	3.0 - 4.9	5.0 - 5.9	6.0 - 6.9	≥ 7.0

A probabilistic coastal vulnerability assessment was conducted by Bosom & Jimenez (2011) for the northwest Mediterranean coast. Using preexisting extreme event data, a probability function for extreme hazards was created. The vulnerability of the coast to inundation and erosion is quantified using predictors of storm waves and storm induced erosion, respectively. These predictors are compared with the ability of the coast to cope with stressors. Finally, this data is used to create the probability function, where the vulnerability of the coast is ranked from 0 (least vulnerable) and 1 (most vulnerable).

Kumar & Kunte (2012), Yin *et al.* (2010), and Le Cozannet *et al.* (2013) conduct coastal vulnerability assessments following past methodologies (Gornitz, 1991; Gornitz *et al.,* 1994;

Shaw *et al.,* 1998; Thieler & Hammar-Klose, 2000), but include new variables to quantify the CVI. Kumar & Kunte (2012) add the variable of bathymetry to define the nearshore slope of the coastal zone, and Yin *et al.* (2012) and Le Cozannet *et al.* (2013) include a land use variable. Yin *et al.* (2012) and Le Cozannet *et al.* (2013) also incorporated a Analytical Hierarchy Process (AHP) in order to weigh each vulnerability index variable.

Tibbetts & van Proosdij (2013) conduct the most recent coastal vulnerability assessment of a macrotidal environment in the Bay of Fundy. The methodology of this work is based on the previous methods of the ranking of variables and the use of a coastal vulnerability matrix (i.e. Gornitz, 1991; Thieler & Hammar-Klose, 2000). However, the work includes unique variables to better measure the vulnerability of a macrotidal environment, such as freeboard, coastline exposure in terms of wave energy, width of the foreshore, presence of vegetation, and morphological resiliency; also included are two variables commonly used in CVAs: slope and observed erodibility of the coast. Finally, Tibbetts & van Proosdij (2013) incorporate an innovative variable of coastal anthropogenic and natural protection.

Table 2 summarizes each of the variables considered in the aforementioned review of the physical coastal vulnerability assessment literature. They are listed in order of instances used in the literature; geomorphology, shoreline change, mean wave height, sea-level rise, mean tidal range, slope, and elevation are the criteria most used in the assessments. Unique variables found in a single work are listen in chronological order.

Table 2: Coastal vulnerability index criteria, summarized from literature

Coastal Vulnerability Index Criteria	
Variable/Criteria	**Work Present In**
Geomorphology	Dwarakish et al., 2009; Gaki-Papanastassiou et al., 2010; Gornitz *et al.*, 1994; Kumar *et al.*, 2010; Kumar & Kunte, 2012; Le Cozannet *et al.,* 2013; Pendleton, Thieler, & Jeffress, 2005; Pendleton, Thieler, & Williams, 2010; Thieler & Hammar-Klose, 2000; Shaw et al., 1998; Yin *et al.*, 2012
Erosion/ Shoreline Change	Dwarakish et al., 2009; Gaki-Papanastassiou et al., 2010; Gornitz *et al*., 1994; Kumar *et al.*, 2010; Le Cozannet *et al.*, 2013; Kumar & Kunte, 2012; Pendleton, Thieler, & Jeffress, 2005; Pendleton, Thieler, & Williams, 2010; Thieler & Hammar-Klose, 2000; Tibbetts & van Proosdij, 2013; Yin *et al*, 2012
Mean Wave Height	Dwarakish et al., 2009; Gaki-Papanastassiou et al., 2010; Gornitz *et al.*, 1994; Kumar *et al.*, 2010; Kumar & Kunte, 2012; Pendleton, Thieler, & Jeffress, 2005; Pendleton, Thieler, & Williams, 2010; Thieler & Hammar-Klose, 2000; Shaw et al., 1998; Yin *et al.*, 2012
Sea-level Rise	Dwarakish et al., 2009; Gaki-Papanastassiou et al., 2010; Gornitz *et al.*, 1994; Kumar *et al.*, 2010; Kumar & Kunte, 2012; Pendleton, Thieler, & Jeffress, 2005; Pendleton, Thieler, & Williams, 2010; Thieler & Hammar-Klose, 2000; Shaw et al., 1998; Yin *et al.,* 2012
Mean Tidal Range	Dwarakish et al., 2009; Gaki-Papanastassiou et al., 2010; Gornitz *et al.*, 1994; Kumar & Kunte, 2012; Pendleton, Thieler, & Jeffress, 2005; Pendleton, Thieler, & Williams, 2010; Thieler & Hammar-Klose, 2000; Shaw et al., 1998; Yin *et al*, 2012
Slope	Gaki-Papanastassiou et al., 2010; Dwarakish et al., 2009; Kumar *et al.*, 2010; Pendleton, Thieler, & Jeffress, 2005; Pendleton, Thieler, & Williams, 2010; Thieler & Hammar-Klose, 2000; Tibbetts & van Proosdij, 2013; Yin *et al*., 2012
Elevation	Gornitz *et al*., 1994; Le Cozannet *et al.*, 2013; Kumar et al., 2010; Kumar & Kunte, 2012; Shaw et al., 1998; Yin *et al.*, 2012
Geology	Gornitz *et al*., 1994; Le Cozannet *et al.*, 2013; Shaw et al., 1998
Hurricane Criteria*	Gornitz *et al*., 1994
Shoreline Displacement	Shaw et al., 1998
Coastal Form	Pethick & Crooks, 2000
Wave Run-up	Kumar *et al.*, 2010
Extreme Event Criteria*	Bosom & Jimenez, 2011
Bathymetry	Kumar & Kunte, 2012
Storm Surge	Kumar & Kunte, 2012
Exposure Extreme Storms	Le Cozannet *et al.*, 2013
Hydrographic Network	Le Cozannet *et al*., 2013
Freeboard	Tibbetts & van Proosdij, 2013
Coastline Exposure	Tibbetts & van Proosdij, 2013
Width of Foreshore	Tibbetts & van Proosdij, 2013
Vegetation	Tibbetts & van Proosdij, 2013
Anthro & Natural Protection	Tibbetts & van Proosdij, 2013
Morphological Resiliency	Tibbetts & van Proosdij, 2013
Ice Cover	Pendleton, Thieler, & Williams, 2010
Land Use	Yin *et al*, 2012
***Group of variables are unique to study**	

2.4.2. Issues in Physical Coastal Vulnerability Assessments

Predictive models inherently simplify complex systems. This simplification of the real world produces errors in model results (Hanson et al., 2010). Variables of importance to real world system dynamics may be omitted, and biased or incorrect assumptions may affect model results. This is true when conducting physical coastal vulnerability assessments to predict future risk of a coast to the effects of climate change.

Romieu et al. (2010) note that uncertainty of the future impact of climate change can be problematic when conducting physical CVAs. Many CVAs follow an impact-based approach which measures loss potential with a constant hazard; however, climate change will result in these hazards no longer being constant in nature, and methodologies will need to consider how these dynamic hazards will be modeled within the CVA. Furthermore, a purely physically-based CVA without the inclusion of socioeconomic variables limits the evaluation of vulnerable coastal areas (McLaughlin, McKenna & Cooper, 2002).

Yates, Le Cozannet, & Lenotre (2011) provide a summary of errors in coastal hazard assessments; these errors include oversimplification of the real word, model assumptions that are unmet, and data unavailability and limitations. Pilkey & Cooper (2004) have summarized an extensive list of limitations to the use of numerical models to predict coastal change and suggest the use of historical change rates with expert knowledge when evaluating coastal vulnerability. Pilkey et al. (1994) note that many empirical models do not incorporate new methods in model verification and validation. In conclusion, assessing coastal vulnerability to determine feasibility of coastal engineering projects is invaluable; however, the limitations and inaccuracies must be fully known and assessed when using CVA results for policy and adaptation purposes.

2.5. Chapter Summary

The term vulnerability has varying definitions across the literature; in this study, it is defined as the degree of risk which the geophysical coastal system experiences adverse impacts of climate change hazards as well as the coastal systems resiliency to the hazard. The vulnerability of the coastal system to climate change is dependent on two variables: sea-level rise and extreme storm event intensification. This literature review presented a review of the methods of physical coastal

vulnerability assessment. There have been numerous physical CVAs conducted; across the literature, the indicators of vulnerability that were most numerous were geomorphology, shoreline change, mean wave height, sea-level rise, mean tidal range, slope, and elevation. This is reflected in Pendleton, Thieler, & Williams (2010) assertion that 99% of CVI results were dependant on four variables: geomorphology, coastal slope, sea-level change, and wave height.

The next chapter of this body of work focuses on providing insight in to the study area where the research was conducted: the North Shore of Prince Edward Island. This chapter will discuss the geomorphological characteristics of the area, as well as discuss similarities and differences in the regions across the North Shore.

3. Study Area

3.1. Introduction

The North Shore study area is located along the northern coast of the island province of Prince Edward Island, as seen in **Figure 4**. This site extends from Lennox Island (46.636, -63.878) to Savage Harbour (46.432, -62.833) along the coast of the Gulf of St. Lawrence and is comprised of both the mainland island and a sequence of barrier islands. The area has a maritime temperate climate, with average temperature ranging from -5 to 0□C in the winter and 18 to 20□C in the summer. Midlatitude cyclones, hurricanes, and tropical storms produce the most extreme cases of coastal change, with the most intense storms occurring between October and January (Mathew, Davidson-Arnott, & Ollerhead, 2010).

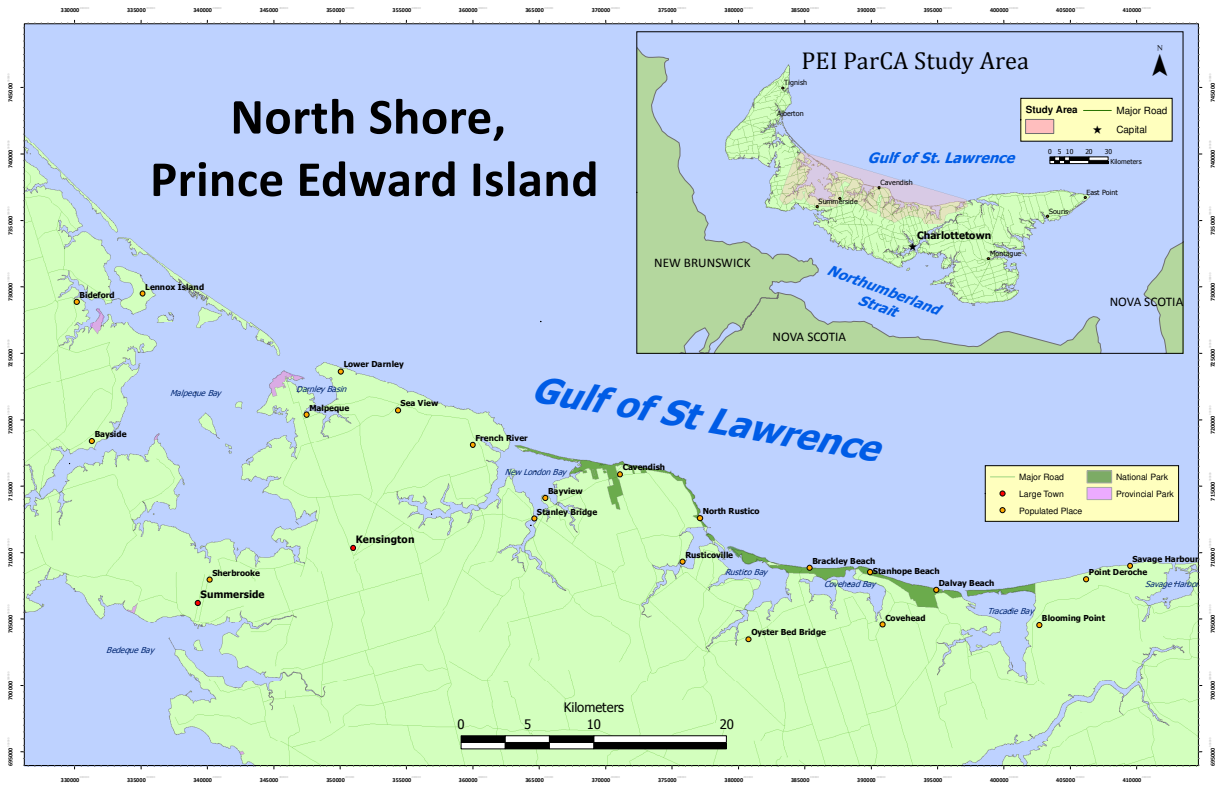

Figure 4: Map of the ParCA Prince Edward Island study area of the North Shore

The North Shore is comprised of highly erodible Pennsylvanian-Permian sandstone and shale (Mathew, Davidson-Arnott, & Ollerhead, 2010). Geomorphological classification of the

study area determined that the open coastline consists of bluffs and cliffs (47%), sand dunes and beaches (31%), where as the estuaries are composed of wetlands (54%), cliffs (19%), low plains (14%) (Davies, 2011).

3.2. Geomorphologic Characteristics of the North Shore

3.2.1. Structure

(a) (b)

Figure 5: (a) Dune system, Cavendish Beach, May 14, 2013 (b) Backshore wetland, Lennox Island; May 27, 2014

As stated in Davies (2011); Mathew, Davidson-Arnott, & Ollerhead (2010); and Stephenson & Stephenson (1954), the controlling factors which determine the geomorphological structure of the North Shore coast are the elevation, type and hardness of the exposed sandstone bedrock. Davis (2011) succinctly describes the general characteristics of the PEI shoreline: the backshore is comprised of sand dunes, plains and wetlands, or bluffs and cliffs as seen in **Figures 5a, 5b, 6a and 6b**, respectively; the foreshore is composed of bedrock, cobble, or sand (**Figures 7a, 7b, and 8)**; and the nearshore consists of sand of varying degrees of thickness over sandstone bedrock (**Figure 9a, Figure 9b**).

(a) (b)

Figure 6: (a) Backshore unconsolidated bluff, Lower Darnley Beach; May 18, 2013 (b) High cliffs at Orby Head, Cavendish; May 15, 2013

(a) (b)

Figure 7: (a) Foreshore bedrock, Seaview Beach; May 30, 2013 (b) Cobble foreshore, Cavendish; May 14, 2013

Figure 8: Foreshore sand beach, Robinson's Island; May 31, 2013

In areas of cliffs and bluffs, the sandstone bedrock is susceptible to the effects of wind, wave, and tidal action. The erodibility of the bedrock ranges spatially; areas of greater erosion resistance lead to low-relief headlands interspersed with pocket beaches, for example the headland with pocket beach seen in **Figure 10**. Exposed bedrock of higher erodibility produce low relief cliffs and bluffs. Pocket beaches are supplied by this eroded sediment in addition to offshore glacial sediment moved in to the area through wave and tidal action.

(a) (b)

Figure 9: (a) Thick layer of beach sediment, Belmont Provincial Park; May 26, 2013 (b) Exposed bedrock interspersed amongst sand, Flat Rock, Cavendish; May 15, 2013

Dynamic sand beach systems occur in areas of lower bedrock relief or along barrier islands. The systems are comprised of quartz and feldspar sand of find to medium grain size (Mathew, Davidson-Arnott, & Ollerhead, 2010). In some instances, beaches are beige colored where sediment is supplied by glacial till (**Figure 11a**); however, most beaches in the study area are rust red in color due to erosion of sandstone (**Figure 11b**).

Figure 10: Headland pocket beach, Cavendish; May 14, 2013

(a) (b)

Figure 11: (a) Glacial till beach, Cavendish; May 14, 2013 (b) Bedrock sand beach, North Rustico; May 15, 2013

(a) (b)

Figure 12: (a) Embryo dune, Lower Darnley Beach; May 18, 2013 (b) Mature dune, Point Deroche; June 2, 2013

Beaches are often characterized by extensive dune systems. Dune systems grow from initial small embryo dunes through the entrapment of windblown sediment in vegetation along the beach (**Figure 12a**) (Mathew, Davidson-Arnott, & Ollerhead, 2010). Further growth of the dune is dependent on the amount of input sediment and the location and amount of vegetation, with some dunes reaching heights of over four meters, as seen in **Figure 12b**.

Degradation of the dune through erosion is dependent on the amount of input energy from the Gulf of St. Lawrence (Mathew, Davidson-Arnott, & Ollerhead, 2010) and is exacerbated through anthropogenic forcings, such as trampling. Salt marshes and low plains are typically found behind the beach and dune systems (Mathew, Davidson-Arnott, & Ollerhead, 2010).

Barrier islands (**Figure 13**) and spits are located along the majority of the North Shore; these structures reduce the energy reaching the mainland from the Gulf of St. Lawrence (Mathew, Davidson-Arnott, & Ollerhead, 2010) and thus help reduce the amount of coastal change along the mainland coast. These barrier islands and spits are comprised of unconsolidated materials and this exposure to high energy forces leads these structures to be highly dynamic (Webster, 2012). The migration of these structures over sometimes small periods of time (annually) changes the amount of energy which reaches the mainland coast thus increasing the complexity of determining where coastal change will occur.

Figure 13: Hog Island, a barrier system, seen from Lennox Island; May 27, 2013

3.2.2. Littoral Zone

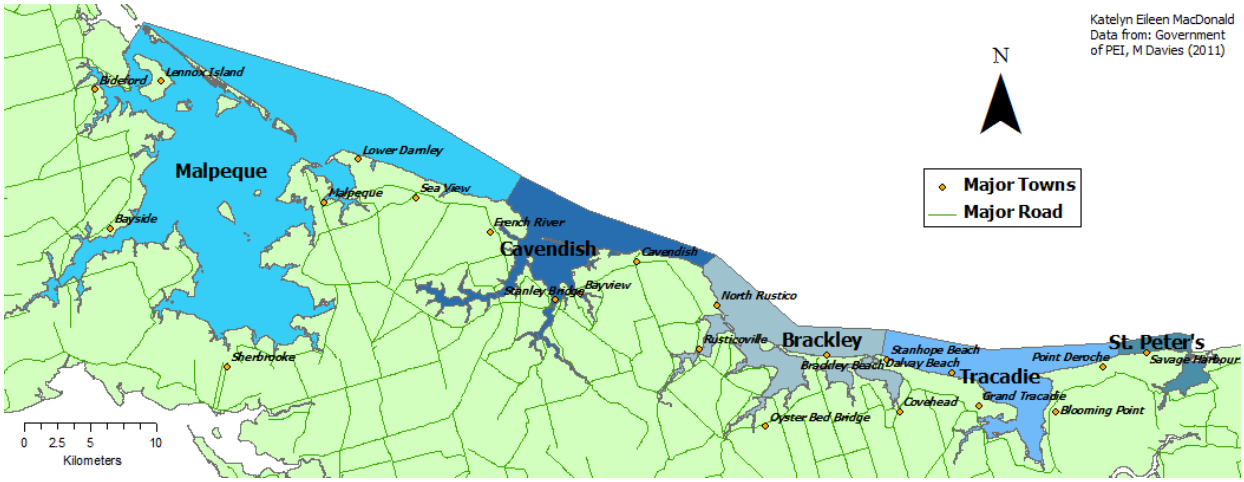

Figure 14: Map of littoral cell units, North Shore, PEI

Locations of major headlands as well as shore sediment exchange processes define the littoral cells of the North Shore (Forbes *et al.,* 2004). Five littoral cells have been identified within the study area: Malpeque, Cavendish, Brackley, Tracadie, and St. Peter's (**Figure 14**); within these cells alongshore sediment transport generally moves from west to east with open coasts having larger transport rates than estuaries (Davis, 2011). Mathew, Davidson-Arnott, & Ollerhead (2010) concluded that increases in sediment volume into the cells occur through aeolian and

overwash sediment transport. Sediment sinks within the cells include estuarine flood deltas, barrier islands, as well as coastal beach and dune systems (Davis, 2011; Forbes *et al.,* 2004).

Wave activity primarily moves from the north-northwest direction, although less severe waves occur from the northeast and southwest. Wave action is more severe and frequent in the fall. Sea ice in winter reduces the fetch distance along the open water which consequently reduces wave height, and summer storms are uncommon (Davis, 2011; Shaw, 2001).

3.3. Vulnerability of the North Shore to Climate Change

The coast of the Gulf of St. Lawrence has been identified as a Canadian region most vulnerable to sea-level rise (Shaw *et al.,* 1998), particularly due to its unique geology and geomorphology. PEI is comprised of erodible sandstone bedrock, a low elevation, frequent incidences of shoreline retreat, and a coastline exposed to large wave-generating fetches. These factors contribute to the high risk coastal hazards of coastal erosion and coastal flooding, which are exacerbated by climate change. Each hazard poses unique risks to the fisheries and tourism industry along the North Shore (Davies, 2011; Richards & Daigle, 2011). Examples of severe coastal erosion can be seen in **Figure 15a and 15b**.

The migration of sand dunes, spits, and barrier islands is a natural process; however, human intrusion in this system causes pressures which alter the system from its natural equilibrium. Coastal change along the North Shore can largely be attributed to anthropogenic forcings along the coastline. Davies (2011) states that due to long-term sea-level rise, the coasts of PEI are generally experiencing erosion rather than accretion. Climate change will compound these problems as it has been forecasted to cause sea-level rise, increase the intensity of extreme storm events and associated waves and storm surge, and alter the seasonal extent and duration of sea ice (Forbes *et al.,* 2004) . Increased levels of sea-level rise as well as increased frequency of extreme storm events will lead to amplified rates of coastal change both along the mainland and with barrier islands and sand spits (Mathew, Davidson-Arnott, & Ollerhead, 2010; Shaw 2001).

(a) (b)

Figure 15: Severe erosion at (a) Robinson's Island (May 31, 2013) and (b) Cavendish Campsite (May 14, 2013)

Extreme storms can cause increased rates of cliff, beach, and dune erosion based on coastal morphology in addition to potential overwash of barrier islands and dunes and mainland inundation (Forbes *et al.,* 2004) Furthermore, climate change has been projected to reduce the amount and duration of sea ice cover in the Gulf of St. Lawrence. This decrease in sea ice will leave the North Shore with a greater degree of exposure to extreme storm events, thus increasing the areas vulnerability.

The effects of climate change have been observed by residents of the North Shore. Over the past three decades residents have witnessed a greater frequency of high intensity storms (ACASA, n.d. a). Growing seasons are longer for farmers and residents state that winters are warmer than in past years. Rain is occurring in January, causing freeze thaw events which many species cannot tolerate (ie. White Birch) (R. Angus, personal communication, May 8, 2013). Annual precipitation is expected to increase by 10% of the 1980 rates over the next century, with more rain than snow occurring with an increase in temperature (ACASA, n.d. a) As the North Shore climate continues to change, accounts of these local effects can be expected to continue.

3.4. Regions of the North Shore

The study area of the North Shore is comprised of over 100 kilometers of coastline; thus, characteristics of the area vary regionally. This section intends to provide the reader with a brief introduction to six important regions of the study area: Lennox Island, Malpeque Bay, New London Bay, Cavendish, Rustico, and the Eastern portion of PEI National Park.

3.4.1. Lennox Island

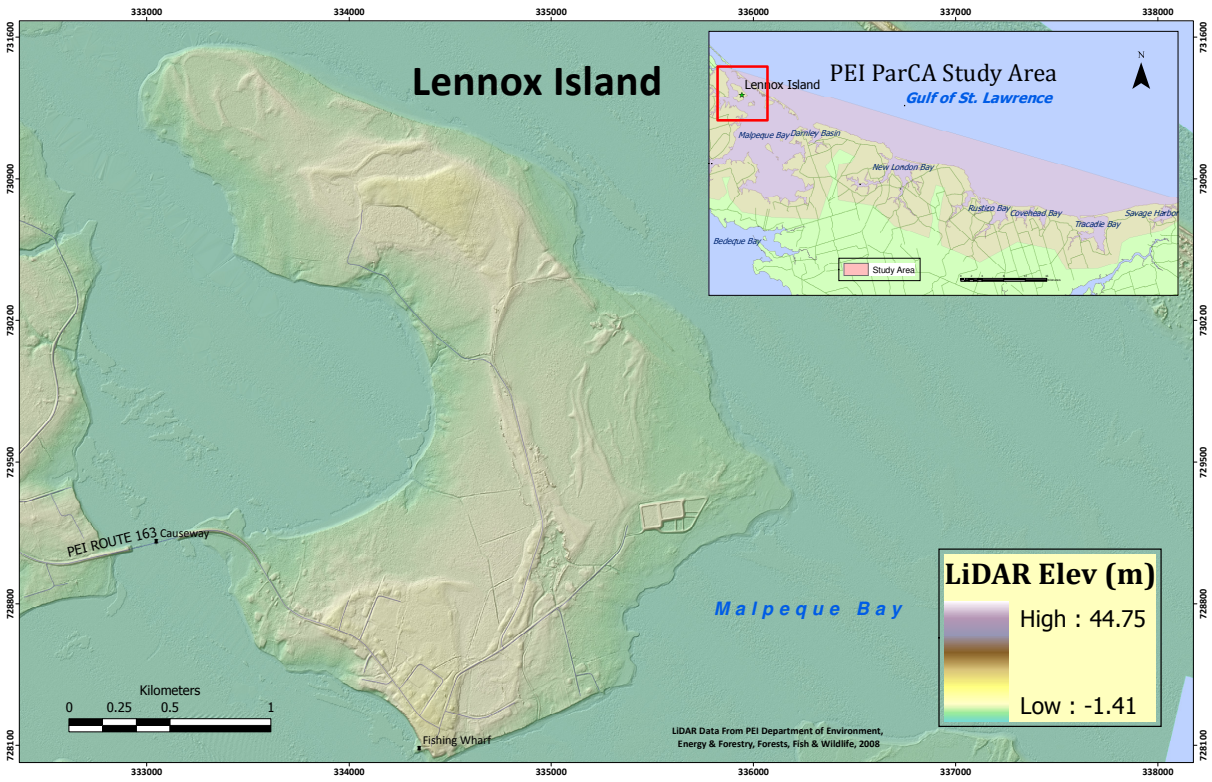

Figure 16: Map of Lennox Island; LiDAR elevation relative to CGVD28

Lennox Island is located within Malpeque Bay and is home to the Mi'kmaq people of the Lennox Island First Nation. The island is experiencing a large degree of coastal change, with the highest degree of erosion occurring along the northwestern peninsula (**Figure 17**) (R. Angus, personal communication, May 8, 2013). The causeway connecting Lennox Island to mainland PEI has experienced overwash during storm events. In December 2010 a strong storm caused structural damage from a storm surge breach. Thus, in March 2013 the anthropogenic hard

structure of riprap was added to further protect the causeway (**Figures 18a and 18b**) (R. Angus, personal communication, May 8, 2013).

Figure 17: Erosion at NW peninsula; May 27, 2013

(a) (b)

Figure 18: a) Riprap at fisherman's wharf; May 27, 2013 (b) Riprap at Lennox Island causeway, May 27, 2013

A fishing wharf located on the southwestern portion of the island is also experiencing erosion. Gabian baskets and riprap were put in place in order to decrease coastal change along the wharf and the adjacent cemetery. During an extreme storm event the cemetery experienced a high degree of erosion which caused grave sites to be exposed. Erosion has also caused emergency

evacuation at a archeological site at George's Island (R. Angus, personal communication, May 7, 2013). Issues of saltwater intrusion from sea level rise are causing concern for the residents of Lennox Island as fresh water is provided by an aquifer. Sea level rise will cause further issues in regards to a newly constructed sewage pond, as it is only 3 meters above mean sea level (R. Angus, personal communication, May 8, 2013).

3.4.2. Malpeque Bay

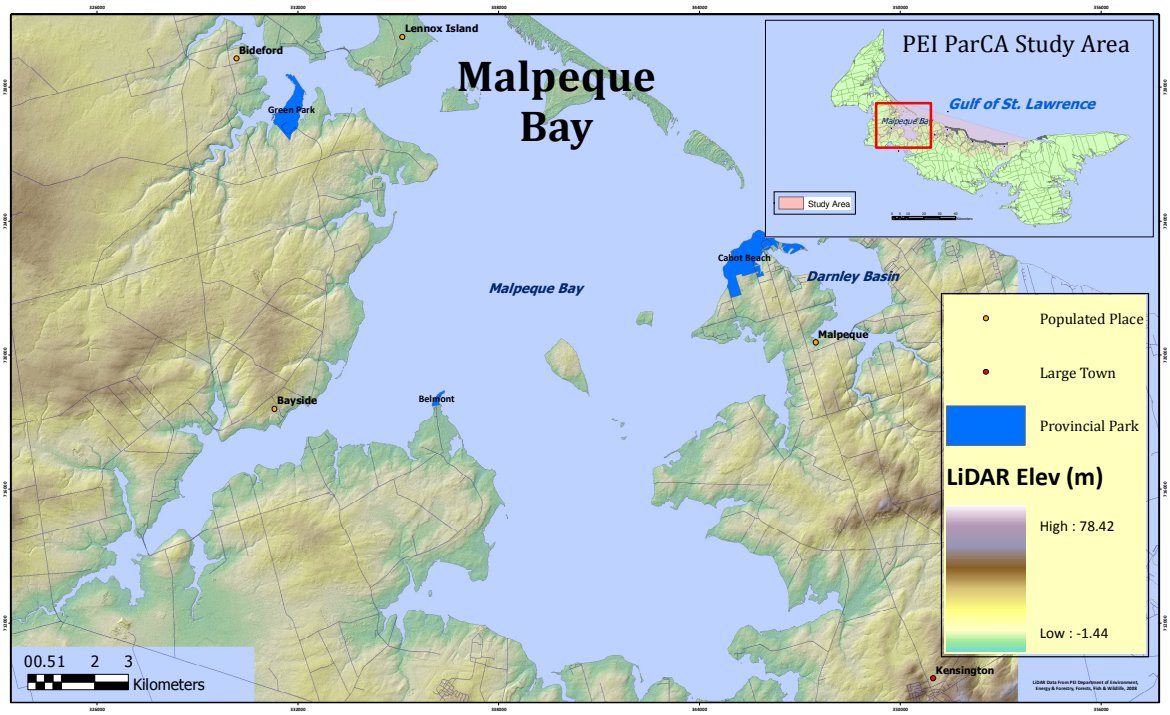

Figure 19: Malpeque Bay region of the North Shore; LiDAR elevation relative to CGVD28

Malpeque Bay is an important fishing and shellfish harvesting location. The region is home to three provincial parks (Cabot Beach, Belmont, and Green Park) (**Figure 19**) and an important fishing wharf. The coast is protected from the waters of the Gulf of St. Lawrence by a series of barrier islands. These barrier islands are dynamic in nature and are experiencing coastal change; the islands are decreasing in width while lengthening through accretion. The opening in to Malpeque Bay from the larger barrier island Hog Island has been rapidly changing over the past ten years (Webster, 2012). The area is very dynamic and experiencing rapid coastal change. A

moving sand dune has been annually filling in the bay. The area of Port Hill is experiencing erosion around an archeological site (D. Jardine, personal communication, May 8, 2013).

3.4.3. New London Bay

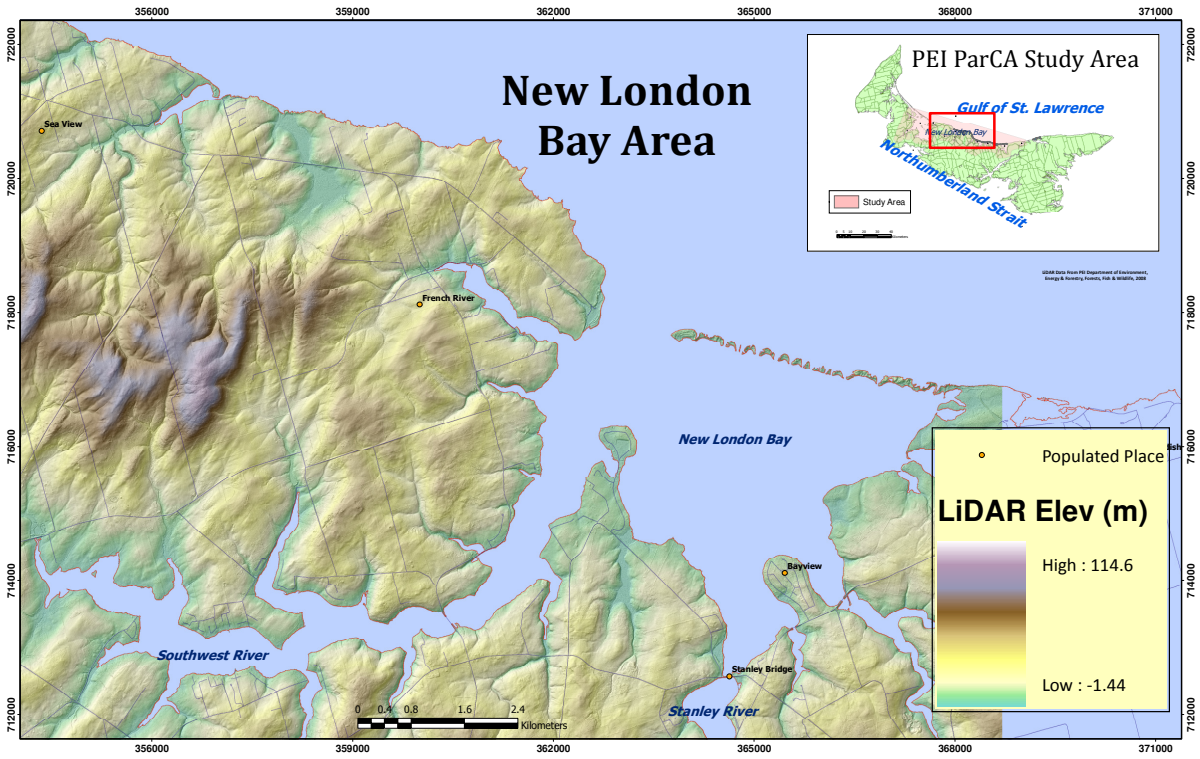

Figure 20: New London Bay and surrounding area; LiDAR elevation relative to CGVD28

New London Bay is a popular cottage location as well as an area of farming, fishing, and shellfish harvesting. The bay is protected from the Gulf of St Lawrence by a large spit and barrier island chain characterized by a large sand dune system, as seen in the map in **Figure 20**. These dunes add further protection to the bay. In recent years the coast of New London Bay has been particularly vulnerable to extreme weather. Two peninsulas within the area, Hebrides residential area and Bayview, are densely populated with summer cottages and residential properties. The peninsulas are protected from the Gulf of St. Lawrence by the spit and barrier island chain. However, if further degradation of the associated dune systems occurs, these properties could be at risk to direct impact from extreme storm surge events and sea-level rise as seen in **Figures 21a and 21b**.

(a) (b)

Figure 21: (a) Hebrides, an extremely low elevation residential area; May 31, 2013 (b) Severe erosion at Bayview; May 23, 2013

3.4.4. Cavendish

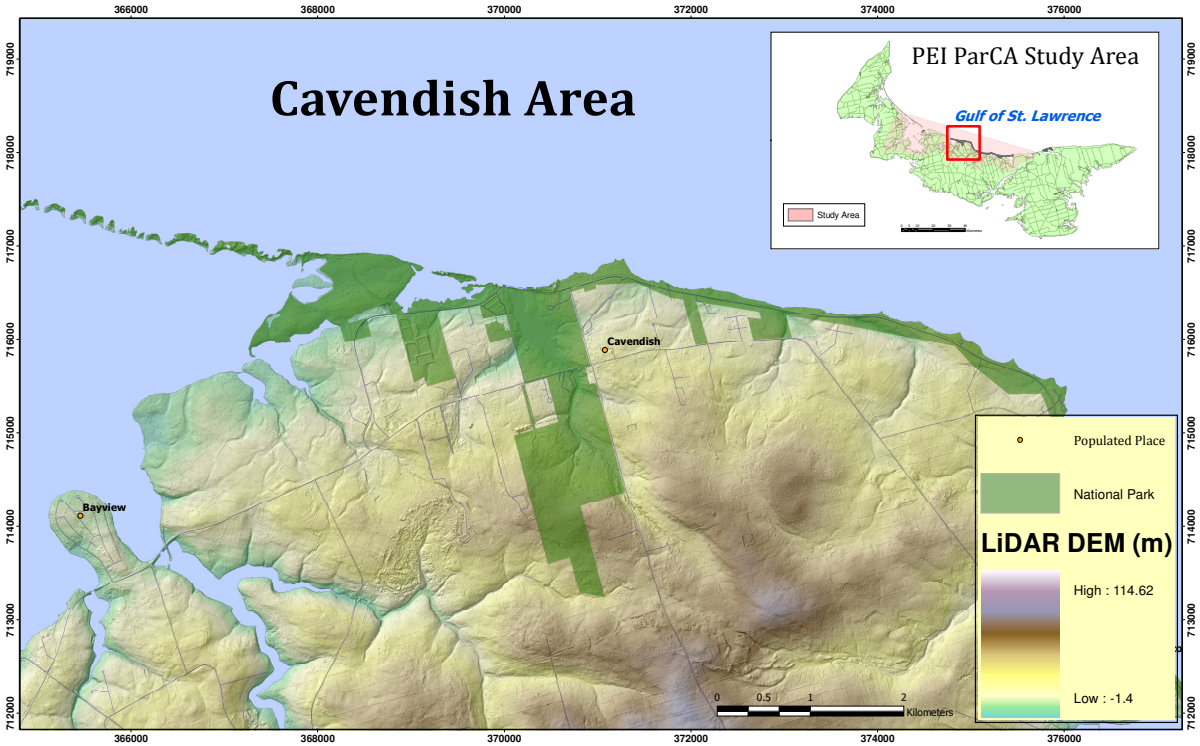

Figure 22: Map of Cavendish portion of PEI National Park; LiDAR elevation relative to CGVD28

Figure 23: Damage to dune at Cavendish Beach; May 14, 2013

Cavendish is one of PEI's most popular tourist destinations. The area is home to a portion of the PEI National Park and is the location of Green Gables attractions, as depicted in **Figure 22**. The seasonal influx of beach users has caused extensive damage to the coastal system, most particularly the Cavendish dune system (**Figure 23**). Paul Giroux, a park monitoring ecologist with Parks Canada, has stated the within PEI National Park, the most extensive damage and change has been located at the Cavendish dunes. This area will soon be designated an official wilderness site (P. Giroux, personal communication, May 10, 2013). Bluff erosion is also a very serious issue within the PEI National Park as it is causing loss of land at the Cavendish Campground.

3.4.5. Rustico

Important fishing and shellfish harvesting locations are found in the region of Rustico. A highly dynamic spit and barrier island system protects a portion of the area from the Gulf of St. Lawrence, as seen in (Webster, 2012). The fishing community of North Rustico is highly vulnerable to storm surge inundation and climate change induced sea-level rise. An extreme storm event in December 2012 inundated the town and flooded the only access road leaving the town. The North Rustico fire department is located in the current flood zone and is thus highly vulnerable to inundation (ACASA, 2012). A breakwater extending eastward into the Gulf of St. Lawrence was constructed in order to reduce wave energy in to the harbor and the associated

erosion (**Figure 24**), however erosion continues to occur along the northern coastline (Webster, 2012).

Figure 24: North Rustico breakwater extending into the Gulf of St. Lawrence

Oyster Bed Bridge, which connects the major highway through the region, is frequently washed out due to storm surge and strong wave action (**Figure 26a**). The bridge is routinely rebuilt after each blowout event. Recently, hard adaptation measures such as riprap and gabion baskets have been put in place (A. Fenech, personal communication, May 9, 2013). Robinson's Island, a portion of the PEI National Park, is experiencing severe erosion (**Figure 26b**). The sand spit was once a beach day area and was connected by road to the main park in the 1930s. Over a few decades, the spit eroded back one kilometer due to the addition of the roadway. In the 1970s the beach day area and road were abandoned due to severe erosion. The spit is now rotating landward (ACASA, 2013a; P. Giroux, personal communication, May 10, 2013; R. Angus, personal communication, May 7, 2013).

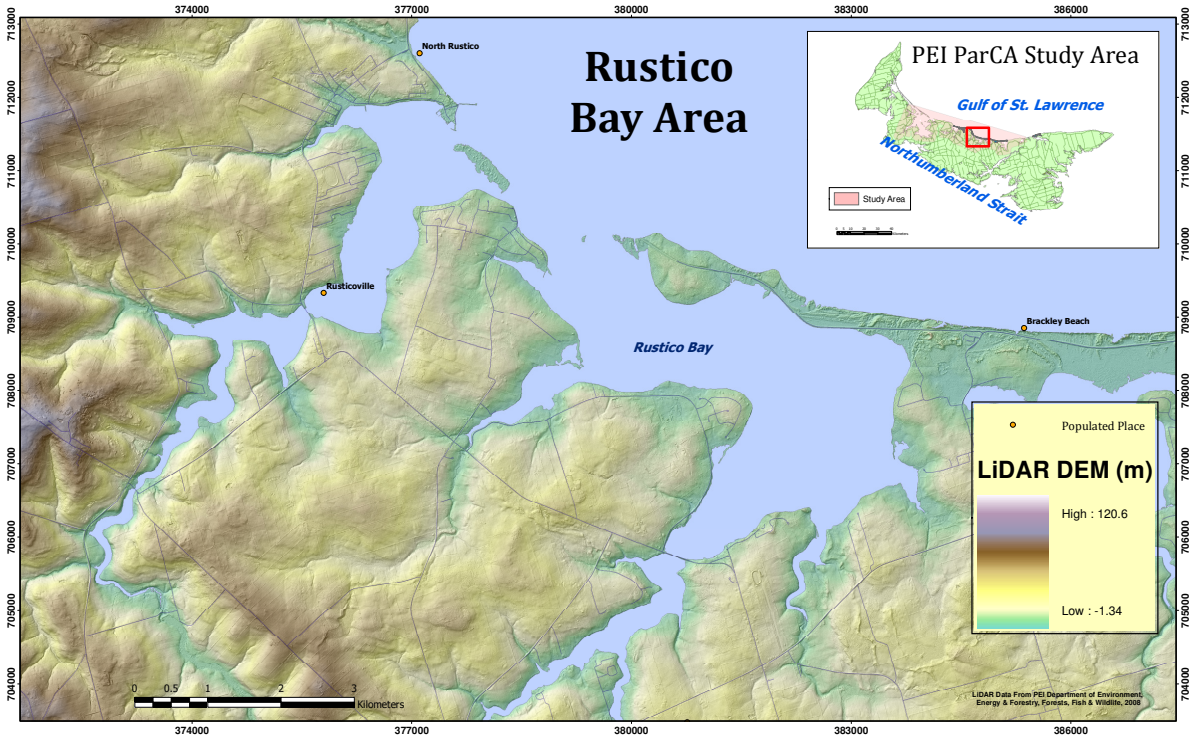

Figure 25: Rustico Bay and surrounding area; LiDAR elevation relative to CGVD28

(a) (b)

Figure 26: (a) Riprap at Oyster Bed Bridge; May 23, 2013 (b) Severe erosion at Robinson's Island; May 31, 2013

3.4.6. Brackley-Dalvay

The region of Brackley-Dalvay is located along the eastern portion of the PEI National Park (**Figure 27**). The area is a popular tourist destination with 47 kilometers of beach coastline. The park has a history of dune and bluff degradation due to anthropogenic forcings caused by this influx of visitors; the primary purpose for the creation of the park was to control dune and bluff damage, as seen in **Figure 28a** (Mathew, Davidson-Arnott, & Ollerhead, 2010). For example, before strict monitoring was enacted visitors to the beach would climb the dune, causing a "reverse mohawking" of the dune, increasing erosion and degradation as shown in **Figure 28b**. Soft adaptation techniques, such as placement of pine trees to entrap sediment and encourage dune growth, have recently been put in to restore the dune systems (ACASA, 2013a). Furthermore, in 2000 beach side parking was removed to reduce beach users from walking over dunes to reach the beach.

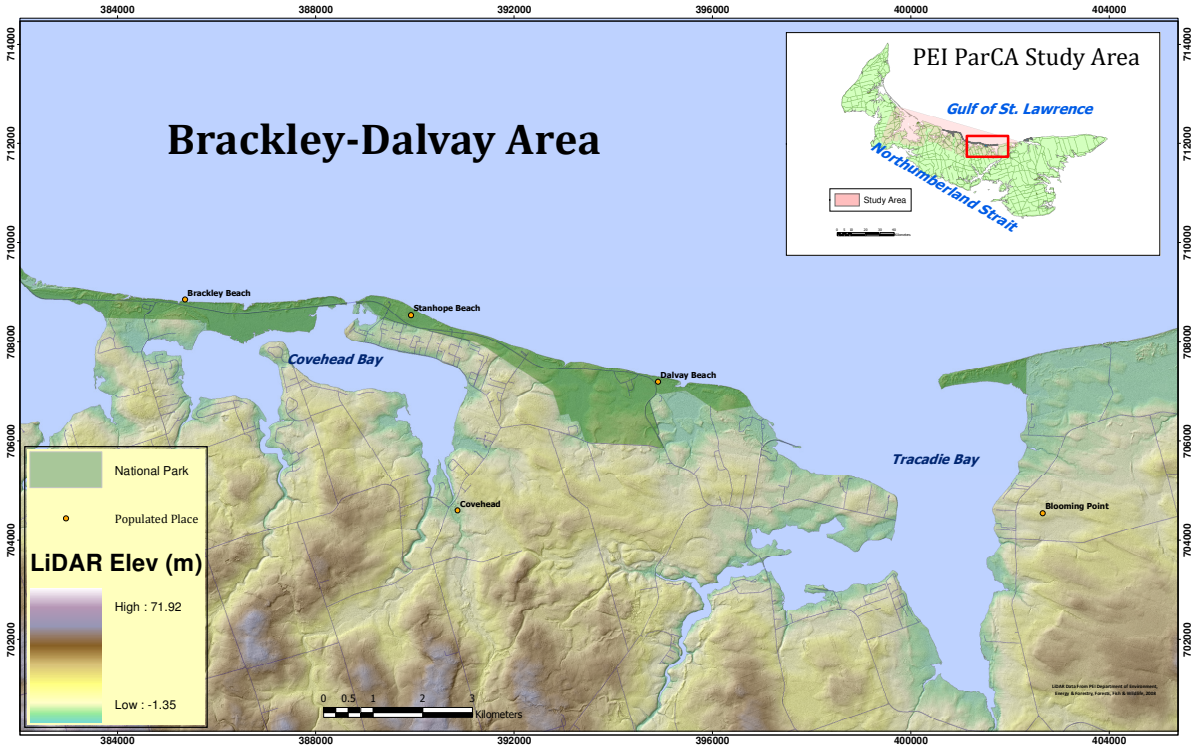

Figure 27: Region of Brackley Dalvay, eastern portion of PEI National Park; LiDAR elevation relative to CGVD28

(a) (b)

Figure 28: (a) Bluff erosion at PEI National Park; May 16, 2013 (b) Dune monitoring, May 16, 2013

4. Methodology

4.1. Criteria Selection

The North Shore of Prince Edward Island has historically experienced a high degree of coastal change from forces including erosion, accretion, and permanent inundation. To quantify the physical vulnerability of the North Shore to climate change, three criteria were selected to evaluate the exposure-sensitivity of the study area. The initial factor which governs the magnitude and direction of change in a coastal system is the exposure condition, or the potential amount of stress acted upon the coastline. Exposure condition was evaluated through the ArcMap 9.3 extension Wave Exposure Model (WEMo) version 4.0 developed by Fonseca and Malhotra (2010). The coastal system's level of morphological resiliency is defined as the ability of the system to return to a state of equilibrium following a stress event. Morphological resiliency was evaluated area in terms of volumetric sediment change and alongshore sediment transport with both GIS and mathematical analysis. As the exposure condition and morphological resiliency quantifications did not capture the vulnerability of the study area shoreline to storm surge and sea-level rise flooding, a separate vulnerability criteria to assess flood risk was included. These three criteria were incorporated in a coastal vulnerability assessment (CVA). The CVA was conducted for three time steps (2010, 2050, and 2100) in order to evaluate the change in vulnerability the North Shore will experience as a result of increasing climate change hazards.

4.2. Overview of Methods

Three criteria were quantified in a CVA for three time steps (2010, 2050, and 2100) in order to assess the physical coastal vulnerability of the North Shore. The three criteria included exposure condition, morphological resiliency, and risk to permanent and episodic flooding. Each criteria was independently quantified through the use of GIS and mathematical modeling. The exposure condition was evaluated through the input of five data in to WEMo, including fetch, shoreline position, local bathymetry, top wind frequency, and top hourly wind. Morphological resiliency was assessed through the quantification of annual volumetric sediment change and sediment budget. The risk of the shoreline to permanent and episodic flooding due to relative sea-level rise

and storm surge was assessed utilizing estimates of mean sea-level rise calculated by Rahmstorf (2007) along with storm surge return periods estimated by Richards & Daigle (2011). An overview of the data needs and integration process for each criteria is shown in **Figure 29**.

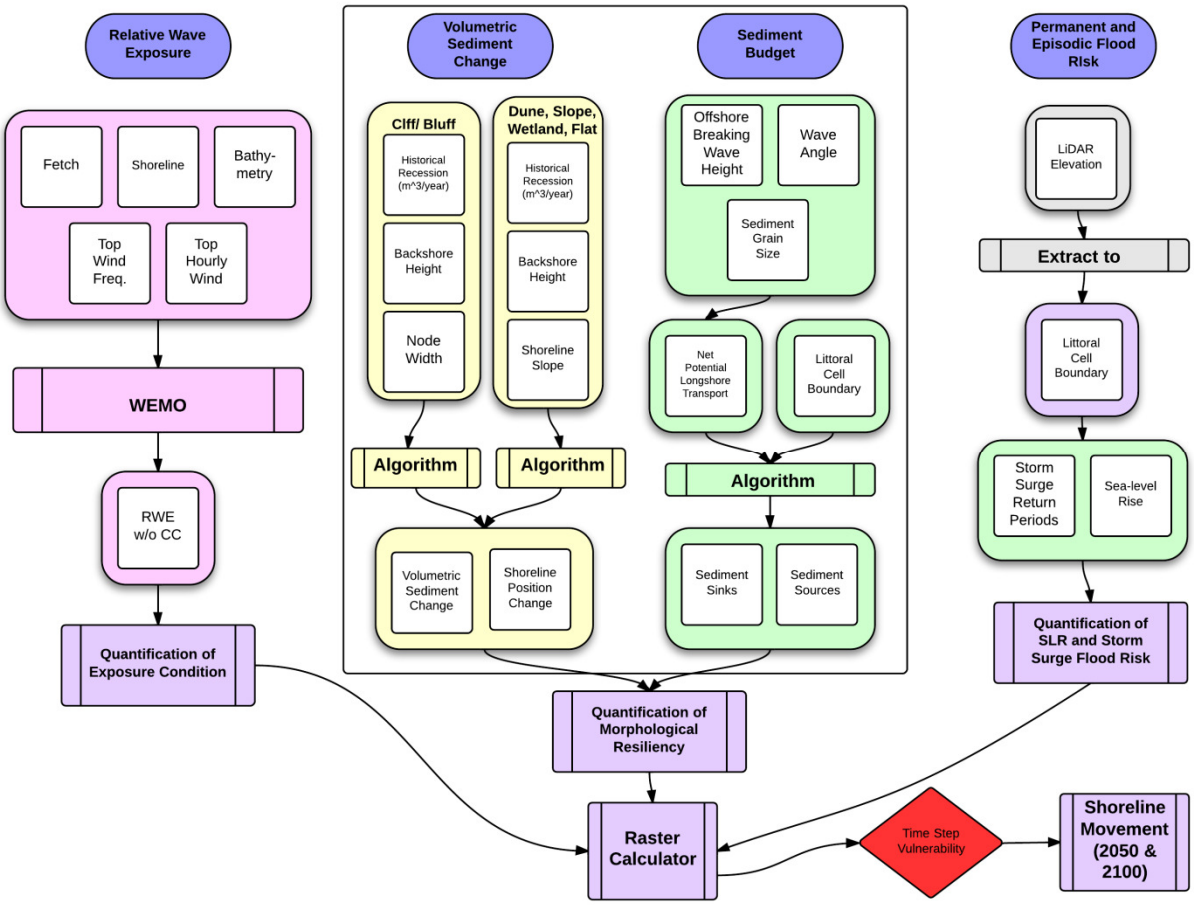

Figure 29: Data inputs for quantification of vulnerability criteria, time steps 2010, 2050, and 2100

4.2.1. Wind-Wave Exposure Condition

The Wave Exposure Model version 4.0 (Fonseca & Malhotra, 2010) was used to quantify the exposure condition of the North Shore coast. WEMo utilizes linear wave theory to determine wave energy and wave height, known as wind-wave exposure. Local wind generation and water depth features are input in to the model to determine the energy acting on the coastal study area. The model has two modes, the Representative Wave Energy (RWE) mode and Relative Wave Exposure Index (REI) mode. REI mode is simplified in comparison to the RWE mode in that it is

a non-physical relative mode that provides dimensionless outputs. The RWE mode defines the total wave energy and accounts for wave generation and dissipation with wave movement direction. This thesis utilized WEMo in the Representative Wave Energy (RWE) mode to quantify the exposure condition.

Exposure is defined as the potential of the coastal system to experience a climate change induced hazard. Inputs of WEMo used to calculate RWE include a bathymetry DEM, wind data, a shoreline polygon shapefile, and a point shapefile representing the locations RWE will be calculated. RWE mode outputs total wave energy per unit wave crest width in units of J/m or $kg/(m/s^2)$(i.e. wind-wave exposure) at the given location specified by the user using the point shapefile. The greater the relative wind and wave energy reaching the coast, the greater the vulnerability. The shoreline polygon dataset is used to clip fetch rays which are calculated by WEMo to quantify wind generation and dissipation. The polygon must depict the coverage of water, not land (Davidson-Arnott, 2010).

Bathymetric data represents the measured depth of the ocean relative to a given sea level. It is critical to know what tidal reference the data used in order to accurately understand the outputs of the model. Bathymetry data is utilized in WEMo in order to determine the propagation of waves over the area of study. Changes in bathymetry alter wave processes including refraction, diffraction, shoaling, and energy dissipation, which alter the wave energy reaching the coast.

Digital bathymetry data were not available for the study area. Thus, Canadian Hydrographic Services (CHS) chart 4023 of the 2002 shoreline of Prince Edward Island was scanned and digitized, as seen in **Figure 30**. Point depths and contour depths were digitized to point and polylines shapefiles respectively and fathoms were converted into meter depths. Since CHS Chart 4023 depicts the shoreline at mean low water line which is chart datum, the created point and polyline depth shapefiles were converted to CGVD28 by subtracting 0.52 meters to all measurements . This process follows a similar approach described in literature (King *et al*., 2002). The point and polyline depth shapefiles were used in conjunction with LiDAR contours of the shoreline to create a bathymetric DEM through the spatial analyst tool 'Topo to Raster' in ArcMap 9.3. The DEM represented the depths of the coastal waters of the North Shore and was used as the input bathymetry in the RWE analysis.

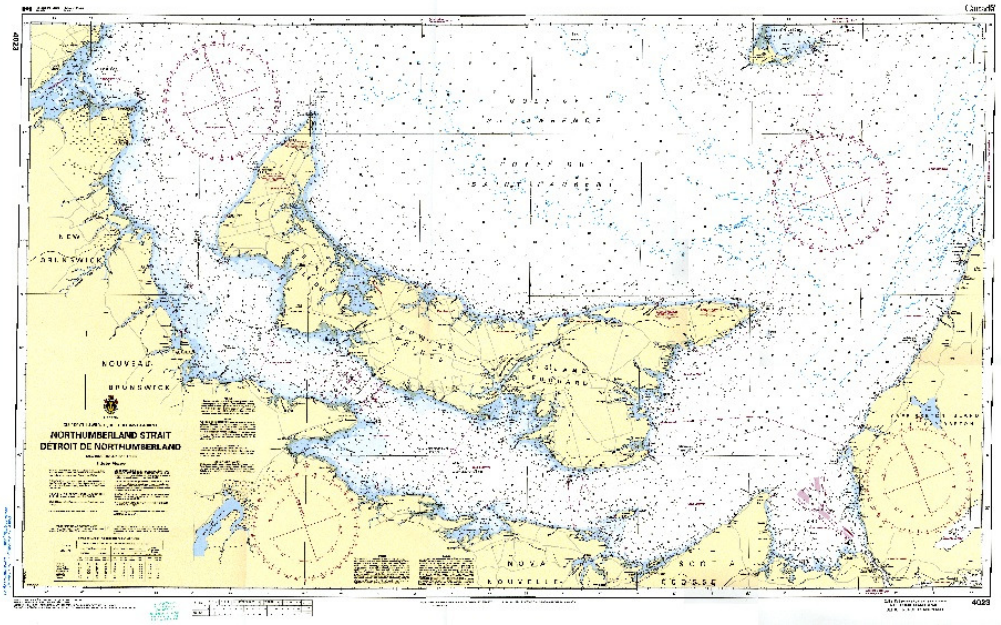

Figure 30: CHS Chart 4023 of Northumberland Strait

Data for the top wind frequency and top hourly wind were available from the St. Lawrence Global Observatory (SLGO) website (St. Lawrence Global Observatory, n.d.). Buoy IML 6 at Shediac was chosen due to its proximity to the study area (47° 47.000’ N, 64° 2.000’ W). This buoy is at a station depth of 82 meters. The data ranged from the years 2004-2010, however the monthly range for each year varied.

WEMo requires the input wind data to be in .txt file type with comma separated values specifically in the order of year, month, day, hour, month, wind speed (meters per second) and wind direction (angular degrees). The SLGO IML 6 buoy data was thus edited to conform to these standards.

4.2.2. Morphological Resiliency

Morphological resiliency is defined as the ability of the coastal system to return to a state of equilibrium after a disturbance. This resiliency is a factor of the amount of sediment supply to the coastal system, the morphology of the system, and the duration of time between disturbance events. For the purpose of this research, morphological resiliency of the North Shore study area was evaluated through the quantification of annual volumetric sediment change and the sediment budget. The morphological resiliency criteria is similar to the "relaxation time" Coastal

Vulnerability Index (CVI) component used in Pethick & Crooks (2000). Relaxation time is defined as the period of recovery of a coastal system after a disturbance event, and is divided by the return period of disturbance events to evaluate coastal vulnerability (Pethick & Crooks, 2000).

Within this area, coast lines classified as dunes, slopes, wetlands, or flats have a higher morphological resiliency as they are largely sinks of sediment; cliffs and bluffs are typically characterized by a low morphological resiliency as they are sediment sources.

Morphological resiliency is a function of volumetric sediment change and the sediment budget measures whether the unit of shoreline has the capacity to recover after a disturbance event. In terms of vulnerability, an area that has a positive volumetric sediment change and a low net potential transport will have a higher morphological resiliency and thus less vulnerability. In comparison, an area with high net potential longshore transport and a negative sediment budget will have lower morphological resiliency and a higher vulnerability. The assumption that a lower morphological resiliency would correlate with sediment sources, and higher with sediment sinks was necessary in order to mathematically quantify the physical vulnerability of the coast, but is not necessarily correct in all situations. For example, a beach was assumed to be a sediment sink; however, during periods of storm events a beach may become a sediment source as wind-wave energy erodes beach sediment and deposits it in to nearby estuaries and bays. However, the assumption that a beach would be an overall sediment sink is reflective of the decadal time scale of the methodology.

The methodology described in this chapter is dependent on the assumption that the geomorphological state of the shoreline will be the largest factor defining it's exposure-sensitivity as well as the degree of coastal change. This change effects the geomorphological dynamics of the area, including the coast's exposure condition, morphological resiliency, and potential to be flooded by nearby water bodies. A shoreline classification entails mapping the physical condition of the shoreline into a GIS database to include data on geomorphology and vegetation (Davies, 2011; Pietersma-Perrott & van Proosdij, 2012). The shoreline classification data by Davies (2011) was created through the classification of the nearshore, foreshore, and backshore of the coast through visual assessment of orthophotos captured in 2010.

As the Davies (2011) shoreline classification was not field validated, shoreline classification of a portion of the study area was conducted during the months of May and June, 2013. To gather this information, a Yuma Tablet was employed *in situ* to collect spatial data on the coastal geomorphology of the North Shore. Coastline data for the year 2010 were also downloaded and three separate polylines were created by Greg Baker to represent the backshore, foreshore, and nearshore of the shoreline; these polyline shapefiles were inputted in to a geodatabase and edited in the field to reflect shoretypes classification of the coastal region. The backshore, foreshore, and nearshore were classified by shoretype along with associated characteristics. For example, the backshore shoretypes consisted of anthropogenic (human-built structures with the purpose of controlling coastal change), outcrop, platform, cliff, bluff, dune, slope (clastic), slope (organogenic), wetland (organogenic), wetland (minerogenic) or waterbody; the foreshore shoretype could be classified by anthro, outcrop, platform, beach, flat, dune, wetland (organogenic), or wetland (minerogenic); and finally the nearshore could be classified as platform, flat, or bar. In order to accurately classify the North Shore of Prince Edward Island, base data including orthoimagery, road networks, and location names to be used as spatial references.

The nearshore, foreshore, and backshore polylines were classified based on a shoreline classification schema first developed by Pietersma-Perrott & van Proosdij (2012). Once in field, the GPS toolbar within ArcMap 9.3 on the Yuma Tablet was used to accurately define the location of the physical coastal region with the shore polyline shapefiles. The Editor toolbar was used to begin the classification of the shoreline shapefiles; each polyline was cut using the split tool within the editor toolbar to create the boundaries of the area being classified. The user then walked the shoreline with the Yuma tablet in order to classify the morphology of the shoreline using the previously designed classification schema; for example, if the backshore changed from a medium height cliff to a low dune, the user would use the split tool on the backshore polyline to split the line between the boundary between the dune and cliff, and then classify each separately. This field work produced three polylines of the classification of the nearshore, foreshore, and backshore and was used to calculate annual volumetric sediment change; in areas that were not classified in the field, the Davies (2011) classification was used.

Coastal change is defined in terms of erosion and accretion, or the change in meters of land lost or gained for a coastal unit. GeoNet Technologies, Inc. (2011) provided the initial calculation of coastal change rates for the North Shore through the digitization of orthophotos of the years 1968, 2000, and 2010. Historical change rates between 1968 and 2010, and recent change rates between 2000 and 2010 were calculated by measuring the shortest Euclidean distance between two shorelines and determining the change in meters per year. Webster (2012) noted that these calculated rates of change did not always correctly reflect areas of erosion and accretion *in situ*. Thus, areas determined to be anomalous were given change rates of zero. Shoreline segments of coastal change were labeled anomalous if the calculated change surpassed greater than three meters annually of change - typically migration of sand spits or inundation of sea-level rise.

The coastal change rates calculated by GeoNet Technologies Inc. (2011) and Webster (2012) only captures the change which the coast either accumulates towards or erodes away from the water and does not incorporate the height of the shoreline unit in question. Thus, in order to determine the sediment lost or gained to the coastal unit, two algorithms were defined based on the geomorphological classification of the segment: either bluffs and cliffs or dunes, plains, wetlands, and flats. The two algorithms presented assume that the volumetric loss rate remains constant during a given time step.

It was assumed that coastal cliffs and bluffs have a predominantly rectangular shape as modeled in **Figure 31**. Annual volumetric change for these geomorphological units was defined in **Equation 2** as:

$$V_r = \left[\left(\left(\frac{elv_N + elv_{N-1}}{2}\right) \cdot \frac{d_{N-1}}{2}\right) + \left(\left(\frac{elv_N + elv_{N+1}}{2}\right) \cdot \frac{d_{N+1}}{2}\right)\right] \cdot r_{cc} \qquad (2)$$

Where elv_N, elv_{N+1} and elv_{N-1} = LiDAR elevation of backshore at node in question, forward node and previous node of the coastal unit (meters)

d_{N-1} and d_{N+1} = distance between N and N-1, N and N+1 respectively

r_{cc} = historical coastal change rate (meters/year) for first year of time step

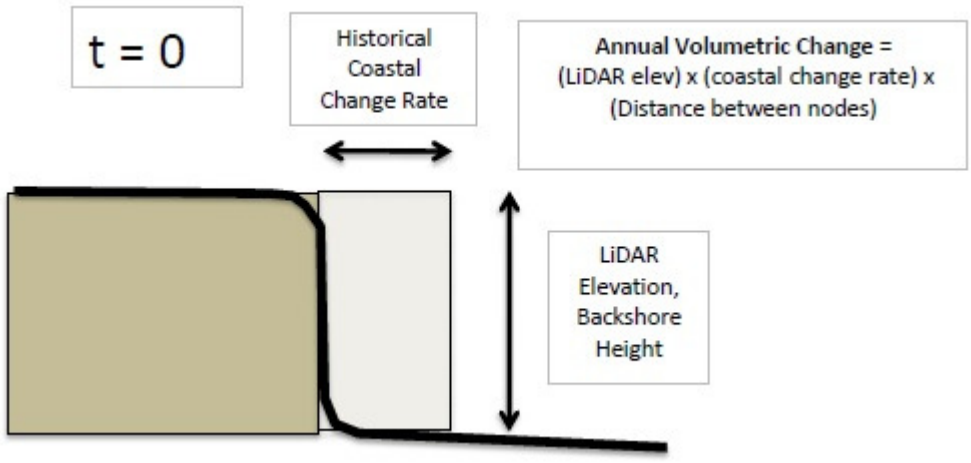

Figure 31: Method for calculation of volumetric sediment change for bluffs and cliffs

Thus, the resulting solution defines the volumetric sediment change in cubic meters for the duration of the time step.

The algorithm for coasts classified as dunes, slopes, wetland, and flats assumed a triangular shape as depicted in **Figure 32**. Annual volumetric change for these geomorphological units was quantified using **Equation 3**:

$$V_t = \frac{1}{2} md \cdot \left(\frac{r}{|r|} \cdot r^2\right) \quad (3)$$

Where m = slope of the coast

d = distance between nodes

r=rate of coastal change at node

This algorithm also provides a solution in cubic meters per total years of the time step.

Alongshore sediment transport is the mechanism which moves sediment within a littoral system. It is a function of oblique wave action on the swash slope, longshore wave-generated currents, and seaward-moving currents; combined, these forces act to transport sediment along the coast in a relatively uniform direction (Davies, 2011). Longshore sediment transport transfers suspended material from areas of sediment sources, such as bluffs and cliffs, to depositional areas of sediment sinks, such as deltas, spits, and barrier islands. A major component of the quantification

of a coastal systems sediment budget is to determine the systems net potential longshore sediment transport, or the calculated amount of sediment able to be transferred along a particular shoreline by tidal and wave forces.

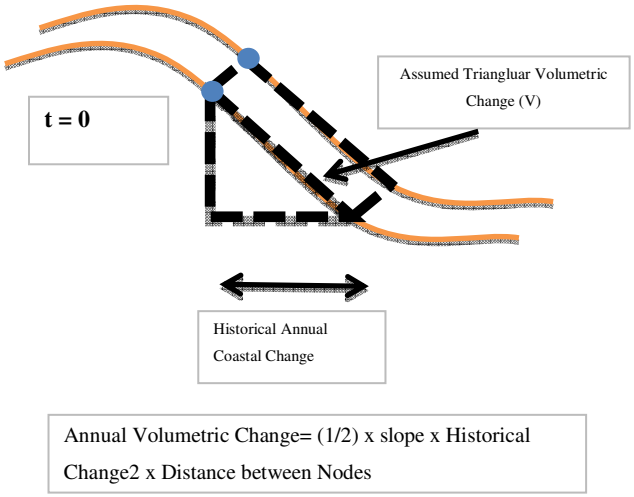

Figure 32: Calculation of annual volumetric change for dunes, slopes, wetlands, and flats

Davies (2011) calculated the net potential longshore sediment transport (Q_n) using the Queen's University Expression for Sediment Transport for the 2010 PEI shoreline. This expression uses wave hindcast data, longshore sediment transport rate field data from the 1980s, sediment grain size, geomorphology, and local wave climate to calculate Q_n. Wave hindcast data over a 58 year period is available from the Meteorological Service of Canada MSC50 database and includes information on breaking wave height and the wave angle relative to the shoreline.

Utilizing the calculated alongshore sediment transport, Davies (2011) defined the littoral cells of the coast of PEI. The littoral cell is a coastal compartment where sediment theoretically does not leave or enter from an adjacent cell. Thus, the spatial boundaries of the littoral cell were used to define the sediment budget of the study area.

Between each time step (2010 and 2050, 2050 and 2100) the shoreline position was assumed to change based on the coastal change rates calculated by Webster (2012). This shoreline position change was calculated within ArcMap 9.3 and Excel. X and Y coordinates of the initial 2010 shoreline nodes were first added as a field to the node shapefile as well as the Webster (2012)

calculate coastal change rates. As the nodes represent segments of the shoreline and thus the main polyline, they represent different segments of the North Shore coast- whether it be the main coast or islands. The nodes were given IDs to represent segments of the shoreline polyline which are the same - for example, the main North Shore polyline and node segment would receive one ID, where as an island polyline would receive another ID. These IDs were labelled "FID_Coast". Areas with anthropogenic hard adaptation measures such as riprap were also indicated in the field "shoretype". This table was then extracted as a CSV to be input in Excel. Within Excel, there are five columns indicating the necessary data for each node: X coordinate, Y coordinate, coastal change rate, FID_Coast, and Shoretype. Each node was then offset based on the magnitude of accretion or erosion, whether it be inland or offshore. This was accomplished through the approximation of the tangent of each node. Once the tangent of the node was quantified, the node moved perpendicular to the shore based on the degree of coastal change. This process was repeated given the size of the time step analysis (40 years between 2010 and 2050, 50 years between 2050 and 2100). Finally, the 2100 coastline was predicted by multiplying the Webster (2012) coastal change rates by a factor of 1.1, known as the storm enhancement factor, which is described in detail in **Section 4.2.3**. The previous method was then followed to create the 2100 coastline of the North Shore. It was assumed that the shoreline classification of each node remained the same through the shore movement from 2010 to 2050 and 2050 to 2100.

4.2.3. Permanent and Episodic Flood Risk

Permanent and episodic flood risk was quantified through the evaluation of permanent climate change induced sea-level rise and episodic storm surge inundation based on coastal elevation. Through the 2010, 2050, and 2100 time steps, relative sea-levels were estimated to increase, and a larger area of land received increased storm surge return periods and heights. Vulnerability ranking calculation assumed that the highest vulnerability of 5 would be associated with elevations that are susceptible to more frequent flooding (10 year return period), that a moderate vulnerability (rankings of 4, 3, and 2) would be associated with elevations which experience flooding between 25 and 100 year return periods, and elevations greater than the 100 year flooding return period were of least vulnerability (ranking of 1). The total area of the North

Shore which would experience the five flood return periods increased through each timestep due to relative sea-level rise; thus, the vulnerability of the study area to permanent and episodic storm surge increases through time.

Simply defined, storm surge is the difference between the forecasted astronomical tide and the measured water level; storm surge may raise or lower sea level. In terms of shoreline risk to storm surge, we refer to storm surges which raise the predicted tide. Storm surges occur during extreme weather events due to higher than average wind speeds and low barometric pressure. They are most damaging during times of high tides which cause episodic coastal flooding (Richards & Daigle, 2011).

Richards and Daigle (2011) estimated extreme total water level for 2-, 10-, 40-, and 100-year return periods for Rustico using results from the Environment Canada Atmospheric Hazards Atlantic Website. Using this information, total estimated return-period sea levels for the years 2025, 2055, 2085, and 2100 were quantified as the sum of the estimated storm surge height and estimated sea-level rise based on the higher high water low tide (HHWLT) chart datum for the specific year, as seen in **Table 3**. The values included estimates of annual permanent sea-level rise, thus including risk of permanent sea-level rise to the evaluation. Estimates for permanent sea-level rise values were extracted from Rahmstorf (2007).

Table 3: Total change of water levels for Rustico, from Richards and Daigle (2011) (cm relative to CGVD28)

Municipality or Area	Global Sea-Level Rise (2100) (Note 1)	Crustal Subsidence (2100)	Total Change (2025) (Note 2)	Total Change (2055) (Note 3)	Total Change (2085) (Note 4)	Total Change (2100)
Rustico	0.90 ± 0.43	0.18 ± 0.05	0.16 ± 0.03	0.44 ± 0.15	0.84 ± 0.36	1.08 ± 0.48
Note 1: Value of 90 cm is the central value from Rahmstorf (2007) year 2100 estimates and ±43 cm error bar represents the associated range Note 2: Total includes linear increase of crustal subsidence (25%) + prorated non-linear (polynomial) increase of 100-year sea-level rise Note 3: Total includes linear increase of crustal subsidence (55%) + prorated non-linear (polynomial) increase of 100-year sea-level rise Note 4: Total includes linear increase of crustal subsidence (85%) + prorated non-linear (polynomial) increase of 100-year sea-level rise						

To determine the areas of vulnerability within the study area to storm surge flooding, LiDAR elevation measurements were utilized. Areas within the storm return periods were considered at risk, and received a vulnerability ranking from most vulnerable (5) to least vulnerable (1).

When predicting future hazards of climate change, a storm enhancement factor can be included to model the proposed rise of storm intensity in the next century. This factor would increase the water levels associated with storm surge using a factor of 10% multiplied for 1:100 and 1:1000 storm surge flood levels. This percentage was determined using the most up to date understanding of climate change science (Dasgupta *et al.,* 2011; Nicholls *et al.,* 2007; Ward *et al.,* 2011). This storm enhancement factor was used when predicting future vulnerability of the North Shore for the years 2050 and 2100 in the form of wind speed increase and coastal change rate increase. This will increase the accuracy of determining coastal vulnerability of the North Shore to climate change.

4.3. Time Step Analysis

As detailed in Chapter 2, coastal vulnerability assessments are typically quantified through the use of criteria indicators. These criteria represent the hazards and risks the coastline experiences. For this work, the criteria used to evaluate the coastal vulnerability of the PEI North Shore to climate change included exposure condition, morphological resiliency, and flooding risk. Each criteria were evaluated and summed together to produce the coastal vulnerability for three years: 2010, 2050, and 2100. These three years were chosen in order to predict the coastal vulnerability as climate change progresses through time.

4.3.1. Exposure Condition

Year 2010

The initial step in the assessment of the year 2010 was to determine the relative wave exposure (RWE) of the coast using WEMo. Four inputs were required – bathymetry of the coast, the coastal polygon to clip the fetch rays, top wind frequency and top hourly wind, and a point shapefile which represent the areas where the 2010 RWE will be calculated. This point shapefile was created from the 2010 coastal polygon, which was converted in to a raster, and then a point shapefile. The resolution of the point grid is dependent on the desired number of points where the RWE needed to be calculated. Because the study area is quite large, a resolution of 1.5 kilometres was used. Furthermore, the WEMo input point shapefile was standardized in that each point was between 200 and 300 meters from the shoreline. With these input data the RWE was

calculated within WEMo. The 2010 extent polygon was created using the 2010 coastline polyline created by Davies (2011). Line segments within the polyline shapefile were closed using topological tools and the tool 'Feature to Polygon' was utilized to create the final polygon. The procedure for creating the bathymetry and wind data was outlined in **Section 4.2.1**. The 2010 input parameters (bathymetry DEM, wind data, shoreline polygon, RWE calculation point) were added to a new WEMo project. The Distribution of Fetch and Bathymetry Interrogation Distance settings were increased to 7,000 meters, otherwise the default options were used.

With the RWE values calculated, these values were spatially joined to a standard 2010 node point shapefile which was used for each of the three vulnerability criteria in the time step. The RWE was not calculated initially at each node as the resolution was too fine for a large study area thus producing a very lengthy computation time. The join was accomplished through the 'Spatial Join' tool based on nearest proximity.

The RWE vulnerability for the 2010 coastline was quantified using Jenks Natural breaks of the initial RWE point shapefile; **Figure 33** is an image of the tool used to classify this field, and **Table 4** lists the resultant divisions. The Jenks Natural Breaks method to organize criteria data sets was used in the creation of a Coastal Vulnerability Index for a macrotidal environment (Tibbetts & van Proosdij, 2013). The method is best used for grouping non-normally distributed data, and seeks to maximize the difference between values for the data range.

The 'Field Calculator' was used to add the vulnerability value. Finally, with the new vulnerability field added, this point shapefile was converted in to a raster of 50 meter resolution using the 'Feature to Raster' tool. This raster thus depicts the areas of the highest (5) to lowest (1) vulnerability.

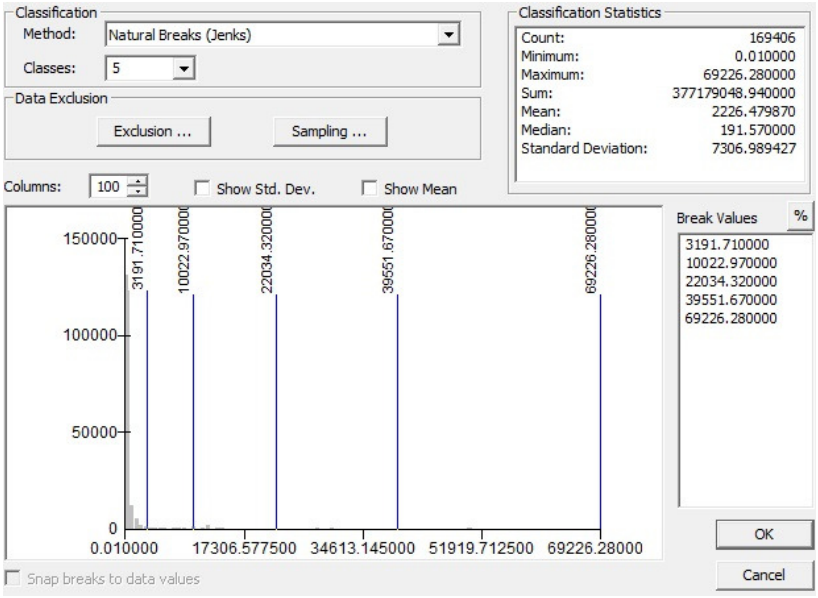

Figure 33: Natural Breaks (Jenks) classification of RWE values for 2010 calculated in WEMo

Table 4: Vulnerability ranking of RWE for year 2010

RWE (J/m)	Vulnerability Index
0.01 - 3191.7	1
3191.71 - 10022.97	2
10022.971 - 22034.32	3
22034.321 - 39551.67	4
39551.671 - 69226.28	5

Years 2050 & 2100

The methodology used to determine the exposure condition of the North Shore coast for years 2050 and 2100 was similar to that of the year 2010. A CSV file containing the shoreline node locations calculated for 2050 and 2100 was first converted in to a ESRI point shapefile and then a polyline shapefile. As the Hog Island coast is very dynamic, an accurate prediction of the coastal change for the years 2050 and 2100 was not possible. The output of the shoreline movement algorithm for Hog Island in the year 2050 is shown in **Figure 34**. Thus, the Hog Island coast was represented as the same as 2010 for the years 2050 and 2100 and was merged in to the new polylines for 2050 and 2100. Figure 6 depicts the resultant node shapefile after the shoreline movement was undertaken, however this node shapefile was no used for the creation of the shoreline.

Figure 34: Unused 2050 predicted shoreline movement of Hog Island

A polygon was created from the 2050 and 2100 shorelines through the extension ET Geowizards. The islands of the North Shore coast were separately converted in to polygons in order to "clip" their extent from the main coast polygon. This was accomplished through the editor toolbar in ArcMap 9.3.

DEM bathymetry of the North Shore coasts for the years 2050 and 2100 were created to be used in WEMo. These DEMs were created through the use of the CHS contours previously created along with the new polygon of the coastal area and the new shoreline polyline. The CHS contour shapefile and the shoreline polyline were merged together to create a new contours for the years 2050 and 2100. The new shoreline for these years was given a depth of "0" in order to represent the new coastal extent. In the tool Topo to Raster, the polygon was input to represent the DEM extent as well as the new contour shapefile. The z extent was limited to 0 in order to accurately represent the bathymetry of the 2050 and 2100 coasts, with the 2050 DEM shown in **Figure 35**.

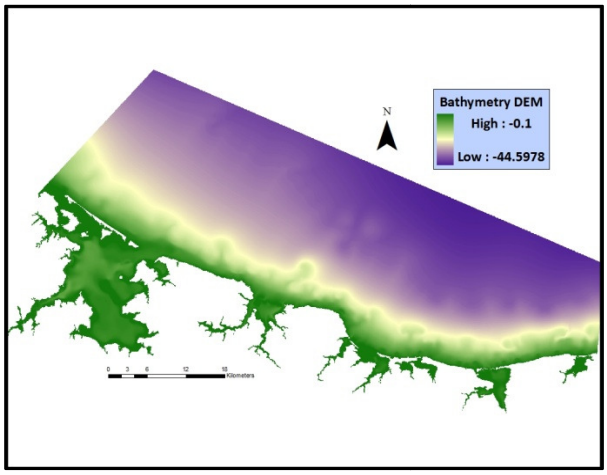

Figure 35: Bathymetry DEM of 2050 North Shore

The next input needed in WEMo was the point shapefile to represent the locations where the RWE would be calculated. For the calculation of RWE for years 2050 and 2100, the 2010 point shapefile was used, however edits were made to ensure the points were only in the newly exposed water locations.

Finally, North Shore wind data for the years 2050 and 2100 was created through the use of the 2010 wind data. In order to represent an increase in wind speeds through stronger storms in the years 2050 and 2100, the 2010 wind speeds were multiplied by 1.1 and 1.21, respectively.

Symbol	Range	Label
◆	35.100000 - 3191.700000	1
◆	3191.700001 - 10022.970000	2
◆	10022.970001 - 22034.320000	3
◆	22034.320001 - 39551.670000	4
◆	39551.670001 - 69226.280000	5

Figure 36: 2050 ranking of 2050 RWE values

Once the inputs for WEMo were completed, RWE was calculated for 2050 and 2100. A new "water level adjustment" was made for 2050 and 2100 to represent sea-level rise for each year and reflect calculations made by RIchards and Daigle (2011). The water level was increased for year 2050 by 0.44 meters and for 2100, 1.08 meters.

The 2050 and 2100 RWE values were divided at the intervals calculated for the 2010 exposure condition vulnerability, as seen in **Figure 36**. These intervals were used in order to compare the growing vulnerability of the North Shore coast through the three time steps.

4.3.2. Morphological Resiliency

Year 2010

Morphological resiliency (MR) of the shoreline of the North Shore is assumed to be a function of the annual volumetric sediment change (VSC) of the shoreline as well as the longshore sediment transport (Q_n) of the study area. MR is assumed to equal the sum of the normalized values of VSC and Q_n, as shown in **Equation 4**.

$$VSC_{norm} + Qn_{norm} = MR \qquad (4)$$

The net potential longshore sediment transport rate (cubic meters annually) for the year 2010 had been quantified by Davies (2011) using a 58 year wave hindcast of breaking wave height relative to the shoreline provided by the Meterological Service of Canada.

Annual volumetric sediment change is a function of the geomorphological classification of each shoreline segment. Calculation of annual volumetric sediment change is dependent on this geomorphological classification, as explained in Section 1.2.2. The initial step in calculating annual volumetric sediment change was to classify the standard shoreline node point shapefile as

one of three classes - "2" for anthropogenic structures; "1" for dune, wetland, slope, or plain; and "0" for cliffs and bluffs. Then, variables for the volumetric sediment change calculation were spatially joined to each class: for class 0, LiDAR elevation and coastal change rate from Davies (2011) and Webster (2012) were joined, and for class 1, coastal change rate from Webster (2012) was joined; although a slope field was available from this database, errors in the slope dataset were found. Thus, it was necessary to recalculate slope for the shoreline.

The calculation of the 2010 coastline slope was accomplished through the use of ArcMap 9.3 and Excel. First, a point shapefile representing the 2010 node points moved 20 meters inland was created. The LiDAR elevation values were then extracted at the original node point and at the 20 meter offset. These two shapefiles were then spatially joined to create one dataset with each node representing the original elevation and the elevation 20 meters inland. This table was then output as a CSV file in order to be read in Excel. Within Excel, slope was calculated based on the 20 meter difference and the difference between the two elevation points. This final column of slope was then input in to ArcMap 9.3.

Once the slope of the shoreline was determined the volumetric sediment change was calculated for the year 2010, which proceeded in the following steps in Excel:

1. Calculated the distance to the previous node using X and Y coordinates to determine distance between nodes (**Figure 37**)

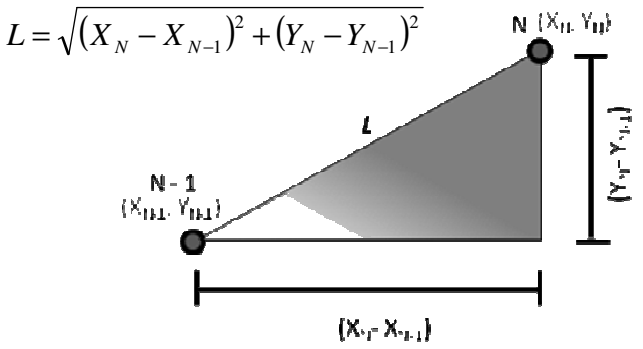

Figure 37: Pythagorean theorem used to calculate distance between nodes

2. Calculated average distance between previous and preceding node to fix errors where gaps occur and to calculate volumetric sediment change (**Figure 38**)

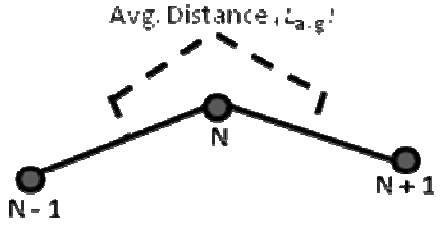

Figure 38: Calculation of average distance between nodes N-1 and N+1

3. Fix average distance at gaps using and if/then statement.

```
If no gap in front
        If no gap behind
                Average distance remains the same
        Else replace with the average distance of N+1
Else if gap behind
        replace with the average distance of N-1
Else
        take average distance of previous node
End
```

4. Calculate volumetric sediment change for types 1 and 0

The volumetric sediment change for each node is thus calculated in m^3/year, with negative and positive change representing areas of accretion and erosion respectively. In order to normalize the values from 0 to 1, the absolute value of the most negative change was added to each value. Then, each value was divided by the greatest value of change.

The next step in determining the MR of the study area was to spatially join the Q_n values supplied by Davies (2011) to the node shapefile of the VSC. Then, each value was normalized by the division of each by the largest Q_n value. The sum of the normalized values of VSC and Qn ranged from a value of 0.055192 to 1.897997.

To rank the vulnerability of the coast in terms of MR, two assumptions were made in terms of VSC and Q_n. The first was that a negative VSC value representing accretion would represent an area of higher morphological resiliency, and thus a lower vulnerability. Similar is assumed for the net potential sediment transport rate: a lower transport rate would assume sediment not being transported away from the node, thus a higher morphological resiliency and low vulnerability, as seen in **Figure 39.** The values of VSC and Q_n were each normalized by dividing each by the greatest value; however, as a portion of the VSC values are negative, the absolute value of the minimum number is added to each number. The normalized values of VSC and Q_n are then added together to calculate the morphological resiliency at each node point, and then ranked for vulnerability on a scale of 1 (lowest vulnerability) to 5 (highest vulnerability) (**Table 5**) using Jenks natural breaks (**Figure 40**).

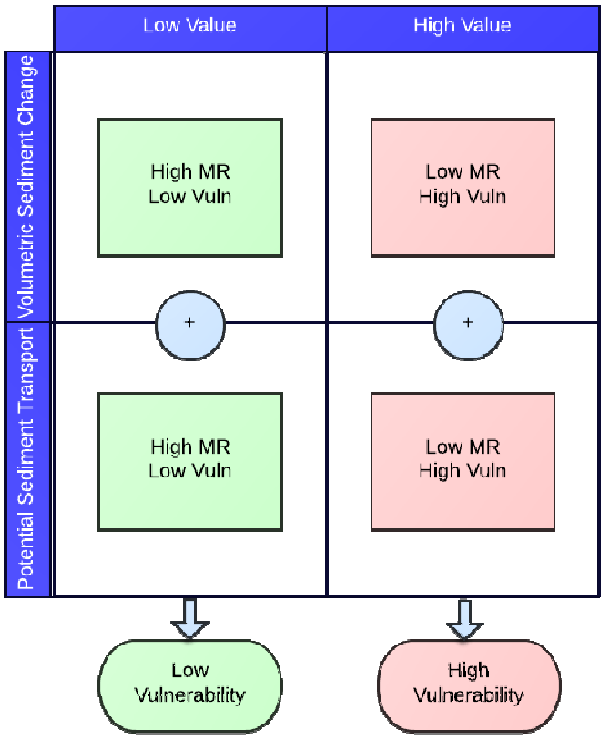

Figure 39: Quantification of vulnerability of the coast in terms of Morphological Resiliency

Years 2050 & 2100

Morphological resiliency of each shoreline segment was assumed to remain the same through the three time steps; although the location of the shoreline may change through time, the geomorphological classification would remain the same, and thus so would the longshore sediment transport rates and annual volumetric sediment change. The VSC and Q_n were spatially joined to the 2050 and 2100 shorelines based on closeness and the vulnerability was ranked using Jenks natural breaks.

Table 5: Vulnerability ranking for morphological resiliency, year 2010

MR Value	Vulnerability Ranking
0.06 - 0.29	1
0.29 - 0.49	2
0.49 - 0.71	3
0.716 - 1.00	4
1.00 - 1.90	5

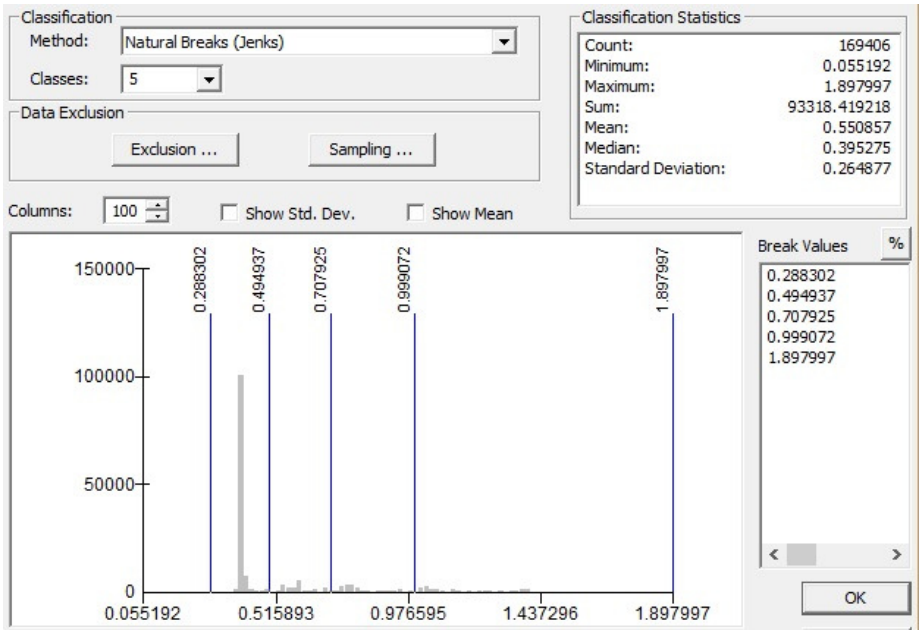

Figure 40: Division of normalized 2010 MR values based on natural breaks (Jenks)

4.3.3. Permanent and Episodic Flood Risk

Year 2010

The vulnerability of the study area to permanent and episodic flood risk (permaent relative sea-level rise and episodic storm surge, respectively) was evaluated based on local sea-level rise estimates and the relative increase of storm surge return period heights. In order to determine the vulnerability of the 2010 coastline to storm surge flooding, LiDAR elevation points were extracted to the 2010 coastal nodes shapefile. The vulnerability of each node was determined

using the Richards & Daigle (2011) storm surge 50-year and 100-year return period values for the year 2010 for Rustico. Because the Richards and Daigle (2011) values were in chart datum, 0.52 meters were subtracted from the extreme total sea level values to convert to CGVD28. **Table 6** displays the level 2000 extreme total sea level in meters chart datum for the CHS representative site of Rustico for four return period years. The residual column lists the annual storm surge height calculated from estimated sea-level rise and crustal subsidence; the Level 2000 column sums the higher high water low tide with this calculated value.

Table 6: Extreme sea level values for Rustico year 2010, developed from Richards and Daigle (2011)

Return Period	Residual	Level 2000 (CD)	Level 2000 (CGVD28)
10-Year	1.07 ± 0.10	2.30 ± 0.10	1.78 ± 0.10
25-Year	1.22 ± 0.10	2.45 ± 0.10	1.93 ± 0.10
50-Year	1.33 ± 0.10	2.56 ± 0.10	2.04 ± 0.10
100-Year	1.45 ± 0.10	2.68 ± 0.10	2.16 ± 0.10

Vulnerability ranking calculation assumed that the highest vulnerability of 5 would be associated with elevations that are susceptible to more frequent flooding (10 year return period), that a moderate vulnerability (rankings of 4, 3, and 2) would be associated with elevations which experience flooding between 25 and 100 year return periods, and elevations greater than the 100 year flooding return period were of least vulnerability (ranking of 1) as seen in **Table 7**. This vulnerability was added to a field in the node shapefile. The tool "Point to Raster" in ArcMap was then used for a cell size of 20 meters to create a raster of the 2010 vulnerability to storm surge flooding.

Table 7: Flooding vulnerability of year 2010; elevation relative to CGVD28

LiDAR Elevation	Vulnerability Ranking
<1.78 m	5
1.781 - 1.93 m	4
1.931 - 2.04 m	3
2.041 - 2.16 m	2
>2.161 m	1

Years 2050 & 2100

Vulnerability of the 2050 and 2100 North Shore coastlines to flooding was calculated similarly to the methods used to calculate the 2010 flooding vulnerability. LiDAR elevations were extracted at the points of the 2050 and 2100 coastal nodes. These elevations were then divided in to five criteria groups to represent those most vulnerable to flooding (5) to least vulnerable (1), with the 2050 divisions shown in **Table 8** and the 2100 in **Table 9**. These divisions were based on the work of Richards and Daigle (2011) for years 2050 (**Table 10**) and 2100 (**Table 11**), respectively. Year 2055 return periods were used for 2050 as they were the predicted values nearest the time step.

Table 8: Flooding vulnerability of year 2050; elevation relative to CGVD28

LiDAR Elevation	*Vulnerability Ranking*
<2.22 m	5
2.221 - 2.37 m	4
2.371 - 2.48 m	3
2.481 - 2.6 m	2
>2.61 m	1

Table 9: Year 2100 flooding vulnerability; elevation relative to CGVD28

LiDAR Elevation	*Vulnerability Ranking*
<2.86 m	5
2.861 - 3.01 m	4
3.011 - 3.12 m	3
3.121 - 3.24 m	2
>3.241 m	1

Table 10: Extreme sea level values for Rustico year 2055, developed from Richards and Daigle (2011)

2055 Extreme Total Sea Level (meters) - Rustico (North Shore)		
Return Period	**Level 2055 (CD)**	**Level 2055 (CGVD28)**
10-Year	2.74 ± 0.25	2.22 ± 0.25
25-Year	2.89 ± 0.25	2.37 ± 0.25
50-Year	3.00 ± 0.25	2.48 ± 0.25
100-Year	3.12 ± 0.25	2.61 ± 0.25

Table 11: Year 2100 Extreme total sea level return periods for the North Shore (Richards & Daigle, 2011)

2100 Extreme Total Sea Level (meters) - Rustico (North Shore)		
Return Period	**Level 2100 (CD)**	**Level 2100 (CGVD28)**
10-Year	3.38 ± 0.58	2.86 ± 0.58
25-Year	3.53±0.58	3.01 ± 0.58
50-Year	3.64 ± 0.58	3.12 ± 0.58
100-Year	3.76 ± 0.58	3.24 ± 0.58

4.3.4. Vulnerability Rasters

Three rasters depicting the physical coastal vulnerability for the years 2010, 2050, and 2100 were created from the input vulnerability criteria- exposure condition, morphological resiliency, and flooding vulnerability. Each of these three rasters for each time step were added together through the use of the Raster Calculator. The resulting raster values ranged from a possible sum of one to 15, and these values were divided in to five vulnerability rankings using Jenks natural breaks, with 1 representing the lowest vulnerability and 5 the highest. Each of the three timestep rasters represent the physical coastal vulnerability of the North Shore coast relative to each year.

5. Results

5.1. Introduction

This chapter outlines and describes the results of the physical coastal vulnerability assessments (CVA) of the North Shore for the years 2010, 2050, and 2100. The three criteria are used to quantify vulnerability, exposure condition, morphological resiliency, and flood risk. The criteria are compared for each time step. Finally, the resultant CVA rasters are described and compared.

5.2. Exposure Condition

The exposure condition is the potential of the coastal system to experience a climate change induced hazard. This thesis utilized WEMo in the Representative Wave Energy (RWE) mode to quantify the exposure condition in RWE values of J/m, calculated through the use of linear wave theory to determine wave energy and wave height, known as wind-wave exposure. The RWE vulnerability of each coastline was quantified using Jenks natural breaks.

5.2.1. 2010

The greatest vulnerability the North Shore identified by the Relative Wave Exposure (RWE) in 2010 occurred exclusively along coastline exposed to the Gulf of St. Lawrence, as seen in **Figure 41**. These locations included a small portion of Hog Island, Lower Darnley, Cavendish, Brackley Beach, Stanhope Beach, Dalvay Beach, and Point Deroche. The bays and estuaries of the study area received lower RWE values and thus had the lowest vulnerability ranking of 1. The frequency of each vulnerability ranking within the 2010 RWE vulnerability raster is depicted in **Table 12**.

The WEMo RWE outputs values ranged from 0.01 J/m to 69226 J/m, with a mean of 2226.48 J/m. The greatest RWE value was experienced along the Cavendish coast. The standard deviation of the values is 7307.011 J/m. These values are summarized in **Table 13**.

Figure 41: 2010 North Shore RWE vulnerability ranking

Table 12: Occurrence frequency of vulnerability rankings in 2010 RWE raster

2010 RWE Vulnerability Raster			
Rank	Vulnerability	Frequency	Percent Frequency
1	Low	16727	90.20%
2		562	3.03%
3	Moderate	737	3.97%
4		363	1.96%
5	High	155	0.84%

Table 13: Descriptive statistics of WEMo 2010 RWE values

	Minimum	**Maximum**	**Mean**	**Standard Deviation**
2010 RWE (J/m)	0.01	69226.28	2226.48	7307.011

5.2.2. 2050

Figure 42: Map of the 2050 North Shore depicting RWE vulnerability ranking, or Exposure Condition

The 2050 North Shore received the highest vulnerability to RWE along the coastline open to the Gulf of St. Lawrence. Moderate vulnerability was also observed along the Cavendish coast and North Rustico, as seen in **Figure 42**. The areas of greatest vulnerability occurred in the same locations as the 2010 RWE vulnerability, although some areas grew from a vulnerability of 4 to 5, the highest ranking of vulnerability. Greatest vulnerability increased from 0.84% of the study area in 2010 to 3.92% of the study area in 2050. **Table 14** lists the occurrence of each vulnerability ranking for the 2050 study area.

The area which received the greatest RWE value was North Rustico at 88,661 J/m. The minimum RWE was 26.83 J/m. The mean of the 2050 RWE values was 4,807.3 J/m with a standard deviation of 12,165 J/m (**Table 15**).

Table 14: Summary of 2050 RWE vulnerability rank occurrence

2050 RWE Vulnerability Raster			
Rank	Vulnerability	Frequency	Percent Frequency
1	Low	14120	83.85%
2		841	4.99%
3	Moderate	509	3.02%
4		710	4.22%
5	High	660	3.92%

Table 15: Descriptive statistics of WEMo 2050 RWE values

	Minimum	Maximum	Mean	Standard Deviation
2050 RWE (J/m)	26.83	88661.17	4807.318	12165.09

5.2.3. 2100

Figure 43: Map of the 2100 North Shore depicting RWE vulnerability ranking, or Exposure Condition

The coastline of the 2100 North Shore experienced an increase in the highest vulnerability rank of 5 from 3.92% in 2050 to 6.99% in 2100 (**Table 16**). The areas which received the greatest RWE values were the open coastlines of Hog Island, Lower Darnley, Seaview, French River,

Cavendish, Brackley Beach, Stanhope Beach, Dalvay Beach, and Point Deroche, as seen in **Figure 43**.

Table 16: Summary of 2100 RWE vulnerability rank occurrence

2100 RWE Vulnerability Raster			
Rank	Vulnerability	Frequency	Percent Frequency
1	Low	7899	52.83%
2		4375	29.26%
3	Moderate	1113	7.44%
4		520	3.48%
5	High	1045	6.99%

The maximum 2100 RWE value of 118,002 J/m was received at Lower Darnley which is exposed to the Gulf of St. Lawrence. The minimum RWE value was 185.59 J/m. The average of the 2100 RWE values was 9,641.4 J/m, an increase of 4834.1 J/m from 2050, with a standard deviation of 18401 J/m (**Table 17**). **Figures 44a, 44b, and 44c** provide a comparison of the RWE vulnerability rank frequency for the years 2010, 2050, and 2100.

Table 17: Descriptive statistics of WEMo 2100 RWE values

	Minimum	**Maximum**	**Mean**	**Standard Deviation**
2100 RWE (J/m)	185.59	118001.5	9641.388	18401.19

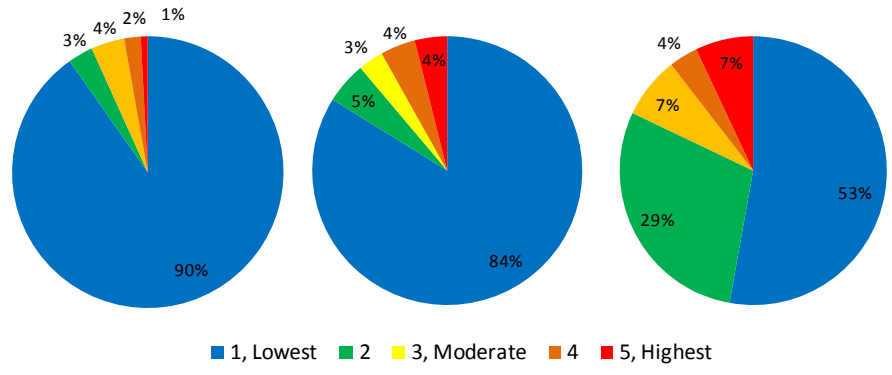

Figure 44: RWE vulnerability rank frequency of (a) 2010 (b) 2050 and (c) 2100

5.3. Morphological Resiliency

Morphological resiliency is defined as the ability of the coastal system to return to a state of equilibrium after a disturbance. This resiliency is a factor of the amount of sediment supply to the coastal system, the morphology of the system, and the duration of time between disturbance events. Morphological resiliency of the area was evaluated through the raster summation of the normalized values of annual volumetric sediment change (VSC) and the longshore sediment transport (Q_n) (**Equation 3**).

5.3.1. 2010

Davies (2011) had calculated the Qn values (m^3/year) for the 2010 study area coastline, and these values were normalized through the division of the largest Qn value. The distribution of the Qn values is shown in **Table 18**. The VSC value calculation method was evaluated based on the geomorphological classification of the shoreline, where cliffs and bluffs were assumed to have a rectangular shape and dunes, wetlands, slopes, and flats were assumed to have a triangular shape (**Section 4.2.2**). The calculated 2010 VSC values (m^3/year) ranged from negative and positive change representing areas of accretion and erosion respectively. In order to normalize the values from 0 to 1, the absolute value of the most negative change was added to each value. Then, each value was divided by the greatest value of change. The resultant VSC values are shown in **Table 19**. The normalized Q_n and VSC values were calculated as a raster and were summed within Raster Calculator to produce the overall morphological resiliency of each cell, which was then divided in to vulnerability rankings from 1 (lowest) to 5 (highest) based on Jenks natural breaks.

The North Shore 2010 coastline experienced the highest vulnerability due to a low morphological resiliency at Lower Malpeque, Lower Darnley, Seaview, French River, Cavendish, North Rustico, Rustico, Rusticoville, Brackley Beach, Covehead Bay and Point Deroche (**Figure 45**). Large portions of the coastlines of Darnley Basin and Covehead Bay had vulnerability rankings of 5. **Table 20** summarizes the frequency of each MR vulnerability ranking for the 2010 coastline.

Table 18: Frequency count of standardized 2010 Qn values

Standardized Qn	Count
0-0.1	113080
0.1-0.2	8580
0.2-0.3	9917
0.3-0.4	11169
0.4-0.5	3881
0.5-0.6	4545
0.6-0.7	8340
0.7-0.8	2853
0.8-0.9	2700
0.9-1	3970
1-1.1	371

Table 19: Frequency count of standardized 2010 VSC values

Standardized VSC	Count
0-0.1	10
0.1-0.2	43
0.2-0.3	98
0.3-0.4	152621
0.4-0.5	15865
0.5-0.6	640
0.6-0.7	100
0.7-0.8	18
0.8-0.9	7
0.9-1	4

Figure 45: Map of the 2010 North Shore depicting Morphological Resiliency vulnerability ranking

Table 20: Summary of 2010 MR rank occurrence

2010 MR Vulnerability Raster			
Rank	Vulnerability	Frequency	Percent Frequency
1	Low	8	0.04%
2		12961	70.18%
3	Moderate	1662	9.00%
4		1965	10.64%
5	High	1872	10.14%

The maximum MR value occurred at French River with a value of 1.8980. The minimum MR value was 0.0552 with a mean of 0.5509. The standard deviation of the MR values was 0.2649 (**Table 21**).

Table 21: Descriptive statistics of 2010 morphological resiliency values

	Minimum	**Maximum**	**Mean**	**Standard Deviation**
2010 MR	0.0552	1.8980	0.5509	0.2649

5.3.2. 2050 & 2100

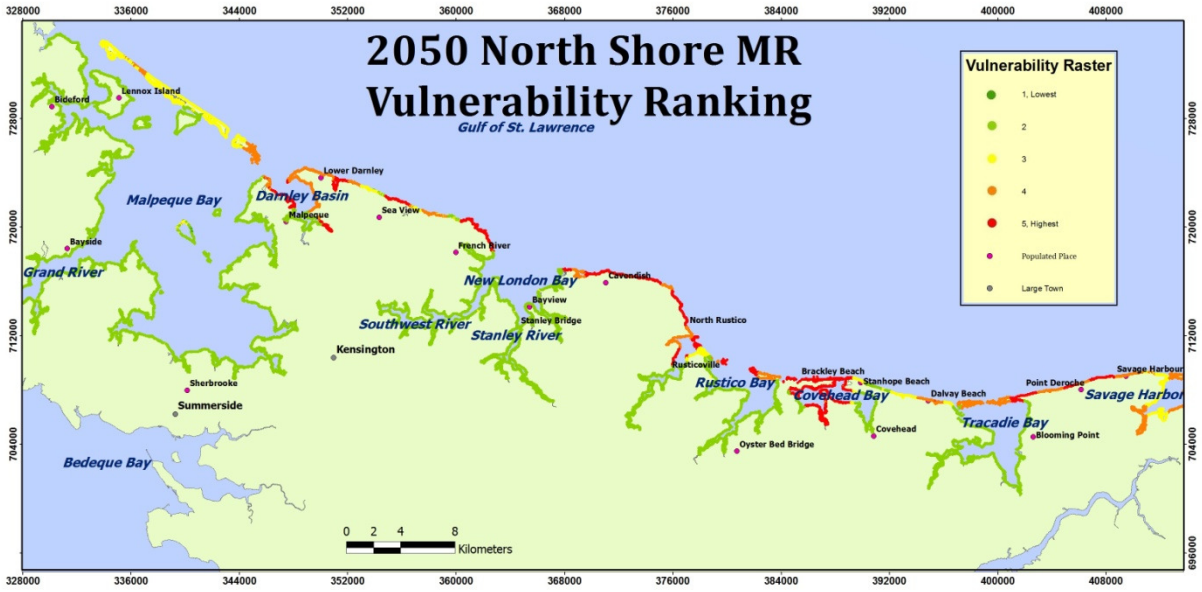

Figure 46: Map of the 2050 North Shore depicting Morphological Resiliency vulnerability ranking

As the morphological resiliency was assumed not to change between time steps, the 2050 and 2100 vulnerability rasters were similar to the 2010 vulnerability rasters; however, due to the shoreline position changing through each time step, the vulnerability ranking frequencies and descriptive statistics of the 2050 and 2100 rasters were different (**Figures 46 and 47**). It was assumed that the shoreline classification of each node remained the same through the shore movement from 2010 to 2050 and 2050 to 2100.

Table 22 illustrates that while the percent frequency of the highest vulnerability ranking of 5 decreased in frequency from 2050 to 2100 (9.09% to 8.88 %, respectively), this is due to the decrease of shoreline nodes through the timestep (16,540 to 14,952 nodes). **Figures 48a, 48b, and 48c** depict the MR vulnerability rank frequency for the years 2010, 2050, and 2100.

Figure 47: Map of the 2100 North Shore depicting Morphological Resiliency vulnerability ranking

Table 22: Summary of 2050 and 2100 MR rank occurrences

		2050 MR Vulnerability Raster		2100 MR Vulnerability Raster	
Rank	Vulnerability	Frequency	Percent Frequency	Frequency	Percent Frequency
1	Low	5	0.03%	5	0.03%
2		12100	71.85%	10788	72.15%
3	Moderate	1371	8.14%	1339	8.96%
4		1833	10.88%	1492	9.98%
5	High	1531	9.09%	1328	8.88%

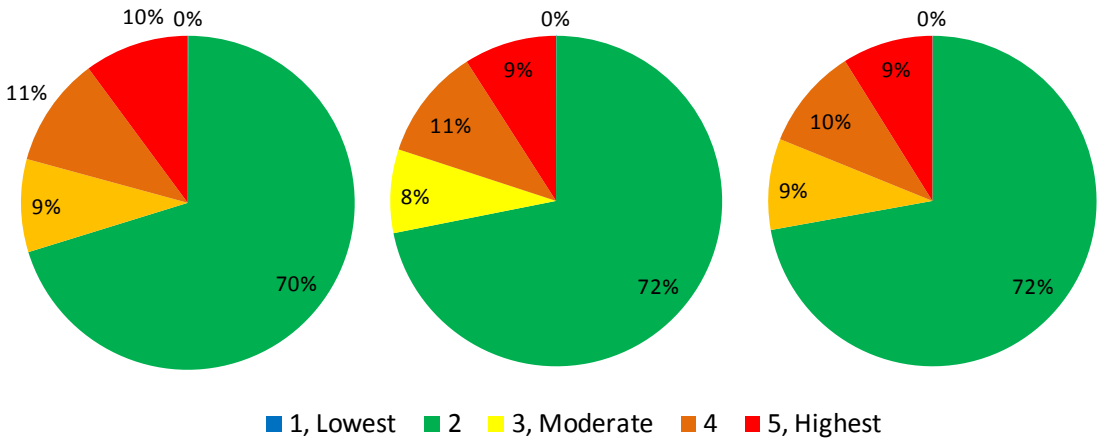

Figure 48: MR vulnerability rank frequency of (a) 2010 (b) 2050 and (c) 2100

5.4. Permanent and Episodic Flood Risk

Permanent and episodic flood risk was quantified through the evaluation of permanent climate change induced sea-level rise and episodic storm surge inundation based on coastal elevation. Through the 2010, 2050, and 2100 timesteps, relative sea-levels were estimated to increase, and a larger area of land received increased storm surge return periods and heights. Vulnerability ranking calculation assumed that the highest vulnerability of 5 would be associated with elevations that are susceptible to more frequent flooding (10 year return period), that a moderate vulnerability (rankings of 4, 3, and 2) would be associated with elevations which experience flooding between 25 and 100 year return periods, and elevations greater than the 100 year flooding return period were of least vulnerability (ranking of 1). The total area of the North Shore which would experience the five flood return periods increased through each timestep due to relative sea-level rise; thus, the vulnerability of the study area to permanent and episodic storm surge increases through time.

5.4.1. 2010

Figure 49: Map of the 2010 North Shore depicting vulnerability ranking to permanent and episodic flood risk

The North Shore coastline experienced the highest vulnerability to flooding largely along bays and estuaries in the year 2010 (**Figure 49**). The largest proportion of high vulnerability areas include the shorelines of Malpeque Bay, Southwest River, Rustico Bay, Covehead Bay, and Tracadie Bay. The frequency of occurrence of each vulnerability ranking for flooding in the year 2010 is summarized in **Table 23**.

The lowest elevation of the study area, and thus the highest vulnerability to flooding, was 0.07 meters at the coastline of an estuary of Malpeque Bay near the town of Bideford. The maximum elevation of 33.06 meters, found along the Gulf of St. Lawrence coast near Park Corner. The mean elevation of the study area was 3.66 meters with a standard deviation of the values of 3.48 meters (**Table 24**). Values are relative to CGVD28.

Table 23: Occurrence frequency of 2010 flood vulnerability rankings

		2010 Flood Vulnerability Raster	
Rank	Vulnerability	Frequency	Percent Frequency
1	Low	11171	60.32%
2		460	2.48%
3	Moderate	425	2.29%
4		658	3.55%
5	High	5806	31.35%

Table 24: Descriptive statistics of 2010 elevation values in meters, relative to CGVD28

	Minimum	Maximum	Mean	Standard Deviation
2010 Elevation (m)	0.07	33.060001	3.663101	3.4802384

5.4.2. 2050

Figure 50: Map of the 2050 North Shore depicting vulnerability ranking to permanent and episodic flood risk

The greatest vulnerability to permanent and episodic flooding grew in frequency from 31.55% in 2010 to 39.89% in 2050, as seen in **Table 25**. Areas experiencing the greatest vulnerability include Malpeque Bay, Rustico Bay, Covehead Bay, and Tracadie Bay seen in the 2010 flood vulnerability, but also Darnley Basin, French River, and Savage Harbor (**Figure 50**).

The minimum elevation of the 2050 coastline was 0.17 meters at Covehead Bay and the maximum was 33.06 meters. The mean of the elevation values was 3.91 meters with a standard deviation of 3.58 meters (**Table 26**). Values are relative to CGVD28.

Table 25: Occurrence frequency of 2050 flood vulnerability rankings

	2050 Flood Vulnerability Raster		
Rank	Vulnerability	Frequency	Percent Frequency
1	Low	8971	53.27%
2		287	1.70%
3	Moderate	351	2.08%
4		514	3.05%
5	High	6717	39.89%

Table 26: Descriptive statistics of 2050 elevation values in meters, relative to CGVD28

	Minimum	Maximum	Mean	Standard Deviation
2050 Elevation (m)	0.17	33.06	3.910115	3.575274

5.4.3. 2100

The areas of greatest vulnerability to permanent and episodic flooding of the 2100 coastline were the same as those of the 2050 coast, as seen in **Figure 51**, however, the frequency of the highest rank grew from 39.89% in 2050 to 46.82% in 2100. **Table 27** summarizes the frequency of occurrence of each rank of vulnerability to flooding of the 2100 coast.

Figure 51: Map of the 2100 North Shore depicting vulnerability ranking to permanent and episodic flood risk

Table 27: Summary of 2100 flood risk vulnerability rank occurrence

2100 Flood Vulnerability Raster			
Rank	Vulnerability	Frequency	Percent Frequency
1	Low	7092	47.43%
2		227	1.52%
3	Moderate	257	1.72%
4		375	2.51%
5	High	7001	46.82%

The minimum elevation of the 2100 North Shore coast, and thus the location of greatest vulnerability, occurred at Covehead Bay with a value of 0.17 meters. The maximum elevation was 33.06 meters. The mean elevation of the 2100 coast was 4.08 meters with a standard deviation of 3.63 meters. Values are relative to CGVD28. **Table 28** outlines the descriptive statistics of the 2100 coast elevation values. **Figures 52a, 52b, and 52c** provide a comparison of the flood risk vulnerability rank frequency for the years 2010, 2050, and 2100.

Table 28: Descriptive statistics of 2100 elevation values, relative to CGVD28

	Minimum	Maximum	Mean	Standard Deviation
2100 Elevation (m)	0.17	33.06	4.081888	3.628866

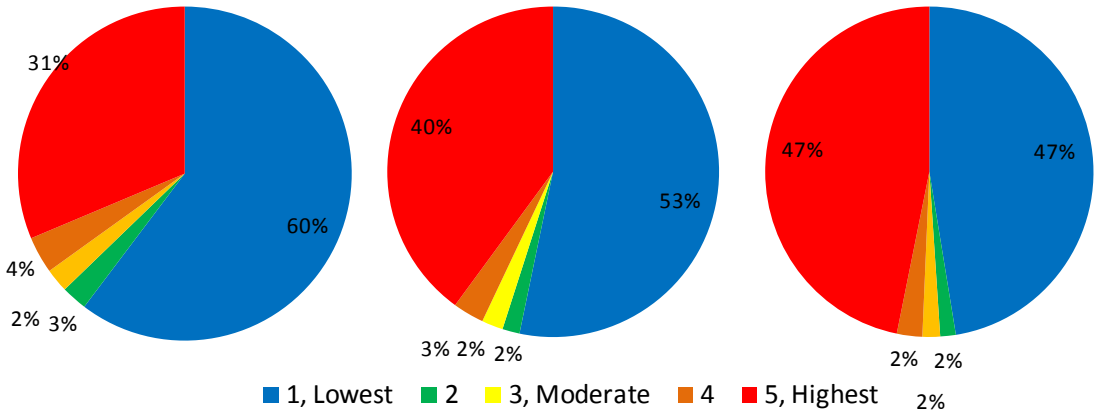

Figure 52: Flood risk vulnerability rank frequency of (a) 2010 (b) 2050 and (c) 2100

5.5. Relative Physical Coastal Vulnerability Raster

The node shapefiles representing each of the ranked three criteria (exposure condition, morphological resiliency, permanent and episodic flood risk) were converted in to rasters. These three rasters were summed together for each timestep to produce the relative physical coastal vulnerability of the 2010, 2050, and 2100 North Shore coastlines.

5.5.1. 2010

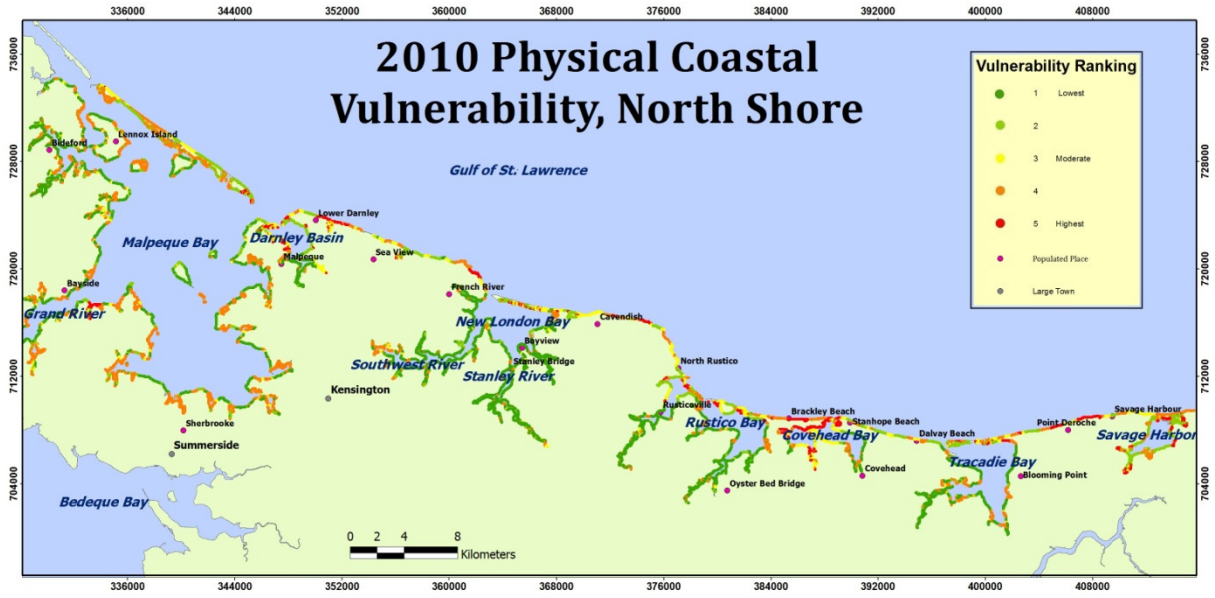

Figure 53: Map of the physical coastal vulnerability of the 2010 North Shore

The quantification of relative physical coastal vulnerability was achieved through the summation of the exposure condition, morphological resiliency, and flood risk rasters for each of the years 2010, 2050, and 2100. The total physical vulnerability raster values for the year 2010 ranged from 3 to 13. These values were divided based on Jenks Natural Breaks into vulnerability ranks from 1 (lowest vulnerability) to 5 (highest vulnerability). The physical coastal vulnerability of the 2010 coastline experienced the greatest vulnerability (rank of 5) of 5.78% of the coastline, a rank of 4 for 31.97% of the coastline, and a moderate rank of 3 for 9.74% of the coast (**Table 29**). The areas of greatest vulnerability included the coasts of Covehead Bay and Savage Harbor, as well as the coastlines of the towns of Lower Darnley, French River, Cavendish, North Rustico, Brackley Beach, and Point Deroche. The coastline of Malpeque Bay experienced a majority vulnerability ranking of 4 (**Figure 53**).

Table 29: Summary of 2010 physical coastal vulnerability of the North Shore

2010 Physical Coastal Vulnerability Raster					
Vulnerability	**Rank Percent Frequency**	**Estimated Shoreline Length (km)**	**Raster Value**	**Frequency**	**Percent Frequency**
1, Lowest	38.22%	348.55	3	7	0.04%
			4	6708	38.18%
2	14.29%	134.32	5	1070	6.09%
			6	1440	8.20%
3	9.74%	90.87	7	1711	9.74%
4	31.97%	313.56	8	4730	26.92%
			9	887	5.05%
5, Highest	5.78%	55.49	10	572	3.26%
			11	422	2.40%
			12	13	0.07%
			13	9	0.05%

5.5.2. 2050

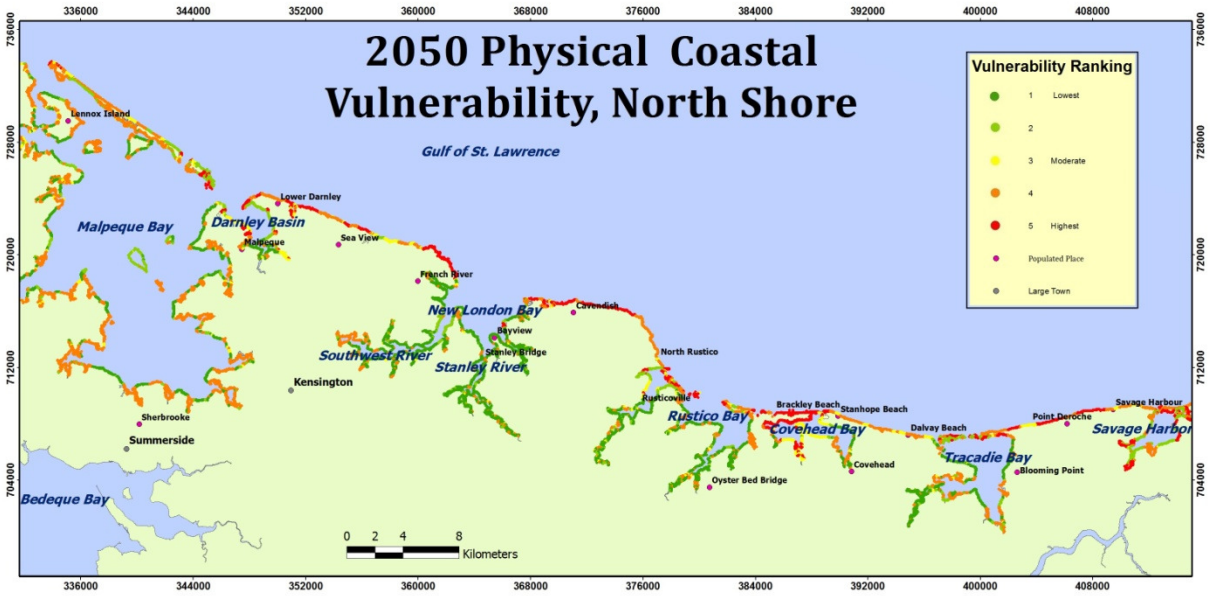

Figure 54: Map of the physical coastal vulnerability of the 2050 North Shore

The 2050 coastal physical vulnerability raster values ranged from 4 to 14. The raster values were divided into vulnerability ranks from 1 (lowest vulnerability) to 5 (highest vulnerability) based on the 2010 divisions. The areas of highest vulnerability included the coastlines of the towns of Lower Darnley, French River, Cavendish, Rustico, Brackley Beach, and Point Deroche. The coasts of Covehead Bay and Savage Harbor also experienced the greatest vulnerability ranking of 5 (**Figure 54**). Furthermore, areas receiving a ranking of 4, great vulnerability, include the coast of Malpeque Bay, as well as Hog Island, Seaview, Southwest River, North Rustico, and Lennox Island. The percentage frequency of the highest vulnerability ranking of 5 grew from 5.78% in 2010 to 9.47% in 2050, and the percent frequency of the lowest vulnerability ranking of 1 decreased from 38.22% in 2010 to 32.38% in 2050 (**Table 30**).

Table 30: Summary of 2050 physical coastal vulnerability of the North Shore

2050 Physical Coastal Vulnerability Raster					
Vulnerability	**Rank Percent Frequency**	**Estimated Shoreline Length (km)**	**Raster Value**	**Frequency**	**Percent Frequency**
1, Lowest	32.38%	308.82	4	5453	32.38%
2	10.17%	97.96	5	729	4.33%
			6	984	5.84%
3	6.22%	59.34	7	1047	6.22%
4	41.76%	401.41	8	5838	34.67%
			9	1194	7.09%
5, Highest	9.47%	92.00	10	777	4.61%
			11	762	4.52%
			12	25	0.15%
			13	13	0.08%
			14	18	0.11%

5.5.3. 2100

The 2100 coastal physical vulnerability raster values ranged from 4 to 15 and these values were divided into vulnerability ranks using the same divisions as the 2010 coastal vulnerability raster. The percent frequency of the greatest vulnerability rank of 5 increased from 9.47% in 2050 to

13.28% in 2100, while the percent frequency of the lowest vulnerability rank of 1 decreased from 32.38% in 2050 to 18.00% in 2100 (**Table 31**).

Table 31: Summary of 2100 physical coastal vulnerability of the North Shore

2100 Physical Coastal Vulnerability Raster					
Vulnerability	**Rank Percent Frequency**	**Estimated Shoreline Length (km)**	**Raster Value**	**Frequency**	**Percent Frequency**
1, Lowest	18.00%	139.62	4	2692	18.00%
2	16.50%	126.49	5	1594	10.66%
			6	873	5.84%
3	4.57%	34.76	7	684	4.57%
4	47.64%	357.87	8	4078	27.27%
			9	3045	20.37%
5, Highest	13.28%	99.06	10	884	5.91%
			11	686	4.59%
			12	302	2.02%
			13	86	0.58%
			14	20	0.13%
			15	8	0.05%

The areas which experienced the greatest coastal physical vulnerability included the coasts of Hog Island, Lower Darnley, Seaview, French River, Cavendish, North Rustico, Rustico, Rusticoville, Brackley Beach, Covehead Bay, Dalvay Beach, Point Deroche, and Savage Harbor. Areas which experienced a vulnerability ranking of 4, or high vulnerability, included the coasts of Malpeque Bay, Seaview, Southwest River, North Rustico, Stanhope Beach, Dalvay Beach, Tracadie Bay, and Lennox Island (**Figure 55**). **Figures 56a, 56b, and 56c** depict the frequency of each physical coastal vulnerability rank for the years 2010, 2050, and 2100 respectively.

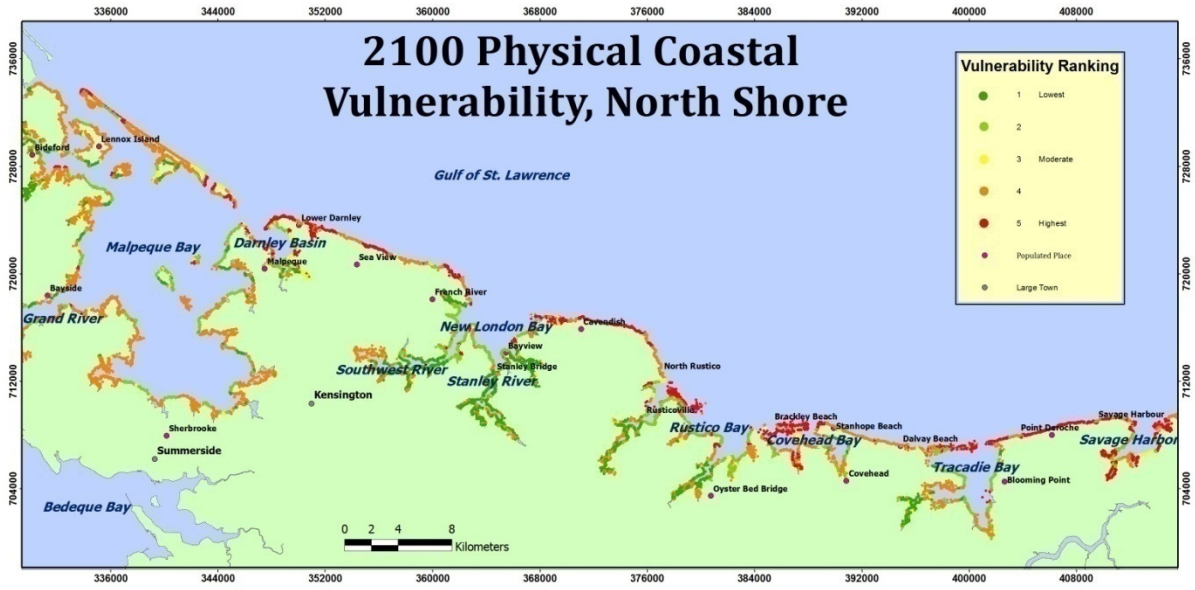

Figure 55: Map of the physical coastal vulnerability of the 2100 North Shore

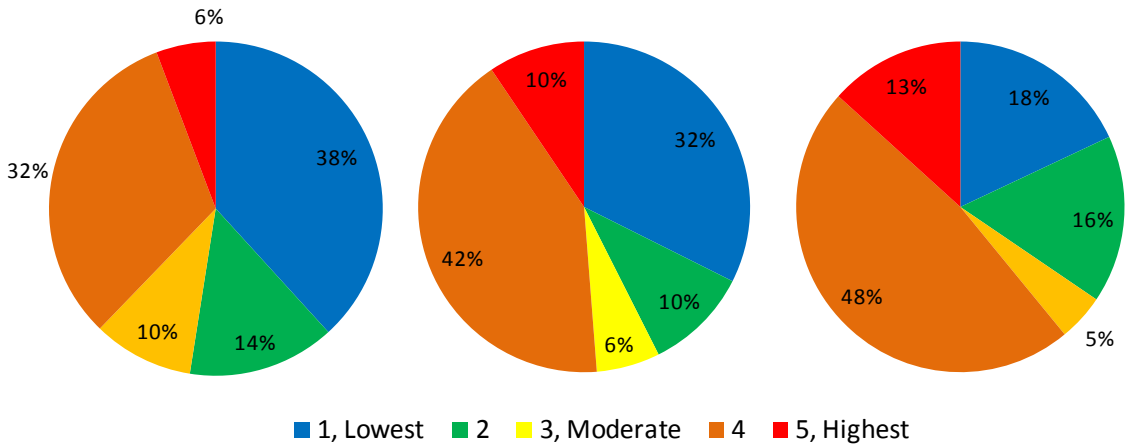

Figure 56: Relative physical coastal vulnerability rank frequency for (a) 2010 (b) 2050 and (c) 2100

5.6. Shoreline Position Change

The North Shore shoreline was assumed to change between each timestep (2010 and 2050, 2050 and 2100) based on annual erosion and accretion rates calculated by Webster (2012) for the year 2010. Each rate, symbolized as a node within ArcMap, was multiplied by the total years which passed through each timestep (40 years between 2010 and 2050, 50 years between 2050

and 2100) in order to quantify the magnitude and direction of coastal change. Areas with anthropogenic hard adaptation measures such as riprap were assumed to remain at the 2010 node locations. The 2100 shoreline estimation included the increase of 2010 coastal change rates by a factor of 1.1, known as the storm enhancement factor (please refer to section 4.2.3). The results of the shoreline movement estimation can be viewed in **Appendix A**.

It was assumed that the shoreline classification of each node remained the same through the shore movement from 2010 to 2050 and 2050 to 2100. Furthermore, truncation of the estimated 2050 and 2100 nodes was undertaken in order to simulate a smooth, continuous shoreline. This process eliminated some barrier islands and spits in both the 2050 and 2100 coasts, where in the real world this sediment would either remain in a new shape or be carried through longshore sediment transport to a new location.

5.7. Chapter Summary

In summation this chapter described the results of the physical Coastal Vulnerability Assessments of the North Shore for the years 2010, 2050, and 2100. The physical CVAs determined that the highest ranking vulnerability of 5 for the physical coastal vulnerability of the North Shore increased from 5.78% in 2010 to 13.28% in 2100, while the lowest rank of 1 decreased from 38.22% in 2010 to 18.00% in 2100 (**Table 32**). **Table 33** depicts the range of vulnerability raster values (3-15) after the summation of the three criteria indicators for each time step. The greatest percent frequency for 2010 was the raster value of 4, and for years 2050 and 2100 it was the raster value of 8.

The areas which will experience the greatest physical vulnerability to climate change in the year 2050 included Lower Darnley, French River, Cavendish, Rustico, Brackley Beach, and Point Deroche as well as the coasts of Covehead Bay and Savage Harbor. In 2100 these areas of highest vulnerability grew to include Hog Island, Lower Darnley, Seaview, North Rustico, Rustico, Rusticoville, and Dalvay Beach. Chapter 6 will continue to analyze and discuss the results of the three timesteps of the physical CVAs as well as discuss the implications these vulnerabilities will have in terms of the fishing and tourism communities.

Table 32: Summary of physical coastal vulnerability rank percent frequency for years 2010, 2050, and 2100

Physical Coastal Vulnerability Rank Percent Frequency				
Rank	Vulnerability	2010	2050	2100
1	Low	38.22%	32.38%	18.00%
2		14.29%	10.17%	16.50%
3	Moderate	9.74%	6.22%	4.57%
4		31.97%	41.76%	47.64%
5	High	5.78%	9.47%	13.28%

Table 33: Raster values of 2010, 2050, and 2100 time steps before division in to ranks

Relative Physical Vulnerability Raster Values			
Raster Value	2010 Percent Frequency	2050 Percent Frequency	2100 Percent Frequency
3	0.0%	0.0%	0.0%
4	38.2%	32.4%	18.0%
5	6.1%	4.3%	10.7%
6	8.2%	5.8%	5.8%
7	9.7%	6.2%	4.6%
8	26.9%	34.7%	27.3%
9	5.0%	7.1%	20.4%
10	3.3%	4.6%	5.9%
11	2.4%	4.5%	4.6%
12	0.1%	0.1%	2.0%
13	0.1%	0.1%	0.6%
14	0.0%	0.1%	0.1%
15	0.0%	0.0%	0.1%

6. Discussion

6.1. Introduction

The fundamental goal of this research was to evaluate the physical coastal vulnerability of the North Shore to climate change for the years 2010, 2050, and 2100 using a Coastal Vulnerability Assessment (CVA). The CVA quantified three criteria indicators ranked from lowest (1) to highest (5) vulnerability:

- Assessed the exposure condition using the Wave Exposure Model and GIS
- Determined morphological resiliency using numerical and GIS modeling
- Used GIS to identify coastal vulnerability to sea-level and storm surge flooding

The approach used to quantify physical coastal vulnerability is similar to assessments conducted in the literature (i.e. Gornitz 1991; Gornitz *et al.,* 1994; Shaw *et al.,* 1998; Thieler & Hammar-Klose, 2000; Pendleton, Thieler, & Jeffress, 2005; and Gaki-Papanastassiou *et al.,* 2010), but is innovative in the quantification of sediment budget and shoreline movement within a GIS. Genz *et al.* (2007) and Dolan, Fenster, & Holme (1991) both summarize the published techniques used to predict shoreline change rates; these methods mainly rely on statistics (i.e. Ordinary Least Squares, Reweighted Least Squares) to predict shoreline movement through time. This work attempts to estimate the movement of the shoreline using geomorphological principals.

The sediment budget of a coastline relates the inputs and outputs of sediment, with a natural balance between sediment supply and removal promoting stable shoreline. However, areas of accretion or erosion occur where this budget is not balanced (ACASA, 2013a). Including a quantification of sediment budget when assessing coastal vulnerability has been noted to be important in the prediction of future vulnerability as the physical change of the coast will alter the relative physical vulnerability of the coastline through each time step. Thus, estimating shoreline movement through time using the estimation of sediment budget provides a more accurate prediction of future coastal vulnerability.

With the physical coastal vulnerability of the North Shore quantified in terms of the three criteria indicators for three time steps (2010, 2050, and 2100), the results are evaluated, assessed, and compared in the following chapter. This assessment was undertaken through the comparison of the coastal risk of permanent relative sea-level rise and episodic storm surge inundation through the three time steps. These findings were then used to determine tourism areas of highest priority for adaptation measures as identified by the highest relative vulnerability ranking of 5.

6.2. Areas of Physical Coastal Vulnerability

This section discusses the relative physical vulnerability of the regions and parks of the North Shore. Full page versions of the maps shown in this section can be seen in **Appendix B**.

6.2.1. Regional Vulnerability

Lennox Island

The region of Lennox Island has historically experienced a high degree of coastal change along the northwest peninsula of the island (R. Angus, personal communication, May 8, 2013), an area of dense wetland and little encroachment of human infrastructure. The vulnerability assessment found that from the years 2010 to 2100, this area received a vulnerability ranking of 4, or high vulnerability through each time step (**Figure 71**). The causeway between the main island and Lennox Island also disappeared between the time step of 2010 and 2050, even though the shoreline movement algorithm explicitly allowed for anthropogenic shorelines to remain unmoved based on annual volumetric sediment change - this is likely due to relative sea-level rise.

The fishing wharf at the southern most section of the island had also experienced a large degree of coastal change, and this vulnerability is depicted through each time step as a vulnerability ranking of 4, or high vulnerability. **Table 34** provides the frequency of each physical coastal vulnerability ranking for Lennox Island. The lowest vulnerability ranking of 1 decreased through each time step from 42.17% in 2010 to 12.50% in 2100. The vulnerability ranking of 2 (low) decreased from 2010 to 2050, and then increased substantially in the 2100 time step. The vulnerability ranking of 3 (moderate) increased from 2010 to 2050, and then decreased in the 2100 time step. A vulnerability ranking of 4, or high vulnerability, increased through each time

step from 46.39% in 2010 to 70.71% in 2100. There were zero instances of the highest vulnerability ranking of 5 along the Lennox Island coast.

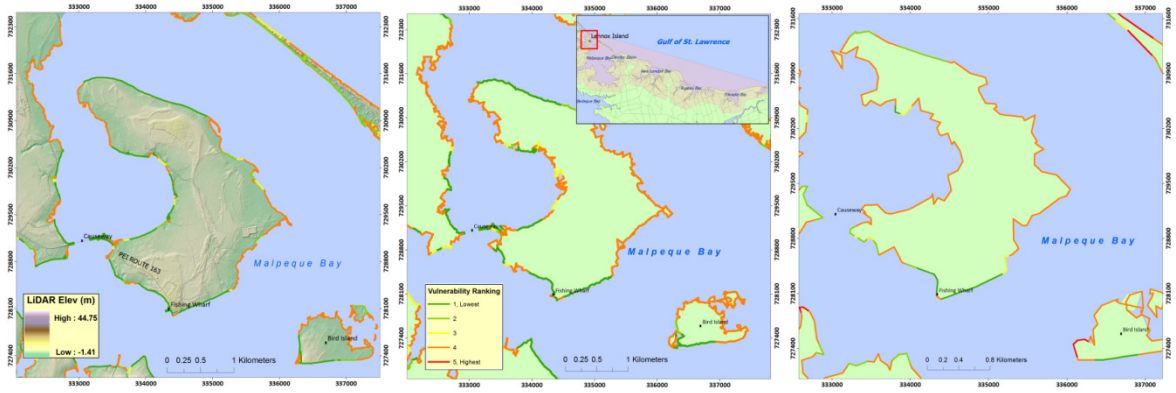

Figure 57: Physical coastal vulnerability of Lennox Island for year (a) 2010 (b) 2050 and (c) 2100

Table 34: Frequency of physical coastal vulnerability ranking for three time steps of Lennox Island

Lennox Island Region Vulnerability Frequency			
Vulnerability	**2010**	**2050**	**2100**
1, Lowest	42.17%	27.13%	12.50%
2, Low	5.72%	3.88%	12.86%
3, Moderate	5.72%	5.94%	3.93%
4, High	46.39%	63.05%	70.71%
5, Highest	0.00%	0.00%	0.00%

Malpeque Bay Region

The barrier islands of Malpeque Bay provide defense against wind and wave energy from the Gulf of St Lawrence which can potentially cause high amounts of coastal change along the coasts of the region. These islands are very dynamic and move on an annual basis due to this input energy as well as longshore sediment transport (Davidson-Arnott, R. 2010). Unfortunately, the highly dynamic nature of barrier islands limited the ability of this research to predict their transgression through time, as the procedure to do so was beyond the scope of the project. The coastline of highest vulnerability (ranking 5) south of the town of Bayside in the year 2010 quickly recedes in time compared to other locations in the region (**Figure 72)**.

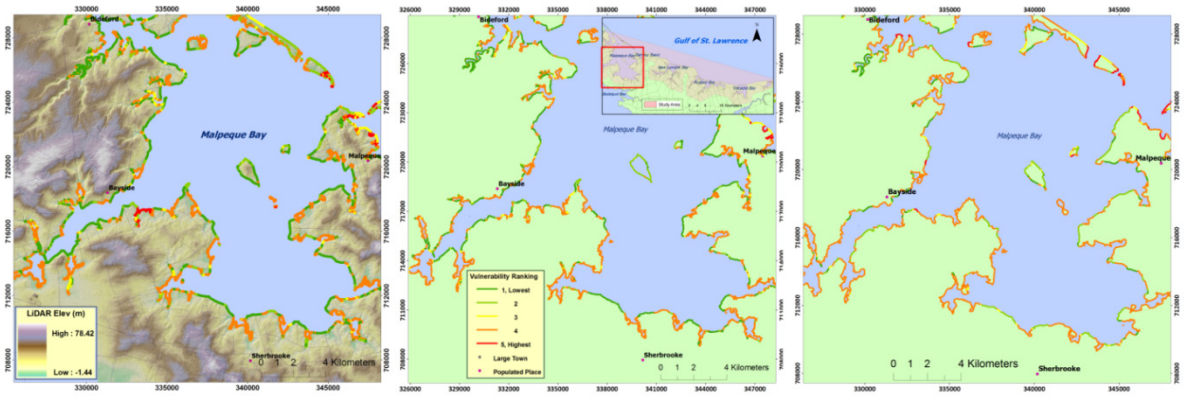

Figure 58: Physical coastal vulnerability of the region of Malpeque Bay for the years (a) 2010 (b) 2050 and (c) 2100

The frequency of the physical coastal vulnerability rankings are summarized in **Table 35**; these statistics included the coastlines of Malpeque Bay to the town of Seaview as well as the barrier islands which protect the bay. The lowest and moderate vulnerability rankings (1 and 3, respectively) decreased through the years 2010 to 2100. A vulnerability ranking of 2 decreased from 2010 to 2050, and then increased in 2100. The vulnerability rankings of 4 and 5 (high and highest) increased through the time steps, from 43.87% to 64.03% and 3.37% to 6.48% respectively. The coast of Malpeque Bay was noted by Dr. Adam Fenech and Randy Angus as a region of high vulnerability, and this coincides with the coastal vulnerability found in this study (A. Fenech, personal communication, May 9, 2013; R. Angus, personal communication, May 7, 2013).

Table 35: Frequency of physical coastal vulnerability ranking for three time steps of Malpeque Bay Region

Malpeque Bay Region Vulnerability Frequency			
Vulnerability	**2010**	**2050**	**2100**
1, Lowest	31.57%	24.10%	10.79%
2, Low	13.41%	9.60%	13.35%
3, Moderate	7.78%	5.61%	5.36%
4, High	43.87%	56.78%	64.03%
5, Highest	3.37%	3.92%	6.48%

New London Bay Region

The region of New London Bay saw an increase in the highest vulnerability ranking of 5 from 1.29% in 2010 to 6.80% in 2100, as well as an increase in the ranking of 4 (high vulnerability) from 14.43% in 2010 to 27.11% in 2100 (**Table 36**). Rankings of 1 and 3 (lowest and moderate) decreased from 2010 to 2100. A ranking of 2 (low vulnerability) decreased from 2010 to 2050, and then increased substantially in the year 2100. The New London Bay region was estimated to encompass the area between the town of Seaview and the beginning of the Cavendish portion of the PEI National Park.

Table 36: Frequency of physical coastal vulnerability ranking for three time steps of New London Bay Region

New London Bay Region Vulnerability Frequency			
Vulnerability	**2010**	**2050**	**2100**
1, Lowest	69.72%	62.79%	42.49%
2, Low	9.52%	8.08%	21.32%
3, Moderate	5.05%	3.68%	2.28%
4, High	14.43%	19.58%	27.11%
5, Highest	1.29%	5.87%	6.80%

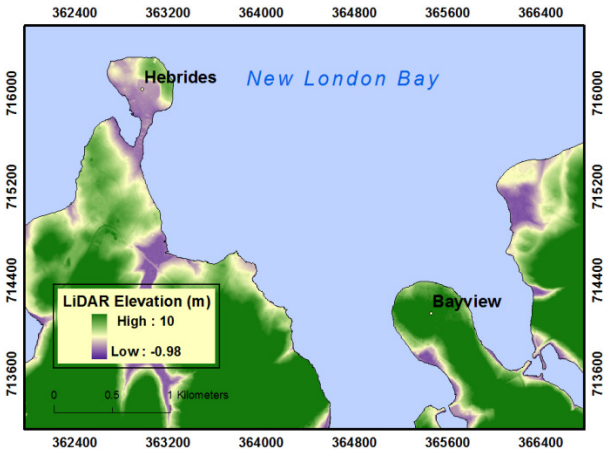

Figure 59: Elevation relative to CGVD28 of Bayview and Hebrides peninsulas, New London Bay region

The physical coastal vulnerability of the New London Bay region from years 2010, 2050, and 2100 is depicted in **Figure 73**. The area contains to two low-lying peninsulas characterized by a substantial amount of tourism and residential infrastructure - Hebrides and Bayview. These locations are potentially areas of vulnerability to permanent relative sea-level rise as well as episodic storm surge. Along the Hebrides coast, the length of coastline of vulnerability ranking 4 (high vulnerability) increases from 2010 to 2050, and then from 2050 to 2100 a significant length of the coastline is ranked a vulnerability of 5, or highest vulnerability. The Bayview coast however does not

receive the same high degree of relative physical coastal vulnerability, and only increases from the lowest vulnerability of 1 to a vulnerability of 2 in 2100. This is potentially due to the peninsula of Bayview having a higher elevation as well as a decrease in wind-wave exposure due to the peninsulas location within New London Bay relative to Hebrides. The elevation of these two peninsulas can be seen in **Figure 74.**

Figure 60: Physical coastal vulnerability of the region of New London Bay for the years (a) 2010 (b) 2050 and (c) 2100

Cavendish Region

The region of Cavendish received a substantially higher percentage of the highest vulnerability ranking of 5 in comparison to every other region of the study area. This is consistent with the assertions of local stakeholders, as a large portion of the Cavendish campsite has been eroded (A. Fenech, personal communication, May 9, 2013; P. Giroux, personal communication, May 10, 2013). The region contains the area of the Cavendish portion of the PEI National Park to North Rustico. The highest vulnerability ranking of 5 increased from 10.86% in 2010 to 56.25% in 2100; the region with the second largest percentage of a vulnerability ranking of 5 for 2100 was the Brackley-Dalvay region at 22.15% (**Table 37**). The vulnerability ranking of 4 (high vulnerability) increased from 25.14% in 2010 to 36.00% in 2100. The lowest vulnerability ranking of 1 decreased from 2010 to 2100, and rankings 2 and 3 (low and moderate, respectively) decreased from 2010 to 2050, and then increased in 2100.

Table 37: Frequency of physical coastal vulnerability ranking for three time steps of Cavendish Region

Cavendish Region Vulnerability Frequency			
Vulnerability	**2010**	**2050**	**2100**
1, Lowest	5.86%	1.94%	0.25%
2, Low	22.00%	2.18%	2.25%
3, Moderate	36.14%	2.91%	5.25%
4, High	25.14%	45.87%	36.00%
5, Highest	10.86%	47.09%	56.25%

Figure 75 depicts the physical coastal vulnerability of the region of Cavendish from years 2010, 2050, and 2100. Between the years 2010 and 2050 it can be seen that a substantial length of the coastline increases in vulnerability to the highest ranking of 5. Furthermore, the Cavendish barrier island system protecting New London Bay also disappears. This is potentially due to the truncation of node loops during the prediction of shoreline movement from years 2010 and 2050; However, the physical basis of the elimination of these features can potentially be due to permanent sea-level rise inundation, severe erosion, and the decrease of coastal sea ice during winter months. Stutz and Pilkey (2011) predict that barrier island systems in the higher latitudes of the Northern Hemisphere will begin to disappear over the next century. The increase of temperatures during the winter months will limit the ability of sea ice to form on barrier islands (Stutz & Pilkey 2011). Winter sea ice buildup limits the erosion of the barrier island through the formation of a solid ice barrier which armors the island from wind and wave energy (Forbes *et al.,* 2004). Prince Edward Island receives the highest energy storms during winter months (ACASA, 2012). Thus, the reduction of sea ice coverage during winter months could eliminate the barrier islands of the North Shore, similar to what is predicted to occur along the US New England coast (Hapke *et al.,* 2011).

The elimination of the barrier island system between the time step of 2010 to 2050 results in an increased vulnerability of the inland coast of New London Bay due to an increase of fetch length and thus wind-wave energy entering the bay. When each new shoreline was estimated for the years 2050 and 2100, the bathymetric DEM of the coast was recreated based on this new position. The change in energy is captured with the recalculation of RWE for the 2050 and 2100

time steps and results in an increase in the vulnerability of the coast due to the change in wind-wave exposure condition.

Figure 61: Physical coastal vulnerability of the region of Cavendish Region for the years (a) 2010 (b) 2050 and (c) 2100

Rustico Region

The region of Rustico is defined as the area extending from the beginning of the town of North Rustico to the beginning of the Brackley-Dalvay portion of the PEI National Park. The region is potentially vulnerable to the impacts of climate change induced permanent sea-level rise and episodic storm surge due to a high density of fishing piers and residential and tourism infrastructure along a low-lying coast. The relative physical coastal vulnerability of the area for years 2010, 2050, and 2100 is shown in **Figure 76**; these maps show that from the years 2010 to 2050, the tributaries of Rustico Bay remain at a low to lowest vulnerability, while the coasts exposed to the Gulf of St. Lawrence, especially the coast of North Rustico, increases from a large amount of rankings of 2 and 3, to rankings of 4 and 5. This continues in to the 2100 time step, where the open coastlines increase in vulnerability to a higher amount of vulnerability rankings of 5. Over the entire region, vulnerability rankings of 4 and 5 (high and highest vulnerability) increased from 2010 to 2100 (**Table 38**). The vulnerability ranking of 4 increased from 18.66% in 2010 to 34.12% 2100, and the vulnerability ranking of 5 increased from 2.07% in 2010 to 9.21% in 2100. The lowest and low vulnerability rankings of 1 and 2 decreased from 2010 to 2100, and the moderate vulnerability ranking of 3 increased from 2010 to 2050 and decreased from 2050 to 2100. The area around Oyster Bed Bridge, a bridge that has historically seen severe damage after storm events (A. Fenech, personal communication, May 9, 2013),

increases in the length of coastline experiencing a vulnerability ranking of 4 or high vulnerability.

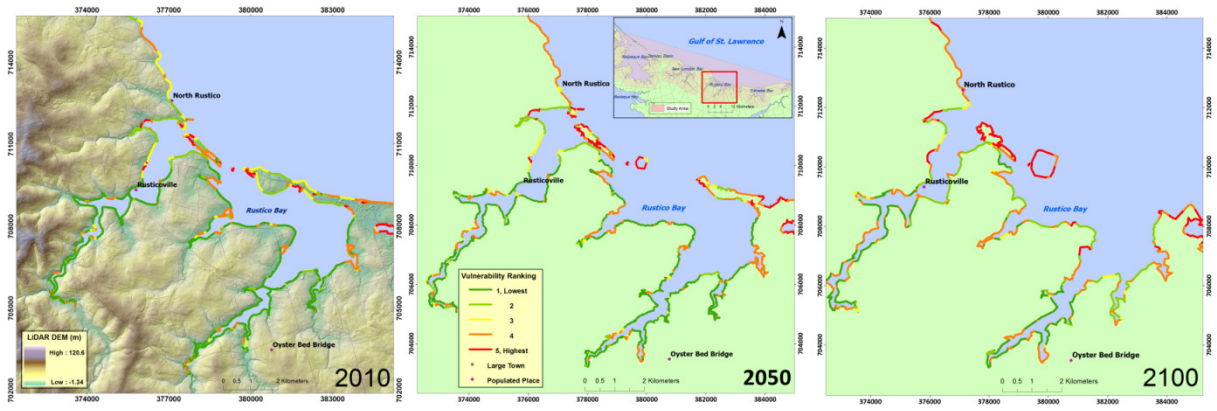

Figure 62: Physical coastal vulnerability of the region of Rustico Region for the years (a) 2010 (b) 2050 and (c) 2100

Table 38: Frequency of physical coastal vulnerability ranking for three time steps of Rustico Region

Rustico Region Vulnerability Frequency			
Vulnerability	**2010**	**2050**	**2100**
1, Lowest	61.73%	52.36%	27.34%
2, Low	12.23%	12.12%	25.03%
3, Moderate	5.31%	6.06%	4.30%
4, High	18.66%	23.90%	34.12%
5, Highest	2.07%	5.56%	9.21%

Brackley-Dalvay Region

The Brackley-Dalvay region is home to the eastern portion of the PEI National Park. The park has experienced a high degree of coastal change historically due both to climactic and anthropogenic forcings. The spit of Robinson's Island is split in to a smaller island and shorter spit from 2010 to 2050, and is almost completely eliminated between the years 2050 to 2100. The eroded sediment from the spit would be entrained in longshore sediment transport and redeposited in areas of accretion (Davidson-Arnott, R. 2010). This accretion can be seen in **Figure 77** where the spit has eroded, however land east of the spit (Stanhope Beach) has gained shoreline width due to accretion.

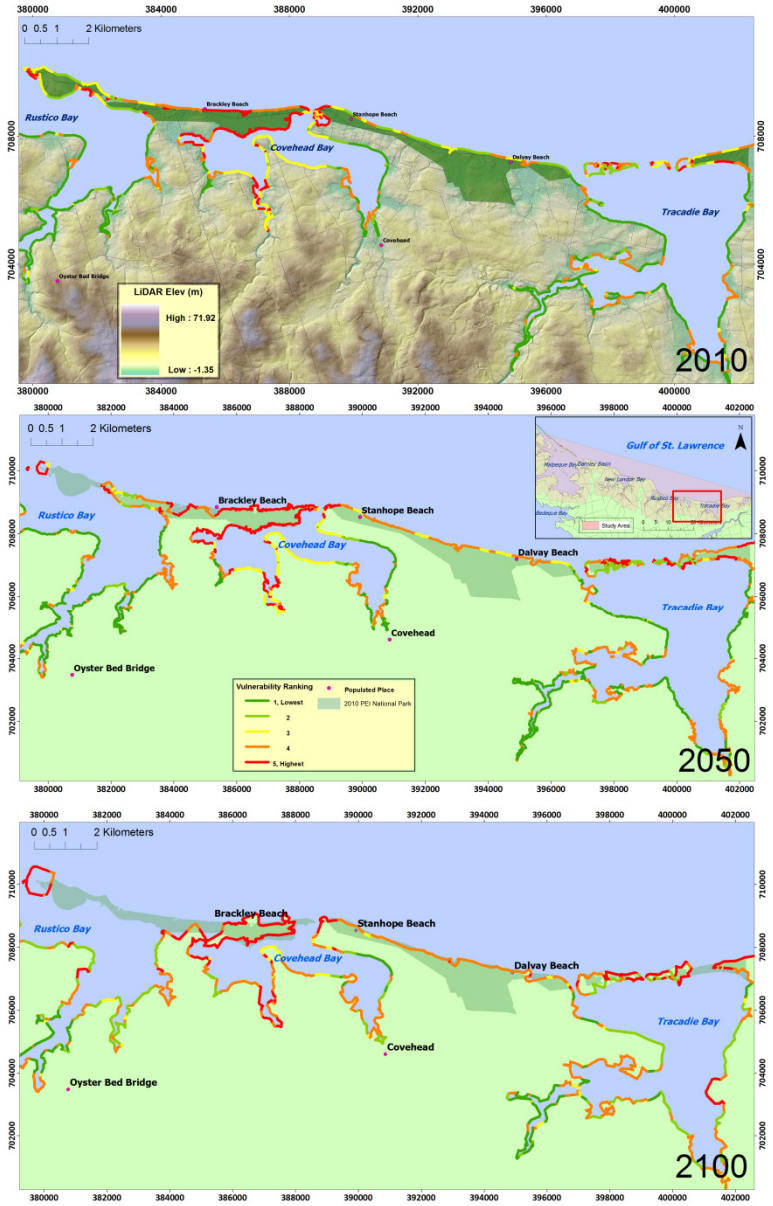

Figure 63: Physical coastal vulnerability of the region of Brackley-Dalvay Region for the years (a) 2010 (b) 2050 and (c) 2100

The elimination of spits and barrier islands during the two shoreline movement time steps can be due to the truncation of loops of nodes created as the shoreline moves inward. However, the physical basis of the elimination of these features can potentially be due to permanent sea-level rise inundation, severe erosion, and the decrease of coastal sea ice during winter months (Stutz & Pilkey, 2011). The physical coastal vulnerability of the region for

the years 2010, 2050, and 2100 can be seen in **Figure 77**. The western portion of Covehead Bay can be seen to have a vulnerability ranking of 5 in the year 2010, and the length of this highest ranking grows into the year 2100. A large fishing pier is located in Covehead Bay and hard adaptation measures were constructed in the Fall of 2012 to protect the pier (P. Giroux, personal communication, May 10, 2013). The coast exposed to the Gulf of St. Lawrence also increases in vulnerability, with the 2100 coast experiencing a large amount of vulnerability rankings of 4 and 5. Overall, the region had the second highest incidence of the highest vulnerability ranking of 5 (**Table 39**). The frequency of this ranking grew from 14.53% in 2010 to 22.15% in 2100. The frequency of the second highest vulnerability ranking of 4 increased from the years 2010 to 2100, from 25.55% to 41.20%. The lowest and moderate vulnerability rankings of 1 and 3 decreased from 2010 to 2100. The low vulnerability ranking of 2 decreased from 2010 to 2050, and increased from 2050 to 2100. Local stakeholders have noted multiple areas within the Brackley-Dalvay region as experiencing extreme coastal change and flooding : these areas include Covehead Golf Course, Covehead Bridge, Brackley Beach Complex, Robinson's Island and Blooming Point (A. Fenech, personal communication, May 9, 2013; R. Angus, personal communication, May 7, 2013 P. Giroux, personal communication, May 10, 2013). These areas were also found to be highly vulnerable (ranking of 5) from the 2010 vulnerability assessment to the year 2100, where Covehead Bay and the Brackley Beach Complex received a majority ranking of 5, and a majority of Robinson's Island and Blooming Point was eliminated by the year 2100.

Table 39: Frequency of physical coastal vulnerability ranking for three time steps of Brackley-Dalvay Region

Brackley-Dalvay Region Vulnerability Frequency			
Vulnerability	**2010**	**2050**	**2100**
1, Lowest	29.64%	26.64%	13.41%
2, Low	13.51%	9.60%	18.39%
3, Moderate	16.77%	11.54%	4.84%
4, High	25.55%	32.41%	41.20%
5, Highest	14.53%	19.80%	22.15%

6.2.2. Vulnerability of Provincial and National Parks

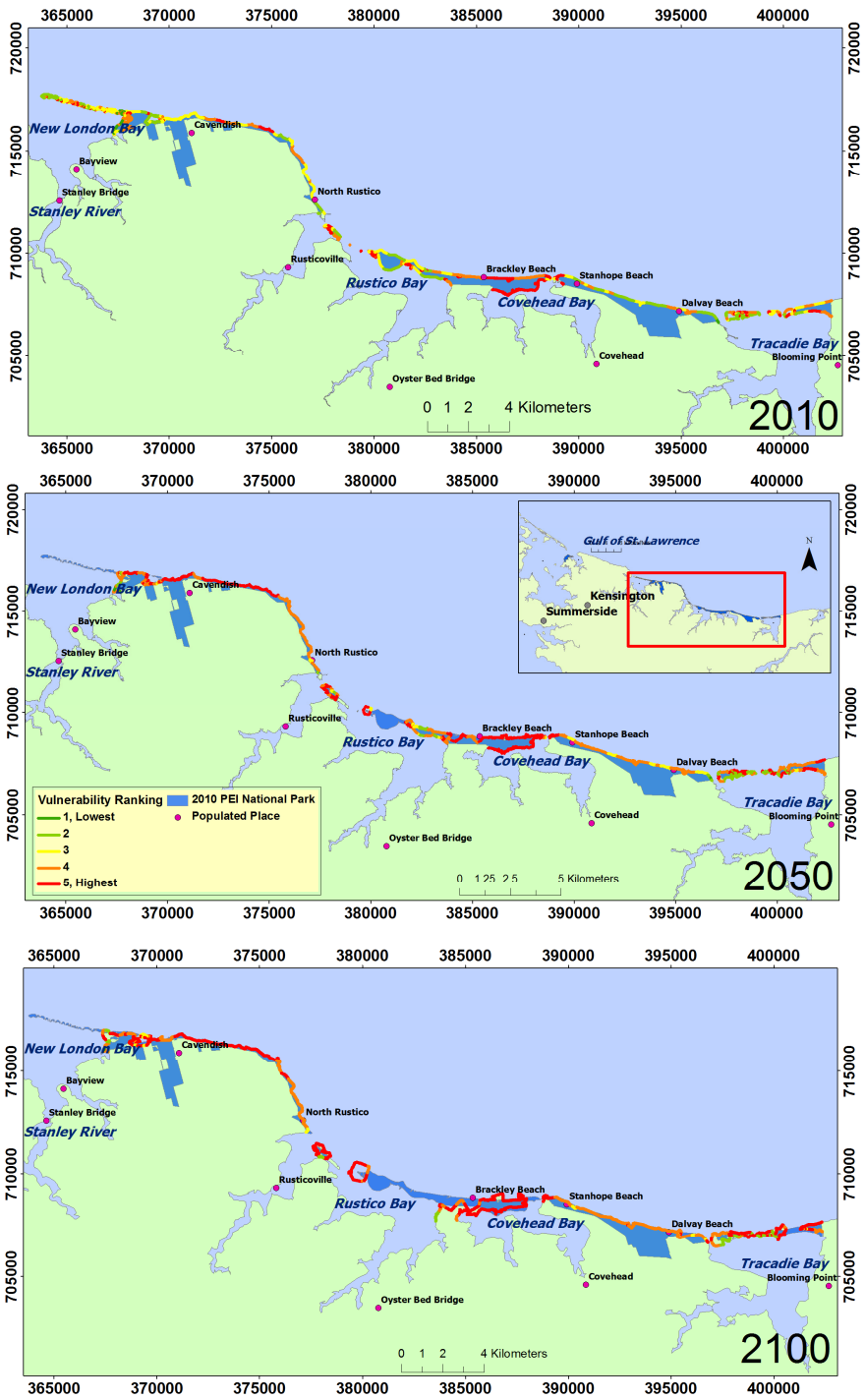

Figure 64: Physical coastal vulnerability of PEI National Park for the years (a) 2010 (b) 2050 and (c) 2100

Prince Edward Island National Park

The Prince Edward Island National Park is a relatively narrow coastal area extending along the coast of the Gulf of St. Lawrence. The park was establish in 1937 in an effort to protect the vulnerable coastal ecosystem (ACASA, 2013a; P. Giroux, personal communication, May 10, 2013). The study area portion of the park stretches from the barrier islands of Cavendish to the spit and barrier island system of Tracadie Bay. The park is split in to two areas, the Cavendish area and the Brackley-Dalvay area, by Rustico Bay. The park is experiencing a high degree of coastal erosion, which is highly detrimental

due to the close proximity of park infrastructure to the open coast. Because of coastal erosion, areas of the park were abandoned, such as the campground at Robinson's Island as well as roads and parking lots at Dalvay (ACASA, 2013a). Mitigation techniques have been used to reduce coastal erosion. Hard anthropogenic infrastructures such as rip rap and gabion baskets have been put in place in segments of the park, as well as soft mitigation techniques such as the relocation of pathways. However, a high degree of coastal erosion continues to occur, and with relative sea-level rise flooding expected to increase in the near future, the park is highly vulnerable to coastal change (ACASA, 2013a).

Figure 78 displays the relative physical coastal vulnerability of the PEI National Park for the years 2010, 2050, and 2100. As the shoreline of the park progresses through the three time steps, it can be seen that the area of both portions of the park is substantially reduced. The coastline across the park encroaches inland and portions of the park are lost.

The Cavendish spit system as well as Robinson's Island is completely eliminated. This may be due to the inability of the shoreline movement algorithm to accurately predict the relocation of sediment of barrier islands and spits through longshore transport through each time step.

Table 40 summarizes the frequency of each physical coastal vulnerability ranking for the PEI National Park. The park substantially increases in the highest ranking of vulnerability from 19.67 % in 2010 to 54.99% in 2100. The ranking of 4, or a high vulnerability, increases from 24.94% in 2010 to 39.00% in 2050, but then decreases to 34.19% in 2100 likely due to the increase of coastline designated a highest vulnerability of 5. The moderate, low, and lowest vulnerability rankings each decrease from 2010 to 2100.

Table 40: Frequency of physical coastal vulnerability ranking for three time steps of PEI National Park

PEI National Park Vulnerability Frequency			
Vulnerability	**2010**	**2050**	**2100**
1	2.63%	0.85%	0.08%
2	26.18%	10.19%	7.28%
3	26.57%	7.64%	3.52%
4	24.94%	39.00%	34.12%
5	19.67%	42.32%	54.99%

Cabot Beach Provincial Park

Cabot Beach Provincial Park is located along the northeastern coast of Malpeque Bay and the western coast of Darnley Basin. The beach is characterized by a sand spit with dune system as well as a system of backshore bluffs and cliffs further inland. Field work conducted in May 2013 found a large degree of coastal erosion occurring along the coast of the park. **Figure 79** depicts a bluff system experiencing a high degree of coastal erosion along an area of the park exposed to the wind and wave energy of Malpeque Bay.

Figure 65: Coastal erosion of bluff system at Cabot Beach Provincial Park, May 2013

The physical coastal vulnerability of Cabot Beach Provincial Park for years 2010, 2050, and 2100 can be seen in **Figure 80**. These maps show that the spit which extends in to Darnley Basin is gradually shortened through the time steps. Furthermore, a significant portion of the park is lost due to coastal erosion, as seen in the northeastern portion of the park. **Table 41** summarizes the physical coastal vulnerability ranking of frequency of the park for the three time steps. The frequency of the highest vulnerability of 5 decreases from 17.11% in 2010 to 13.51% in 2100, possibly due to the loss of land over time. The vulnerability ranking of 4 increases from 2010 to 2100, at 6.42% to 17.57% respectively.

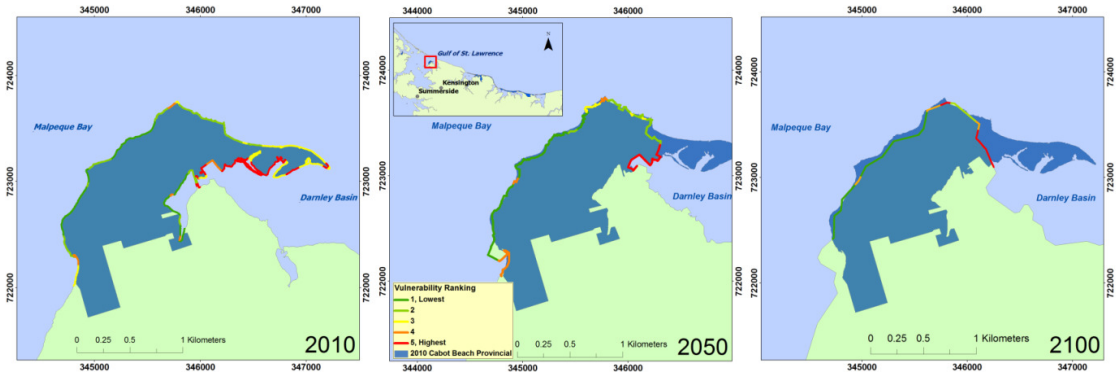

Figure 66: Physical coastal vulnerability of Cabot Beach Provincial Park for years (a) 2010 (b) 2050 and (c) 2100

Table 41: Frequency of physical coastal vulnerability ranking for three time steps of Cabot Beach Provincial Park

Cabot Beach Provincial Park Vulnerability Frequency			
Vulnerability	**2010**	**2050**	**2100**
1	27.81%	47.96%	4.05%
2	24.06%	16.33%	54.05%
3	24.60%	7.14%	10.81%
4	6.42%	15.31%	17.57%
5	17.11%	13.27%	13.51%

Green Park Provincial Park

Green Park Provincial Park is located on a peninsula in the northwestern portion of Malpeque Bay. The park is characterized by extensive brackish wetland systems, as pictured in **Figure 81**. The park does not have a high degree of coastal erosion occurring due to its low relief, however there is a high potential for the park to be inundated with permanent sea-level rise due to this low elevation.

Figure 67: Wetland system of Green Park Provincial Park, May 2013

Figure 82 displays the physical coastal vulnerability of the years 2010, 2050, and 2100 for Green Park Provincial Park. A significant segment of land in the northern portion of the park is lost between the time steps 2050 and 2100, likely due to relative sea-level rise inundation. However, the eastern portion of the park experiences accretion and gains a segment of land.

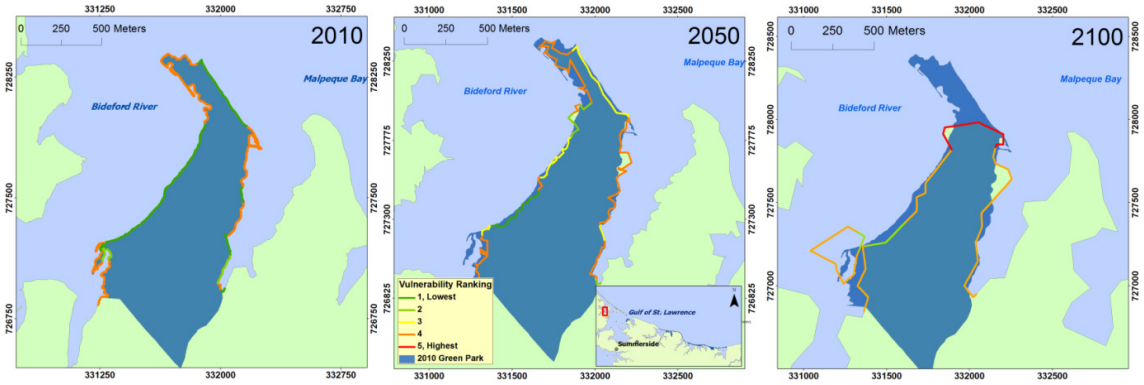

Figure 68 : Physical coastal vulnerability of Green Park Provincial Park for years (a) 2010 (b) 2050 and (c) 2100

The park does not receive a physical coastal vulnerability ranking of any segment of its coast in the year 2010, however by the year 2100, 14.13% of the coast is ranked with having a highest vulnerability (**Table 42**). A large proportion of the park coast is ranked 4 with a high vulnerability, increasing from 50.88% in 2010 to 72.83% in 2100. The park only receives a ranking 4 along any of its shorelines during the year 2050, with a frequency of 20.19%.

Table 42: Frequency of physical coastal vulnerability ranking for three time steps of Green Park Provincial Park

Green Park Provincial Park Vulnerability Frequency			
Vulnerability	**2010**	**2050**	**2100**
1	43.86%	9.62%	13.04%
2	4.39%	6.73%	0.00%
3	0.88%	20.19%	0.00%
4	50.88%	63.46%	72.83%
5	0.00%	0.00%	14.13%

Belmont Provincial Park

Belmont Provincial Park is situated along the southern coast of Malpeque Bay. The coastline is characterized by medium to high elevation bluffs, cliffs, and outcrops comprised of sandstone with cobble sized sediment pocket beaches (**Figure 83**). Belmont is the smallest park located in the North Shore study area.

Figure 69: Cliff and outcrop with pocket beach at Belmont Provincial Park, May 2013

The physical coastal vulnerability of Belmont Provincial Park is depicted for the years 2010, 2050, and 2100 in **Figure 84**. From 2010 to 2050 the western portion of the park experiences erosion, while the eastern portion experiences accretion, thus losing and gaining land respectively. The movement of the shoreline through each time step is based on the 2000 to 2010 coastal change rates created by Webster (2012), and it is assumed that the locations which receive either erosion or accretion will continue to do so with each time step. Coastal change rates for the time step of 2050 to 2100 were assumed to increase by 1.1 times the 2000 to 2010 rates.

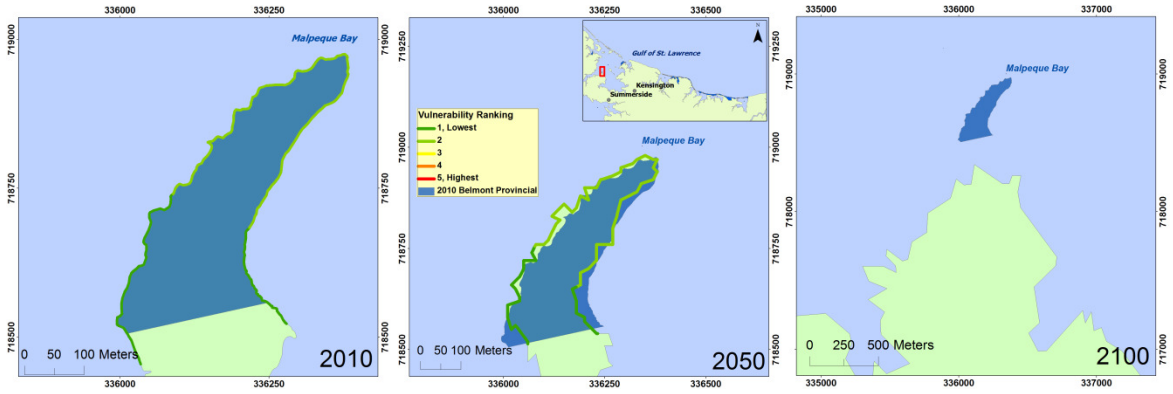

Figure 70: Physical coastal vulnerability of Belmont Provincial Park for years (a) 2010 (b) 2050 and (c) 2100

From 2050 to 2100 the entire area comprising the 2010 extent of the park has been eliminated. This was found to be an error due to the truncation of node loops in the shoreline movement algorithm. The purpose of the truncation of node loops was to automatically smooth the output shoreline to better represent the physical shape the shore would transform into overtime. However, errors may occur where a thin peninsula is removed if the node representing a section of the land erodes beyond the shoreline parallel to it. This creates a loop. In reality, the Belmont Provincial Park shoreline could potentially transform in to an island due to the erosion cutting off the "neck" of the peninsula. The non-truncated 2100 node shapefile can be seen in **Figure 85,** with the location of the two nodes eroding past one another, in to a loop, labeled. Future work would include the ability of the shoreline movement algorithm to transform larger loops in to islands. A similar error occurred when estimating shoreline movement for Hog Island in Malpeque Bay, and thus the resultant 2050 and 2100 shorelines did not predict the movement of this highly dynamic area.

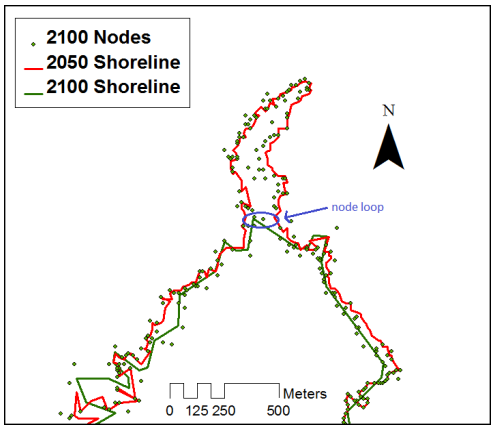

Figure 71: Location of node loop at Belmont Provincial Park, which eliminated the peninsula

The 2010 and 2050 coastlines of Belmont Provincial Park receive vulnerability rankings of 1 and 2, or lowest and low physical coastal vulnerability. The percent frequency of each vulnerability ranking is summarized in **Table 43**.

Table 43: Frequency of physical coastal vulnerability ranking for three time steps of Belmont Provincial Park

Belmont Provincial Park Vulnerability Frequency			
Vulnerability	**2010**	**2050**	**2100**
1	35.29%	36.36%	N/A
2	55.88%	60.61%	N/A
3	0.00%	0.00%	N/A
4	8.82%	3.03%	N/A
5	0.00%	0.00%	N/A

6.3. Climate Change Adaptation Measures

PEI has been identified as a Canadian region most sensitive to coastal erosion (ACASA, 2013a). The coastlines are largely comprised of highly erodible sandstone bedrock beneath glacial till deposits. The North Shore is particularly vulnerable due to the large fetch lengths across the Gulf of St. Lawrence which produce extreme wind and wave energy (ACASA, 2013a). Coastal erosion is most significant during extreme storm events. Human infrastructure is densely populated along the coasts of the study area (ACASA, 2013b) and residents have begun to witness the effects of climate change induced sea-level rise and storm surge. Residents of the North Shore have noticed an increase in the intensity and frequency of Nor'easter storms (ACASA, 2012). This has been similarly witnessed in the Northeast United States, where the 100- year return period extreme storms of the 1950s are now expected to appear once in every 60 years (Horton *et al.,* 2014). An increase in relative sea-level, especially during storm driven swell events, will drive storm surge further inland than historically witnessed. As the greatest loss of land through erosion is caused by storm events, it is imperative that the North Shore continues to plan adaptation measures to reduce the hazards of climate change.

Adaptation is defined by IPCC AR5 as "the process of adjustment to actual or expected climate and its effects" (IPCC, 2013). Anthropogenic adaptation to climate change hazards looks to reduce the risks of climate change through human intervention of the natural system, while

utilizing the potential benefits of climate change (IPCC, 2013). A Community Vulnerability Assessment was conducted in 2012 for the town of North Rustico (ACASA, 2012) which summarizes three categories of adaptation methods prevalent along vulnerable coastlines; these include hard protection, soft protection, and hybrid protection. Hard protection includes man-made structures built to reduce inland flooding and coastal erosion; examples include gabian baskets and breakwaters. Soft protection techniques attempt to use the natural environment to reduce coastal erosion and flooding; techniques include beach nourishment and brush treatments to stabilize dune systems. The hybrid technique utilizes a combination of soft and hard adaptation (ACASA, 2012).

The 2012 Community Vulnerability Assessment of North Rustico provides examples of accommodation adaptation techniques. These methods of adaptation seek to allow use of vulnerable land while planning for its eventual loss due to climate change (IPCC, 2007b). One technique recommended in the report includes the creation of a municipal coastal development setback by-law. This by-law would restrict coastal development close to the water's edge to limit infrastructure damaged by coastal erosion and flooding. Another example is the update of a town's local emergency management plan on an annual basis to best handle the hazards of storm events. These soft adaptation methods would be beneficial not only to North Rustico but also to towns across the North Shore.

Parks Canada have utilized costly and ineffective hard adaptation techniques to protect beaches and the park infrastructure (ACASA, 2013a). Hard shoreline protection can cost over one thousand dollars per linear meter (ACASA, 2013b). Paul Giroux of Park's Canada states that a concrete structure was built in the beach foreshore to protect the backshore dune system at the Brackley Beach complex of PEI National Park. The placement of the structure damaged the dune through the relocation of wave energy, causing the edge of the dune to be removed more frequently and an increase of dune erosion on the seaward side. Another hard adaptation structure at the complex destroyed a dune and caused the sediment to be repeatedly deposited on a nearby boardwalk. Paul Giroux mentions that Dr. Robin Davisdson-Arnott recommends the use of soft adaptation techniques in place of these hard structures to limit these errors; for example, vegetation such as marram grass can be used to stabilize a dune due to the root structure holding

the sediment in place. This advice was followed in 2012 to help stabilize the dunes in the area. Another successful soft adaptation technique occurred at PEI National Park with the relocation of beach side parking to controlled parking lots in order to reduce dune trampling by beach visitors (P. Giroux, personal communication, May 10, 2013). The PEI National Park management plan now incorporates a planned retreat method of adaptation. 12.5 km^2 of land has been purchased since 1974 to make room for the encroaching coastline (ACASA, 2013a).

The limitations of the use of hard adaptation techniques to protect the shoreline at PEI National Park are repeatedly documented. These techniques incur high costs and are frequently ineffective. The placement of hard structures rarely incorporate natural coastal processes when being designed. In comparison, soft adaptation techniques such as brush treatments and the planting of native vegetation have proven to be effective at a much lower cost (ACASA, 2013a; P. Giroux, personal communication, May 10, 2013). In some instances the best adaptation approach is to abandon the coast and allow for re-naturalization (ACASA, 2013b). The PEI National Park has been identified by this research as the area of highest relative physical coastal vulnerability to coastal erosion and flooding. Thus, it is recommended for the park management plan to focus on soft adaptation techniques to reduce the encroachment of the shoreline and to protect against episodic storm surge flooding. However, with permanent sea-level rise, the park will likely need to continue the plan to retreat inland.

6.4. Potential Sources of Error

The evaluation of relative physical coastal vulnerability for the years 2010, 2050, and 2100 for the North Shore, PEI utilized GIS and mathematical modeling techniques. The methodology relied on the use of spatial data from a myriad of sources. Thus, the date range of the data utilized was not always consistent with the three time steps chosen for this research. There is potential error in the creation of the 2010 bathymetric DEM of the study area due to the CHS Chart 4023 used depicted the coast in 2002, and was assumed to be applicable to the 2010 coast. However, the errors were mitigated through the use of LiDAR contour data for the year 2010 with the digitized data collected from the CHS chart when creating the 2010 bathymetric DEM. Furthermore, there were anomalous high elevation instances in the 2010 LiDAR elevation which were not consistent with the 2010 LiDAR contours.

The methodology used to quantify relative physical coastal vulnerability had limitations due to scope. The prediction of annual volumetric sediment change does not incorporate river deposits brought to the shoreline within the sediment budget. Furthermore, the evaluation of coastal change does not include an estimation of change due to changes in sea ice over time. The algorithm used to predict shoreline change between each time step is unable to predict the dynamic nature of barrier islands and spits and thus does not predict their movement well. Finally, spatial data depicting the location of anthropogenic mitigation structures used to reduce coastal change is not up to date and thus these areas may not be correctly predicted when moving the shoreline through each time step.

6.5. Chapter Summary

The evaluation of relative physical coastal vulnerability of the North Shore for the year 2010 found the region of Brackley-Dalvay the most vulnerable to climate change induced with the coastline receiving a ranking of 5, the highest vulnerability, at 14.53% the length of the region. For the time steps of 2050 and 2100, Cavendish was found to be the region most vulnerable, with the area receiving rankings of 5 for 47.95% of the coastline in 2010 and 56.25% in 2100. These two regions are the location of PEI National Park which is a popular tourism destination. The coastline of PEI National Park received a high percentage of the highest vulnerability ranking of 5, increasing from 19.67% in 2010, to 42.32% in 2050, and finally 54.99% in 2100.

This research recommends that the PEI National Park management plan focus on soft adaptation techniques to reduce the encroachment of the shoreline and to protect against episodic storm surge flooding. However, with permanent sea-level rise, the park will likely need to continue the plan to retreat inland. The limitations of the use of hard adaptation techniques to protect the shoreline at PEI National Park are repeatedly documented. These techniques incur high costs and are frequently ineffective. In comparison, soft adaptation techniques have proven to be effective at a much lower cost (ACASA, 2013a; P. Giroux, personal communication, May 10, 2013).

Through each time step of the vulnerability assessment, spits and barrier islands migrated and in times were eliminated during the prediction of shoreline movement. For example, barrier islands protecting New London Bay disappeared between the 2050 and 2100 time step, and the spit of

Robinson's Island was reduced in length, but grew slightly in width from 2010 to 2100. The algorithm used to predict shoreline movement truncated loops of nodes created as the shoreline progressed landward. However, recent scientific evidence suggests that higher latitude barrier island systems may disappear during the next century (Stutz & Pilkey, 2011). The total volume of coastal sea ice is expected to decrease in these systems due to an increase of average winter temperatures. This ice protects barrier systems from erosion through armoring the islands from wind and wave energy, especially during storm events (Forbes *et al.,* 2004). As the North Shore receives the strongest storms during winter months, the elimination of sea ice could potentially cause the barrier islands and spits to disappear (Stutz & Pilkey, 2011).

When the shoreline was estimated for the years 2050 and 2100, the bathymetric DEM of the coast was recreated based on this new position. The resultant change of inland fetch length due to the elimination of barrier islands and spits alters the potential energy entering inland bays. This is captured with the recalculation of RWE for the 2050 and 2100 time steps and the resultant increase in the vulnerability of the coast due to the exposure condition.

This research evaluated the physical coastal vulnerability of the North Shore to climate change for years 2010, 2050, and 2100 using a CVA. The CVA was comprised of three criteria indicators ranked from lowest (1) to highest (5) vulnerability for three time steps. These criteria indicators included exposure condition, morphological resiliency, and relative sea-level rise and storm surge flooding risk. Between each time step, shoreline movement was predicted and new bathymetric data was created. The addition of the quantification of sediment budget and shoreline movement through each time step expands upon methodologies seen in the literature (i.e. Gornitz 1991; Gornitz *et al.,* 1994; Shaw *et al.,* 1998; Thieler & Hammar-Klose, 2000; Pendleton, Thieler, & Jeffress, 2005; and Gaki-Papanastassiou *et al.,* 2010). This component has been noted to be important in the prediction of future vulnerability (Gornitz *et al.,* 1994; Pendleton, Thieler, & Jeffress, 2005) as the physical change of the coast will alter the relative physical vulnerability of the coastline through each time step.

7. Conclusions

This study utilized ArcGIS to conduct a Coastal Vulnerability Assessment to quantify the relative physical vulnerability of the North Shore, Prince Edward Island for the year 2010. Three criteria indicators were used to complete this assessment. The first was the exposure condition of the study area; this criteria represents the potential of the coastal system to experience a climate change induced hazard. This thesis used the open source program WEMo in the Representative Wave Energy (RWE) mode to quantify the exposure condition in RWE values of J/m, calculated through the use of linear wave theory to determine wave energy and wave height, known as wind-wave exposure. The second criteria was the morphological resiliency of the North Shore study area. Morphological resiliency the ability of the coastal system to return to a state of equilibrium after a disturbance. This resiliency is a factor of the amount of sediment supply to the coastal system, the morphology of the system, and the duration of time between disturbance events. Morphological resiliency of the area was evaluated through the raster summation of the normalized values of annual volumetric sediment change (VSC) and the longshore sediment transport (Q_n). The final criteria used to quantify the relative physical vulnerability of the study area was the risk of permanent sea-level rise inundation and episodic storm surge flooding. Through the next century, relative sea-levels were estimated to increase, and a larger area of land will receive increased storm surge return periods and heights atop rising sea-levels. Richards and Daigle (2011) estimated extreme total water level for 2-, 10-, 40-, and 100-year return periods including for Rustico were determined including a quantification of relative sea-level rise. This data was used to calculate the final vulnerability.

The approach used to quantify physical coastal vulnerability is similar to assessments conducted in the literature but is innovative in the quantification of sediment budget and shoreline movement within a GIS. The sediment budget of a coastline relates the inputs and outputs of sediment, with a natural balance between sediment supply and removal promoting stable shoreline. Coastal change occurs where this budget is not balanced (ACASA, 2013a). Estimating shoreline movement through time using the estimation of sediment budget provides a more accurate prediction of future coastal vulnerability. When the shoreline movement was estimated through each time step, the exposure condition was recalculated within WEMo. This

altered the fetch length calculated of each node, thus increasing the relative RWE. Thus, the relative vulnerability changed based on the estimated movement of the shoreline. This method better estimates the effects of compound impacts on physical coastal vulnerability which other studies do not include.

Previous methods in the literature largely employ statistics to predict shoreline movement. This work attempts to estimate the movement of the shoreline using geomorphological principals. Between each time step (2010 to 2050, 2050 to 2100), the position of the shoreline was predicted using 2000 to 2010 coastal change rates calculated by Davies (2011). Between the time step of 2050 to 2100, these rates were increased by a factor of 1.1 in order to mimic increased rates induced by climate by climate change hazards.

The results of the 2010 vulnerability assessment were used to predict the physical vulnerability of the study area for years 2050 and 2100. For the 2050 and 2100 exposure condition criteria, a new bathymetric DEM was created based on the predicted shoreline movement for the year. The morphological resiliency of the study area for each year was assumed to remain constant. Finally, the risk of the 2050 and 2100 shorelines to permanent and episodic flooding were assessed based on storm surge return period data calculated by Richards & Daigle (2011).

This study combines geomorphological principles with the multicriteria evaluation methods of past CVAs within a GIS. This combination of methods provides an innovative tool to quantify the relative physical vulnerability of a coastline. Furthermore, this method utilizes the estimation of shoreline movement within the GIS in order to predict future physical vulnerability. This methodology has the potential to be used to quantify physical coastal vulnerability of regions around the globe as long as the data needs are met.

7.1. Relative Physical Coastal Vulnerability of the North Shore

The CVA results indicated that through each of the three time steps, the regions containing the PEI National Park (Cavendish and Brackley-Dalvay regions) had the highest relative physical vulnerability than other regions of the study area. The PEI National Park was originally formed to reduce the escalating negative effects caused by anthropogenic and climactic forcings, such as trampling and storm surge respectively; these pressures together caused coastal erosion and

ecosystem disruption and loss. With climate change hazards expected to increase over the next century the vulnerability of the park will increase.

The 2010 results of the physical vulnerability assessment found the Brackley-Dalvay region as most vulnerable to climate change, with the coastline receiving the highest vulnerability for 14.53% the length of the coast. For the time steps of 2050 and 2100, Cavendish was found to be the region most vulnerable, with the area receiving rankings of 5 for 47.95% of the coastline in 2010 and 56.25% in 2100. The coastline of PEI National Park received a high percentage of the highest vulnerability ranking of 5 compared to the three other parks in the region, increasing from 19.67% in 2010, to 42.32% in 2050, and finally 54.99% in 2100.

When the 2050 and 2100 shorelines were predicted, many barrier island and spit systems shrank in area or disappeared completely. This phenomena has been witnessed and predicted for the New England region of the eastern United States as well as many Northern Hemisphere locations. The increase of temperatures during winter months will limit the ability of sea ice to form on barrier islands. Winter sea ice buildup limits the erosion of the barrier island through the formation of a solid ice barrier which armors the island from wind and wave energy. As Prince Edward Island receives the highest energy storms during winter months, the reduction of sea ice coverage could eliminate the barrier islands of the North Shore. Between the years 2000 to 2001, three storms caused millions of dollars in damage alone to wharf and fishing infrastructure, tourism facilities, and residential property (Forbes *et al.,* 2004).

An assessment of coastal impacts of climate change for a portion of the North Shore was conducted by Shaw (2001). The study area included 12 kilometers of coast between Tracadie Bay and Savage Harbor. Beach surveys and aerial photograhs were used to calculate erosion rates, which were then used to estimate the value of shorefront properties and farm lands affected by coastal retreat. The case study found net erosion of the study area, effecting coastal cottage property, wetland systems, forests, and tourist attractions such as beaches. Furthermore, the study estimated the flooding extent of Charlottetown, PEI for three flood levels using a "bath tub" approach of raising sea levels relative to CGVD28. This approach only forecasts flooding of areas adjacent to open water, which omits the potential of the flooding of low-lying areas not connected to open waters. The model produced results in a coarse resolution, making it difficult

for local homeowners to determine the potential of their property to be flooded. Thus, there is a an increased value for stakeholders to receive higher resolution vulnerability information when planning adaptation measures to climate change. The method developed in this research provides this increased detail for the North Shore.

7.2. Adaptation Recommendations

Hard adaptation protection measures such as gabian baskets, breakwaters, and riprap have historically used to protect beaches and park infrastructure at PEI National Park. These methods have been concluded to be ineffective in their effort to provide long-term protection measures to reduce erosion and flooding, and can cost over one thousand dollars per linear meter. In comparison, soft adaptation techniques have proven to be successful and lost costly. The planting of marram grass on vulnerable dune systems has proven to be successful at PEI National Park. The vegetation stabilizes the dune due to the root structure holding the sand in place. Furthermore, the removal of beach side parking reduced dune trampling, and the addition of a new parking lot with a single pathway through the dunes allowed beach visitors to park their vehicles, while reducing the traffic across the dune systems. The PEI National Park management plan also has chosen to plan retreat of the park as the shoreline encroaches of the next century.

Due to the limitations of hard protection, this research recommends that not only the PEI National Park management plan focus on soft adaptation techniques, but also regions across the North Shore. In some instances the best adaptation approach is to abandon the coast and allow for re-naturalization. Local policy measures can also be enacted to reduce the risks of climate change. The 2012 Community Vulnerability Assessment of North Rustico recommends the creation of a municipal coastal development setback by-laws. This by-law would restrict coastal development close to the water's edge to limit infrastructure damaged by coastal erosion and flooding.

7.3. Future Research

The methods provided in this research can be further refined in order to reduce errors and automate the process of assessing physical coastal vulnerability. The shoreline movement algorithm used in this work has limitations; the method is unable to predict the movement and

relocation of barrier islands and spits. The incorporation of statistical methods utilized in other literature may provide a reasonable method to predict this relocation. Forbes *et al.* (2004) indicate a need within the literature to improve shoreline change prediction. Furthermore, the CVA process could potentially be automated in a script in either Python or R, however this was beyond the scope of this work.

A important component of the assessment included the geomorphological classification of the study area shoreline. Although a portion of the study area was characterized *in situ,* time constraints limited the classification of the entire region. Davies (2011) remotely classified the nearshore, foreshore, and backshore of the coast through visual assessment of orthophotos captured in 2010, but was completed remotely without field verification. Thus, further field work to complete the geomorphological classification would increase the accuracy of the assessment's results. Furthermore, geospatial data locating anthropogenic adaptation structures across the study area was limited. An updated database including this information would not only produce more accurate shoreline movement results, but could also be used to illustrate a scenario of managed retreat adaptation. For a certain time step, the shoreline could be predicted with the placement of these structures, where it was assumed the shoreline did not move, and with the structures, where it was assumed the shore moved. The resultant magnitude of land loss and the relative value of this land could be compared with the price of anthropogenic structures to evaluate the cost and benefit of their use.

A number of methods of verification and validation may be undertaken in order to assess the veracity of the vulnerability assessment results. For example, coastal change rates for the study area from 1968 to 2000 could potentially be input in to the model barring the availability of other necessary data (year 1968 bathymetry, shoreline classification, alongshore sediment transport rates, etc.). The resultant vulnerability predicted for year 2000 could be compared with locations of greatest coastal transgression and inundation to determine whether the outputs reflect what has actually occurred. Furthermore, many CVAs incorporate weightings to the criteria indictors used to calculate the relative vulnerability ranking of the study area. The weightings are used to reduce the potential of one criteria dominating the results of the CVA. The weightings are calculated through statistical methods (i.e. ANOVA) used to compare the relative impact each

criteria has on the result. The product can be used to determine whether which criteria, if any, had the greatest impact on the resultant physical vulnerability.

The use of the vulnerability assessment results could help demonstrate the potential adverse effects climate change will have on the communities of the North Shore. Expanding upon the current scope of the project could further illuminate the damage potential of climate change. As the greatest impacts of climate change are predicted to occur after the final time step of this assessment (2100), continuing the methodology in to the year 2150 could potentially yield drastic, but interesting, results. The resultant 2100 vulnerability could potentially produce extreme cases of coastal transgression and severe sea-level rise and storm surge flooding. Furthermore, if the necessary input data existed for the entirety of Prince Edward Island, the physical vulnerability assessment outlined in this research could be applied. This assessment would provide a more realistic and higher resolution prediction of potential change than current assessments have supplied for the province due to the incorporation of real world geomorphological principles. For example, Shaw (2001) assesses the flooding potential of Charlottetown for three return periods, but does not incorporate hydrological flow of water through the system nor the geomorphology of the coast and its effects on coastal flooding.

Shoreline classification was assumed to remain the same through each time step of the morphological resiliency methodology. It could be possible to predict the shoreline classification change based on the estimated movement of the shoreline (and thus the resultant change in fetch length) as well as the use of hydrological models. However, this prediction may be difficult due to the degree which humans impact the coast. While the hydrological and geomorphological principals which contribute to the evolution of shoreline classification is mathematically and conceptually difficult, the anthropogenic factors which contribute to this reclassification are nearly impossible to predict. For example, a dune system may be eliminated after a storm event and transformed in to a wetland if permanent flooding occurs. This may be predicted if the dune system was noted to be vulnerable to erosion. However, dune systems are highly vulnerable to anthropogenic disturbance, such as dune trampling, which could cause the elimination of the dune and reclassification of the shore segment. Thus, while it may be possible for the

reclassification of the shoreline through hydrodynamic and geomorphological modeling, it would be difficult to incorporate anthropogenic forcings.

References

ACASA (2012). Climate change vulnerability assessment: North Rustico, Prince Edward Island. *The Atlantic Climate Adaptation Solutions Association.* Retrieved 07 04, 2012, from http://atlanticadaptation.ca/sites/discoveryspace.upei.ca.acasa/files/CC%20Vulnerability%20Assessment%20-%20North%20Rustico%20FINAL%20Combined_1.pdf

ACASA (2013a). Coastal Climate Change in Prince Edward Island Parks: Retreat or Protect? *The Atlantic Climate Adaptation Solutions Association.* Retrieved 10 04, 2012, from http://atlanticadaptation.ca/sites/discoveryspace.upei.ca.acasa/files/DEC-00267-PEI%20Coastal%20Change%20at%20Prince%20Edward%20Island%20Parks%20Case%20Study_HIGHREZ.pdf

ACASA (2013b). Coastal Climate Change in Prince Edward Island: Shoreline Protection. *The Atlantic Climate Adaptation Solutions Association.* Retrieved 06 13, 2012, from http://atlanticadaptation.ca/sites/discoveryspace.upei.ca.acasa/files/DEC-00266-PEI%20Shoreline%20Protection%20Case%20Study_HIGHREZ.pdf

Bamber, J., Riva, R., Vermeersen, B., & LeBrocq, A. (2009). Reassessment of the potential sea-level rise from a collapse of the West Antarctic ice sheet. *Science, 324*, 901-903

Bosom, E., & Jimenez, J.A. (2011). Probabilistic coastal vulnerability assessment to storms at regional scale – application to Catalan beaches (NW Mediterranean). *Natural Hazards and Earth System Science, 11*, 475-484

Briggs, D., Smithson, P., Addison, K., & Atkinson, K. (1997) *Fundamentals of the physical environment, 2nd edition*. London: Routledge

Church, J.A., White, N.J., Hunter, J.R. (2006) Sea level rise at tropical Pacific and Indian Ocean islands. *Global Planetary Change, 53*(3), 155–168

Dasgupta, S., Laplante, B., Murray, S., & Wheeler, S. (2011). Exposure of developing countries to sea-level rise and storm surge. *Climate Change, 106:* 567-579

Davidson-Arnott, R. (2010) *Introduction to coastal processes and geomorphology*. New York: Cambridge University Press

Davies, M. (2011). Geomorphic shoreline classification of Prince Edward Island. *The Atlantic Climate Adaptation Solutions Association.* Retrieved 06 23, 2012, from http://atlanticadaptation.ca/sites/discoveryspace.upei.ca.acasa

Delft Hydraulics (2004). Delft3D modelling suite for integral water solutions. http://www.deltaressystems.com/hydro/product/621497/delft3d-suite

Dolan, R., Fenster, M.S., & Holme, S.J. (1991). Temporal analysis of shoreline recession and accretion. *Journal of Coastal Research, 7*(3), 723–744

Dwarakish, G.S., Vinay, S.A., Natesan, U., Asano, T., Kakinuma, T., Venkataramana, K., Jagadessha Pai, B., & Babita, M.K. (2009). Coastal vulnerability assessment of the future sea level rise in Udupi coastal zone of Karnataka state, west coast of India. *Ocean & Coastal Management, 52,* 467-478

Fonseca, M.S., & Malhotra, A. (2010). WEMo (Wave Expose Model) for use in ecological forecasting. Applied Ecology and Restoration Research Branch NOAA, National Ocean Service. Retrieved 01 19, 2012, from http://www.csc.noaa.gov/digitalcoast/tools/wemo/index.html

Forbes, D.L., & Manson, G.K. (2002). Coastal geology and shore-zone processes. In: Forbes, D.L, & Shaw, R.W. (Eds.), *Coastal impacts of climate change and sea-level rise on Prince Edward Island*. Geological Survey of Canada, Dartmouth, N.S., Open File 4261, Supporting Document 9

Forbes, D. P., Parkes, G.S, Manson G.K., & Ketch, L.A. (2004). Storms and shoreline retreat in the southern Gulf of St. Lawrence. *Marine Geology (210)*, 210, 169-204

Genz, A.S., Fletcher, C.H., Dunn, R.A., Frazer, L.N., & Rooney, J.J. (2007). The predictive accuracy of shoreline change rate methods and alongshore beach variation on Maui, Hawaii. *Journal of Coastal Research, 23*(1), 87–105

GeoNet Technologies, Inc. (2011). Interpretation and extraction of coastline vector data from multi-temporal digital orthophotos and rate of coastline change determination for Prince Edward Island. *The Atlantic Climate Adaptation Solutions Association.* Retrieved 06 24, 2012, from http://atlanticadaptation.ca/sites/discoveryspace.upei.ca.acasa

Gornitz, V. (1991). Global coastal hazards from future sea level rise. *Palaeogeography, Palaeoclimatology, Palaeoecology (Global Planet. Change Sect.), 89*, 379-398

Gornitz, V. M. (1995). Sea-level rise - a review of recent past and near-future trends. *Earth surface processes and landforms*, *20*(1), 7-20

Gornitz, V, Daniels, R.C., White, T.W., & Birdwell, K.W. (1994*). Journal of Coastal Research, SI 12*, 327-338

Gaki-Papanastassiou, K., Karymbalis, E., Poulos, S.E., Seni, A., & Zouva, C. (2010). Coastal vulnerability assessment to sea-level rise based on geomorphological and oceanographical parameters: the case of Argolikos Gulf, Peloponnese, Greece. *Hellenic Journal of Geosciences*, *45*, 109-121

Hansen, B. (n.d.) Identifying and mapping saltwater intrusion and submarine groundwater discharge. *Atlantic Climate Adaptation Solutions Association.* Retrieved 01 22, 2012, from http://atlanticadaptation.ca/sites/discoveryspace.upei.ca.acasa/files/Identifying%20and%20mapping%20saltwater%20intrusion%20and%20submarine%20groundwater%20discharge%20-%20Brian%20Hansen_0_0.pdf

Hanson, S., Nicholls, R.J., Balson, P., Brown, I., French, J.R., Spencer, T., & Sutherland, W.J. (2010). Capturing coastal geomorphological change within regional integrated assessment: An outcome-driven fuzzy logic approach. *Journal of Coastal Research, 26*(5), 831-842

Hapke, C.J., Himmelstoss, E.A., Kratzmann, M., List, J.H., & Thieler, E.R. (2010). National assessment of shoreline change; historical shoreline change along the New England and Mid-Atlantic coasts: U.S. Geological Survey Open-File Report 2010-1118

Hinton, A.C. (2000). Tidal changes and coastal hazards: Past, present and future. *Natural Hazards, 21*(2-3), 173-184

Horton, R., Yohe, G., Easterling, W., Kates, R., Ruth, M., Sussman, E., Whelchel, A., Wolfe, D., & Lipschultz, F. (201). Ch. 16: Northeast. Climate Change Impacts in the United States: *The Third National Climate Assessment*, J. M. Melillo, Terese (T.C.) Richmond, and G. W. Yohe, Eds., U.S. Global Change Research Program, 371-395

IPCC (2007a). *Climate change 2007: The physical science basis. Contribution of Working Group I to the Fourth Assessment Report of the Intergovernmental Panel on Climate Change.* Solomon, S., Qin, D., Manning, M., Chen, Z., Marquis, M., Averyt, K.B, Tignor, M., & Miller, H.L., eds. Cambridge: Cambridge University Press

IPCC (2007b). *Climate change 2007: Impacts, adaptation and vulnerability. Contribution of Working Group II to Fourth Assessment Report of the Intergovernmental Panel on Climate Change*. Parry, M.L., Canziani, O.F., Palutikof, J.P., van der Linden, P.J., & Hanson, C.E., eds. Cambridge: Cambridge University Press

IPCC (2013). *Draft: Working Group I contribution to the IPCC Fifth Assessment Report (AR5), climate change 2013: The physical science basis.* Freeland, H., Garzoli, S., Nojiri, Y, eds. Stockholm, Sweden

Jankowski, P. (1995) Integrating geographical information systems and multiple criteria decision-making methods, *International Journal of Geographical Information Systems, 9*(3), 251-273

Jiang, H., & Eastman, J.R. (2000). Application of fuzzy measures in multi-criteria evaluation in GIS. *International Journal of Geographical Information Science, 14*(2), 173-184

King, G., O'Reilly, G., & Varma, H. (2002). High-precision three-dimensional mapping of tidal datums in the southwest Gulf of St. Lawrence. *Coastal impacts of climate change and sea-level rise on Prince Edward Island.* Edited by Forbes, D.L., & Shaw, R.W. Geological Survey of Canada, Open File 4261, Document 7, 16 p

Kumar, T.S., Mahendra, R.S., Nayak, S., Radhakrishnan, & Sahu K.C. (2010) Coastal vulnerability assessment of Orissa state, east coast of India. Journal of Coastal Research, 26(3) 523-534

Kumar, A.A., & Kunte, P.D. (2012). Coastal vulnerability assessment for Chennai, east coast of India using geospatial techniques. *Natural Hazards, 64,* 853-872

Le Cozannet, G., Garcin, M., Bulteau, T., Mirgon, C., Yates, M.L., Mendez, M., Baills, A., Idier, D., & Oliveros, C. (2013). An AHP-derived method for mapping the physical vulnerability of coastal areas at regional scales. *Natural Hazards and Earth Systems Science, 13*, 1209-1227

Mathew, S., Davidson-Arnott, R. G. D., & Ollerhead, J. (2010). Evolution of a beach-dune system following a catastrophic storm overwash event. *Canadian Journal of Earth Science*, *47*(3)

McLaughlin, S, McKenna, J., & Cooper, J.A.G. (2002). Socio-economic data in coastal vulnerability indices: constraints and opportunities. *Journal of Coastal Research, SI 36*, 487-497

Mitrovica, J.X., Tamisiea, M.E., Davis, J.L., & Milne, G.A. (2001). Recent mass balance of polar ice sheets inferred from patterns of global sea-level change. *Nature, 409*, 1026-1029

Mitrovica, J.X., Gomez, N., Morrow, E., Hay, C., Latychev, K., & Tamisiea, M.E. (2011). On the robustness of predictions of sea level fingerprints. *Geophysical Journal International, 187,* 729-742

Moser, S. C., Davidson, M.A., Kirshen, P. Mulvaney, P., Murley, J. F., Neumann, J. E., Petes, L., & Reed, D. (2014). Ch. 25: Coastal Zone Development and Ecosystems. *Climate Change Impacts in the United States: The Third National Climate Assessment*, J. M. Melillo, Terese (T.C.) Richmond, and G. W. Yohe, Eds., U.S. Global Change Research Program, 579-618

Nicholls, R.J., Hanson, S., Herweijer, C., Patmore, N., Hallegatte, S., Corfee-Morlot, J., Chateau, J., Muir-Wood, R. (2007). Ranking port cities with high exposure and vulnerability to climate extremes. OECD Environment Directorate, Environment Working Papers No. 1

Parkes, G.S., Ketch, L.A., & O´Reilly, C.T.O. (1997). Storm surge events in the Maritimes. in Proceedings, 1997 Canadian Coastal Conference, 21-24 May 1997, Guelph, Ontario, ed, M.G. Skafel. (Can. Coast. Sci. and Eng. Assoc.) 115-129

Pendleton, E.A., Thieler, E.R., & Jeffress, S.W. (2005). Coastal Vulnerability Assessment of Golden Gate National Recreation Area to Sea-Level Rise. USGS Open-File Report 2005-1058

Pendleton, E.A., Thieler, E.R., & Williams, S.J. (2010). Importance of coastal change variables in determining vulnerability to sea- and lake- level change. *Journal of Coastal Research, 26*(1), 176-183

Pethick, J. (2001). Coastal management and sea-level rise. *Catena*, *42,* 307-322

Pethick, J.S., & Crooks, S. (2000). Development of a coastal vulnerability index: A geomorphological perspective. *Environmental Conservation, 27*(4), 359–36

Pietersma-Perrott, B., & van Proosdij, D. (2012). Shore zone characterization for climate change adaptation in the Bay of Fundy. *The Atlantic Climate Adaptation Solutions Association.* Retrieved 09 03, 2012 from http://atlanticadaptation.ca/sites/discoveryspace.upei.ca.acasa

Pilkey, O.H., & Cooper, J.A.G., (2004). Society and Sea Level Rise. *Science, 303*, 1781-178

Pilkey, O.H., Young, R.S., Bush, D.M., and Thieler, E.R. (1994). Predicting the behaviour of beaches: Alternatives to models. *Littoral. 94*, 26-29

Rahmstorf, S. (2007). A semi-empirical approach to projecting future sea-level rise. *Science, 315,* 368-370

Richards, W., & Daigle, R. (2011). Scenarios and guidance for adaptation to climate change and sea level rise – NS and PEI municipalities. *The Atlantic Climate Adaptation Solutions Association.* Retrieved 05 09, 2012, from http://atlanticadaptation.ca/sites/discoveryspace.upei.ca.acasa

Rignot, E., & Kanagaratnam, P. (2006). Changes in the velocity structure of the Greenland ice sheet. *Science*, *311*, 986-990

Romieu, E., Welle, T., Schneiderbauer, S., Pelling, M., & Vinchon, C. (2010). Vulnerability assessment within climate change and natural hazard contexts: revealing gaps and synergies through coastal applications. *Sustainability Science, 5*(2), 159-170

Shaw, J., Taylor, R.B., Forbes, D.L., Ruz, M.-H., & Solomon, S. (1998). Sensitivity of the Canadian Coast to Sea-Level Rise*,* Geological Survey of Canada Bulletin 505

Shaw, R. W. (2001*).* Coastal impacts of climate change and sea-level rise on Prince Edward Island: Synthesis report. *The Atlantic Climate Adaptation Solutions Association.* Retrieved 11 14, 2012, from http://atlanticadaptation.ca/reports

St. Lawrence Global Observatory. (n.d.). *Scientific information: SLGO*. Retrieved 01 19, 2013 from http://slgo.ca/en/th-scientific-info.html

Stutz, M.K.,& Pilkey, O.H. (2011). Open-Ocean Barrier Islands: Global Influence of Climatic, Oceanographic, and Depositional Settings. *Journal of Coastal Research*, *27*(2)2, 207 – 222

Thieler, E.R. & Hammar-Klose, E.S. (2000). National assessment of coastal vulnerability to future sea-level rise: Preliminary results for the U.S. Atlantic Coast. U.S. Geological Survey, Open File Report

Trenberth, K.E. (2005). Uncertainty in hurricanes and global warming. *Science, 308,* 1753-1754 Ward, P.J., Marfai, M.A., Yulianto, F., Hizbaron, D.R., & Aerts, J.C.J.H. (2011). Coastal inundation and damage exposure estimation: a case study for Jakarta. *Natural Hazards, 56*: 899-916

Voogd, H. (1983). *Multicriteria evaluation for urban and regional planning*. London: Pion

Walsh, J., Wuebbles, D., Hayhoe, K., Kossin, J., Kunkel, J., Stephens, G., Thorne, P., Vose, R., Wehner, M., Willis, J., Anderson, D., Doney, S., Feely, R., Hennon, P., Kharin, V., Knutson, T., Landerer, F., Lenton, T., Kennedy, J., & Somerville, R (2014). Ch. 2: Our Changing Climate. *Climate Change Impacts in the United States: The Third National Climate Assessment*, J. M. Melillo, Terese (T.C.) Richmond, and G. W. Yohe, Eds., U.S. Global Change Research Program, 19-67

Webster, T. (2012q). Identification of anomalous coastline change areas and the aggregation of change attributes for littoral cells. *The Atlantic Climate Adaptation Solutions Association.* Retrieved 05 09, 2012, from http://atlanticadaptation.ca/sites/discoveryspace.upei.ca.acasa

Webster, T. (2012b). Coastline change in PEI, 1968-2010 and 2000-2010. *The Atlantic Climate Adaptation Solutions Association.* Retrieved 11 14, 2012, from http://atlanticadaptation.ca/reports

Webster, P.J., Holland, G.J., Curry, J.A., & Chang, H.R. (2005). Changes in tropical cyclone number, duration, and intensity in a warming environment. *Science, 309,* 1844-1846

Whitehouse, P. (2009). *Glacial isostatic adjustment and sea-level change: State of the art report* (TR-09-11). Stockholm, Sweden: SKB Swedish Nuclear Fuel and Waste Management Co. Retrieved from http://www.skb.se/upload/publications/pdf/TR-09-11.pdf

Woodworth, P. L., Tsimplis, M. N., Flather, R. A. & Shennan, I. (1999). A review of the trends observed in British Isles mean sea level data measured by tide gauges. *Geophysical Journal International, 136*, 651-670

Yates, M.L., Le Cozannet, G, & Lenotre, N. (2011). Quantifying errors in coastal erosion and inundation hazard assessments. *Journal of Coastal Research, SI 64*, 260-264

Zheng, N., Takara, K., Yamashiki, Y., & Tachikawa, Y. (2009). Assessing vulnerability to regional flood hazard through spatial multi-criteria analysis in the Huaihe River Basin, China. *Annual Journal of Hydraulic Engineering, 53,* 127-132

Appendix A: Shoreline Change Maps

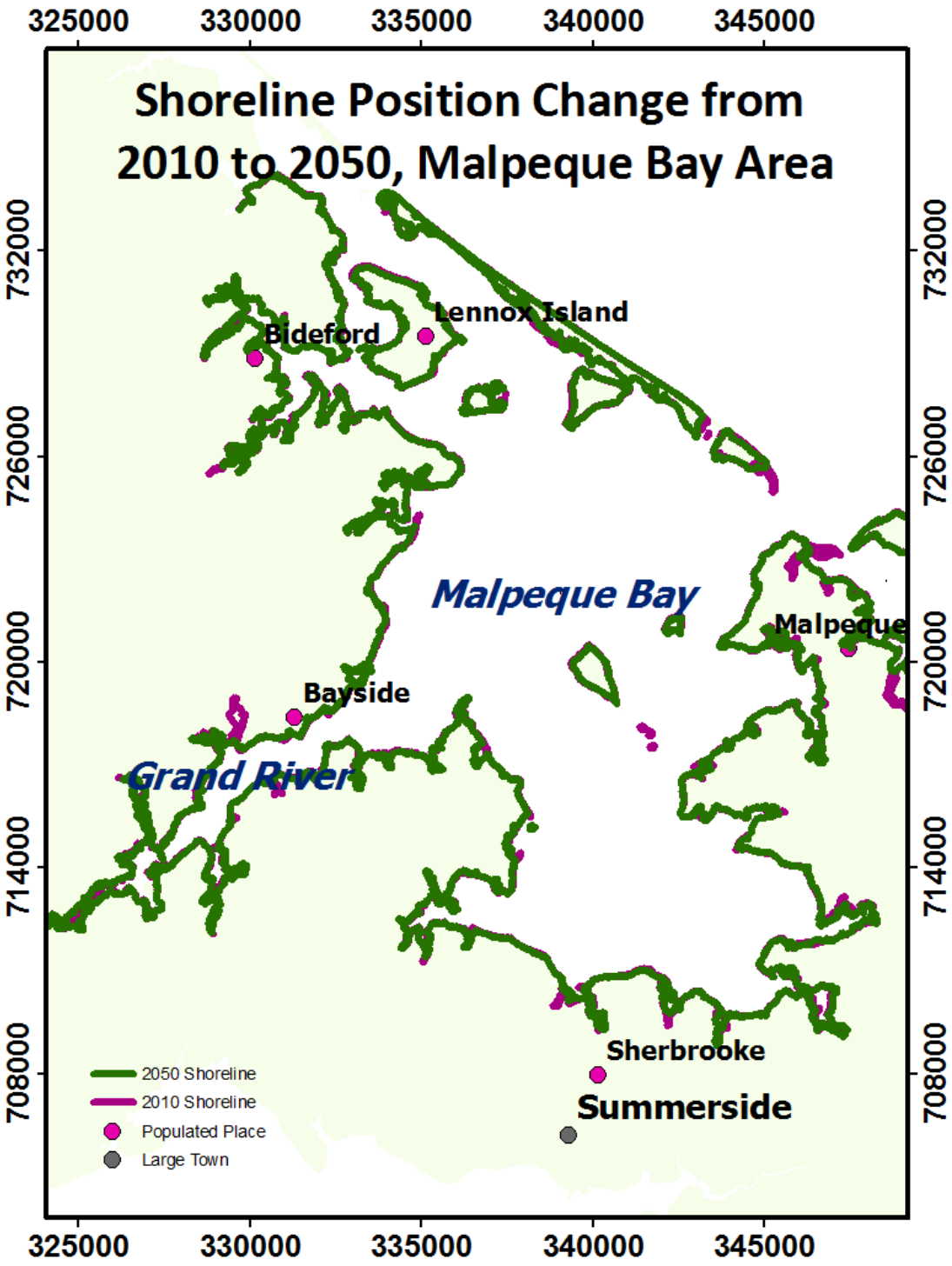

Figure 72: Map of 2010 and 2050 shorelines, Malpeque Bay area

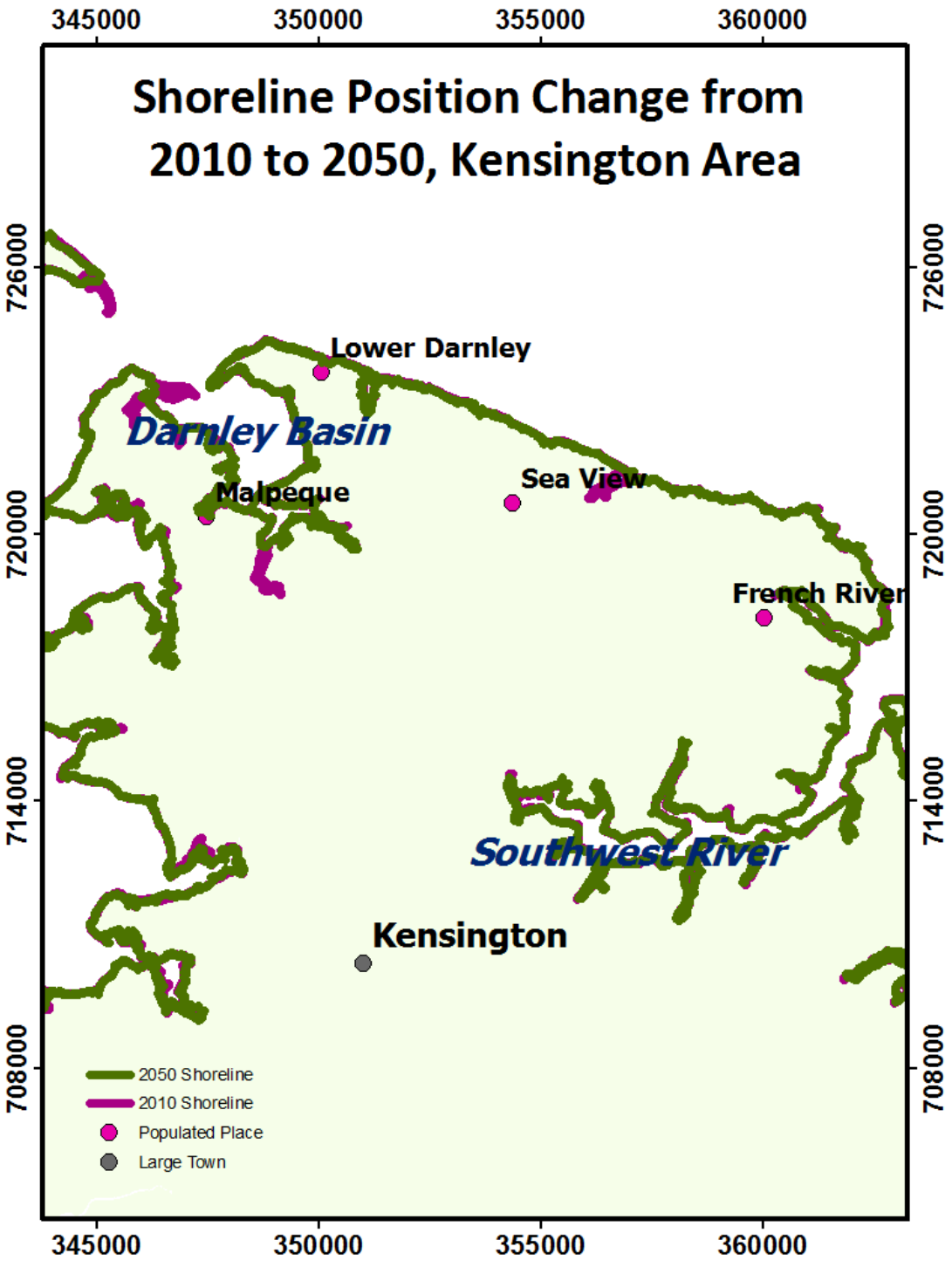

Figure 73: Map of 2010 and 2050 shorelines, Kensington area

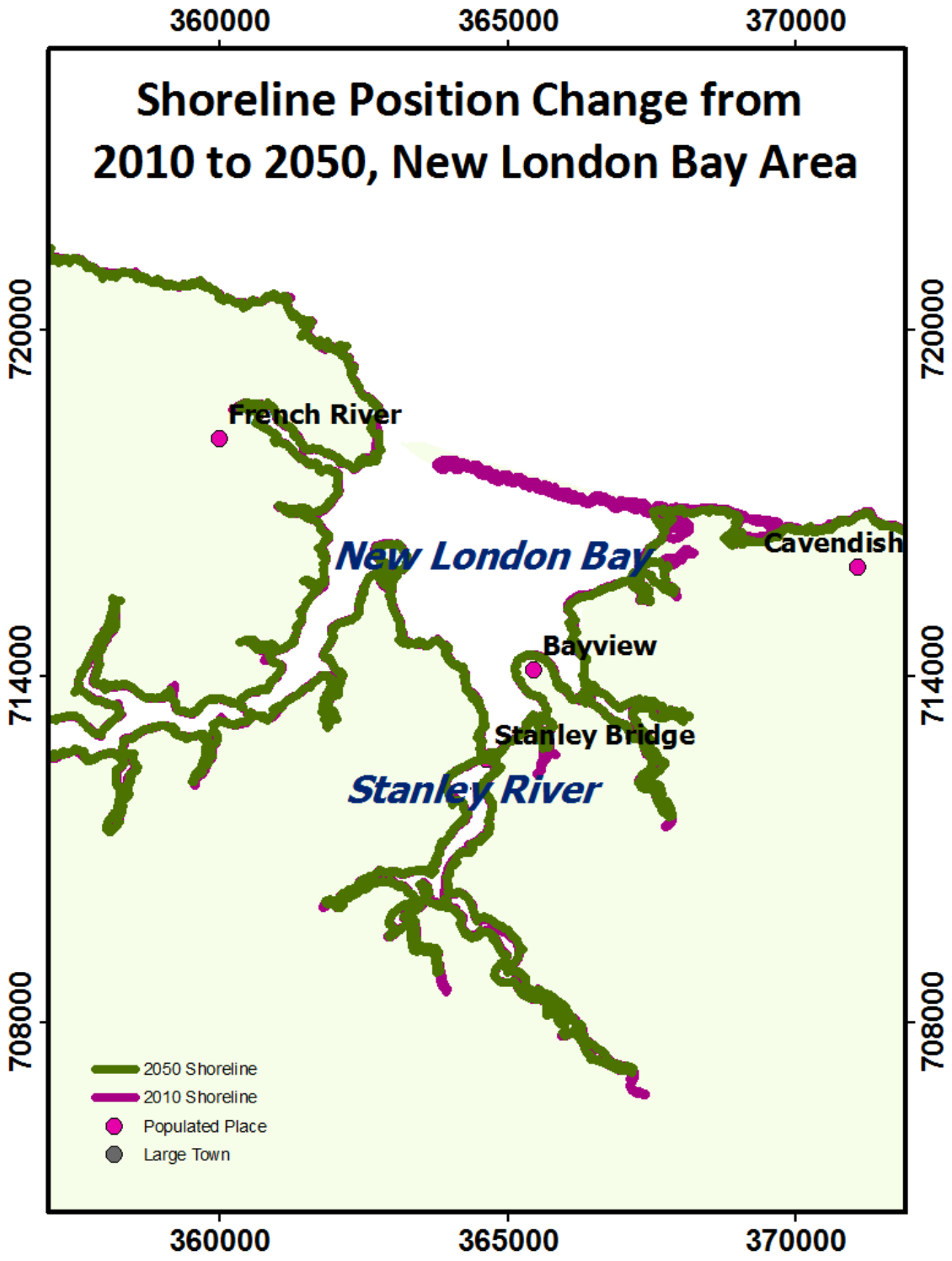

Figure 74: Map of 2010 and 2050 shorelines, New London Bay area

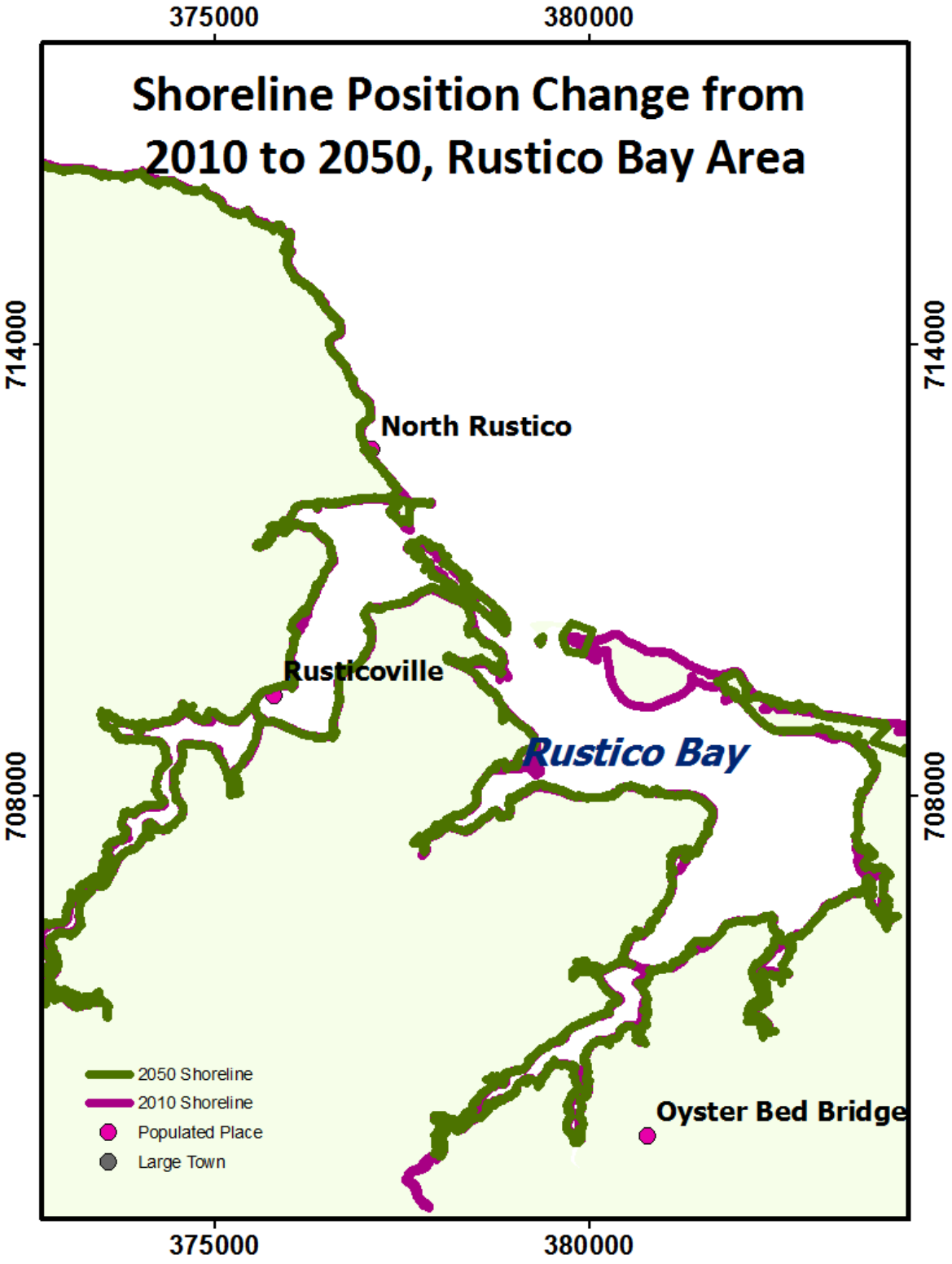

Figure 75: Map of 2010 and 2050 shorelines, Rustico Bay area

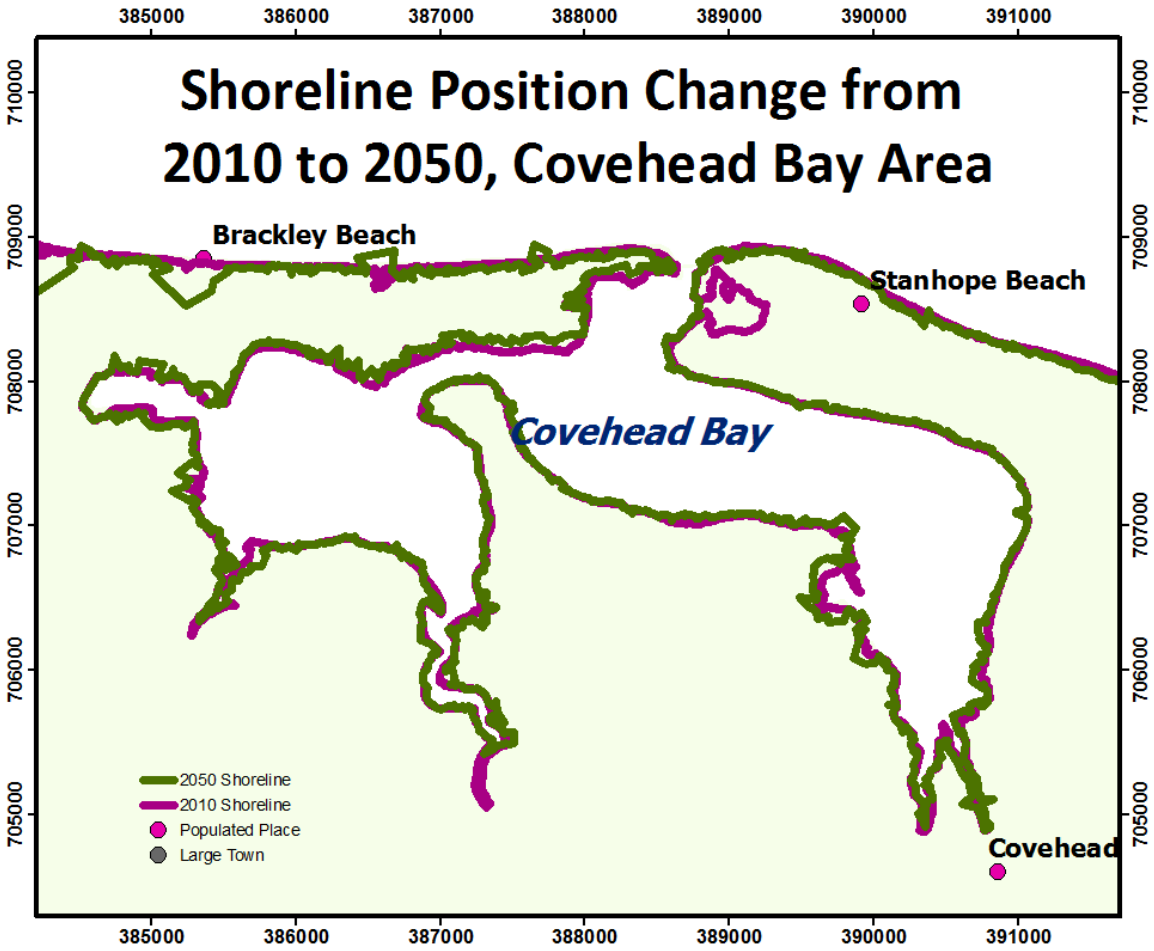

Figure 76: Map of 2010 and 2050 shorelines, Covehead Bay area

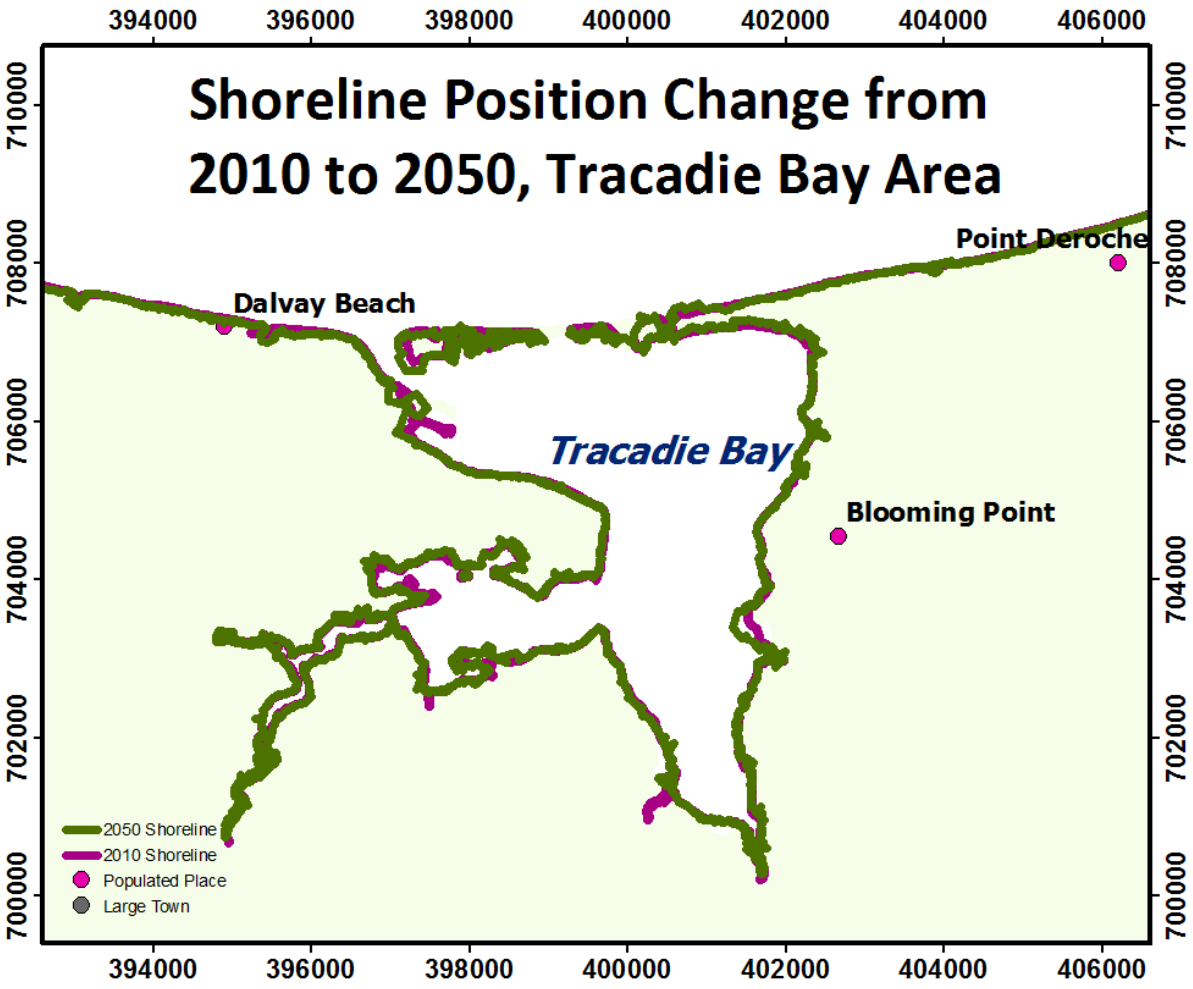

Figure 77: Map of 2010 and 2050 shorelines, Tracadie Bay area

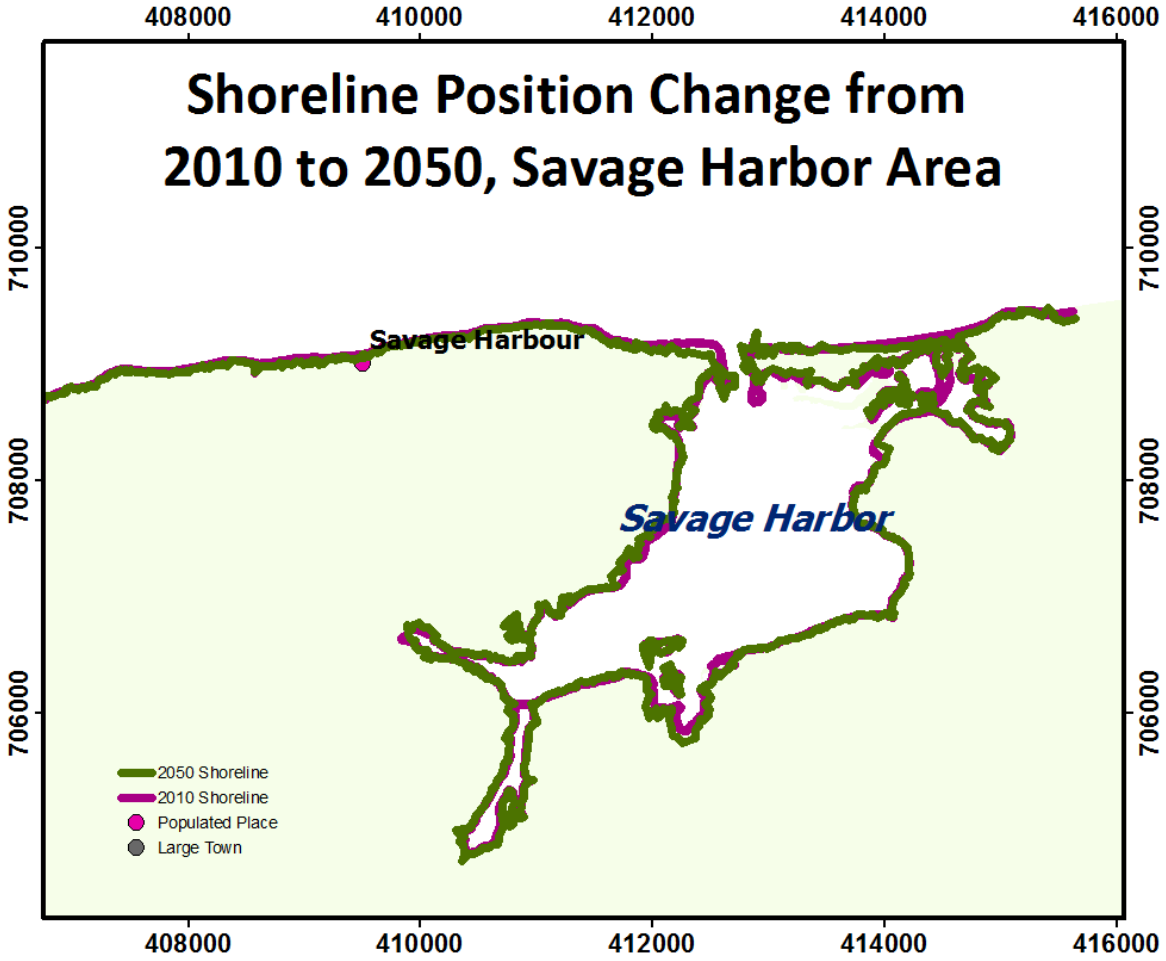

Figure 78: Map of 2010 and 2050 shorelines, Savage Harbor area

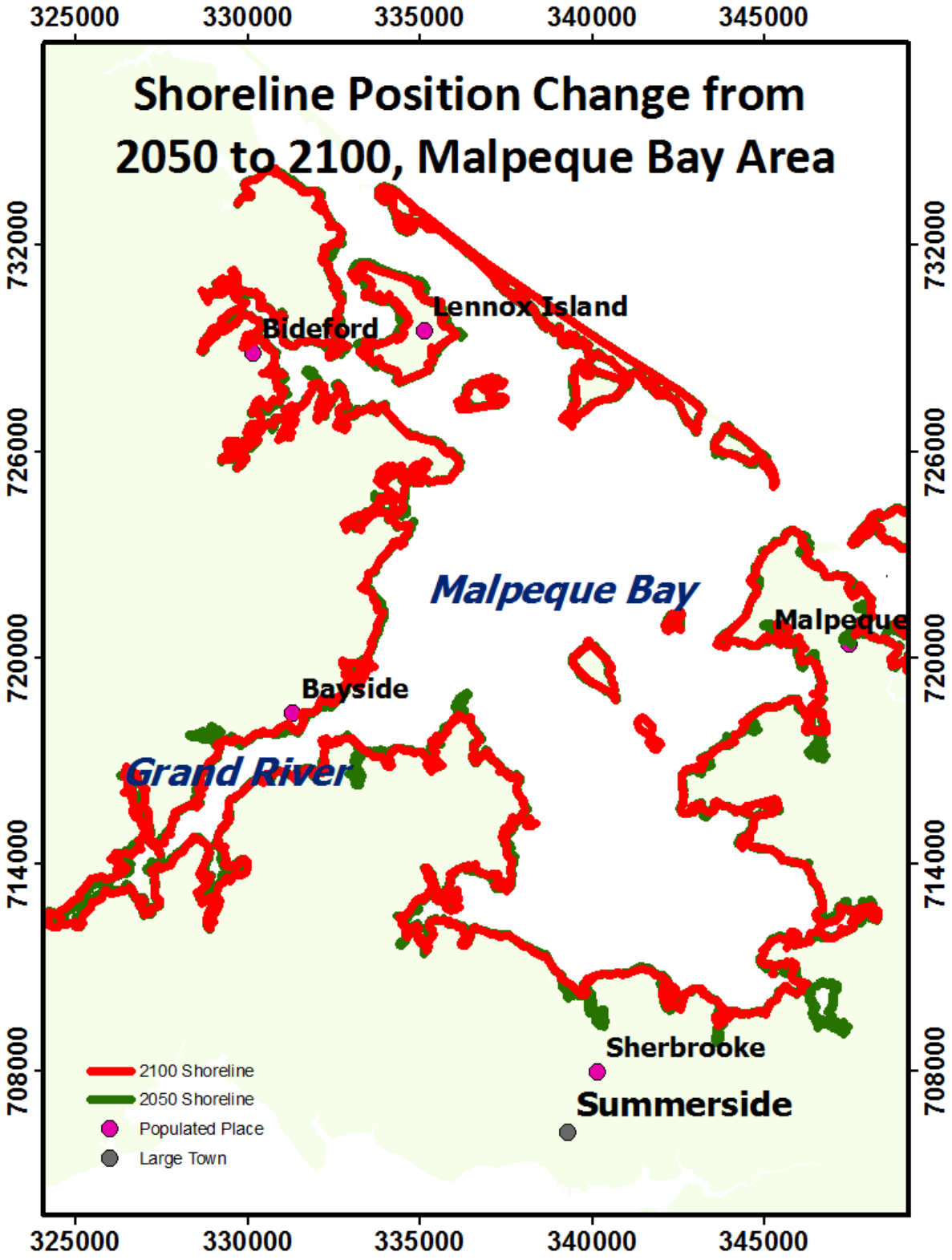

Figure 79: Map of 2050 and 2100 shorelines, Malpeque Bay area

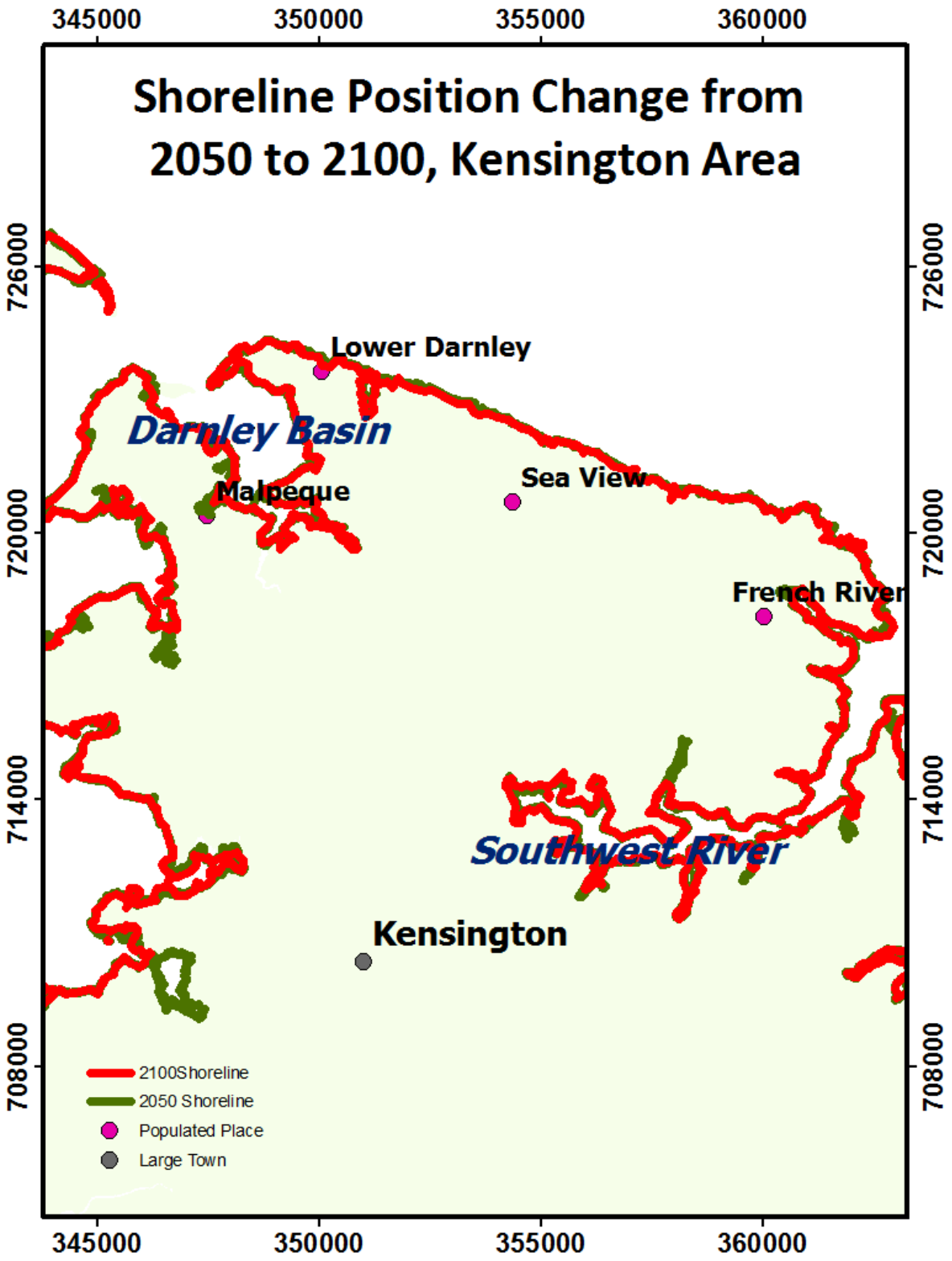

Figure 80: Map of 2050 and 2100 shorelines, Kensington area

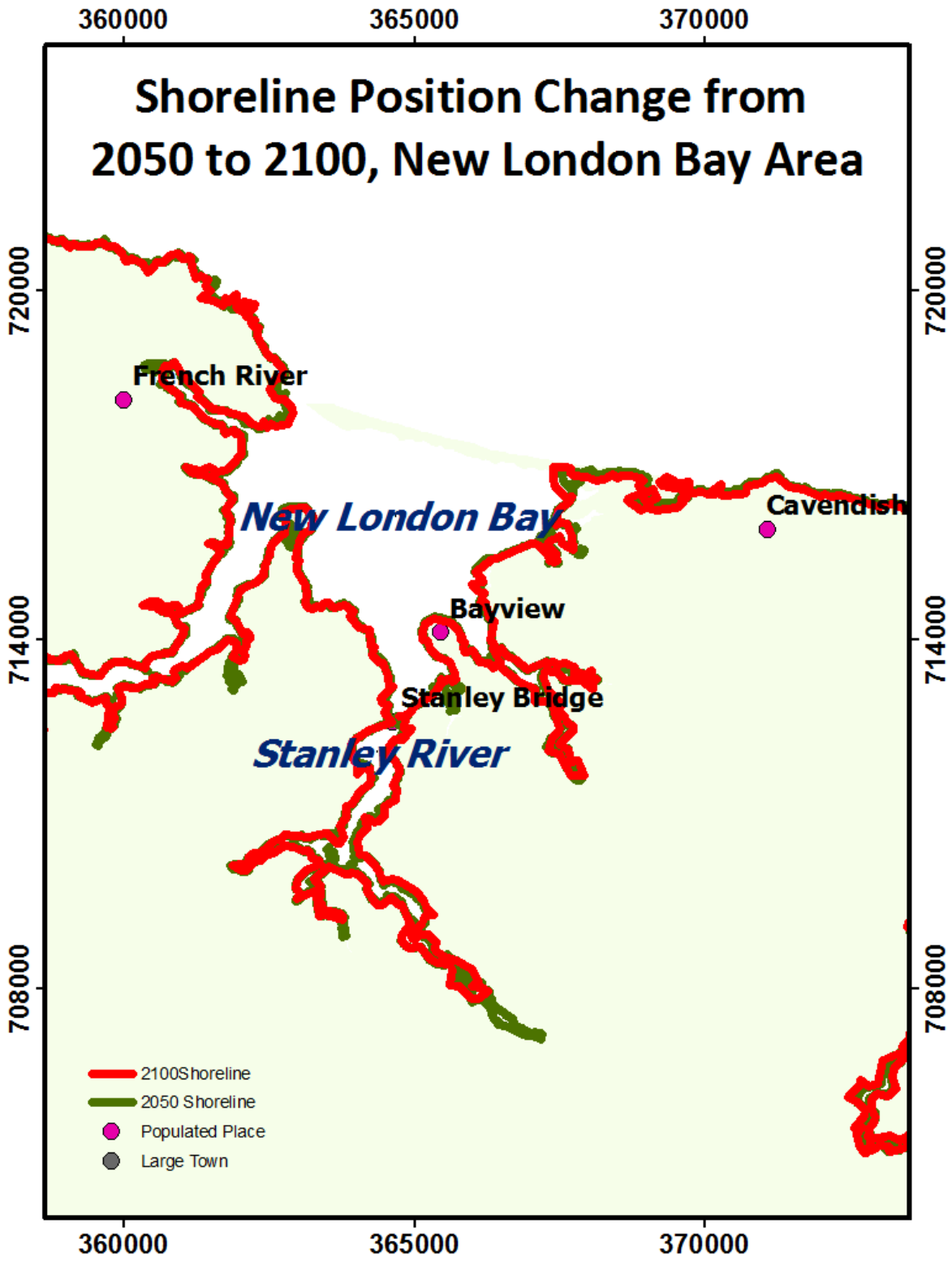

Figure 81: Map of 2050 and 2100 shorelines, New London Bay Bay area

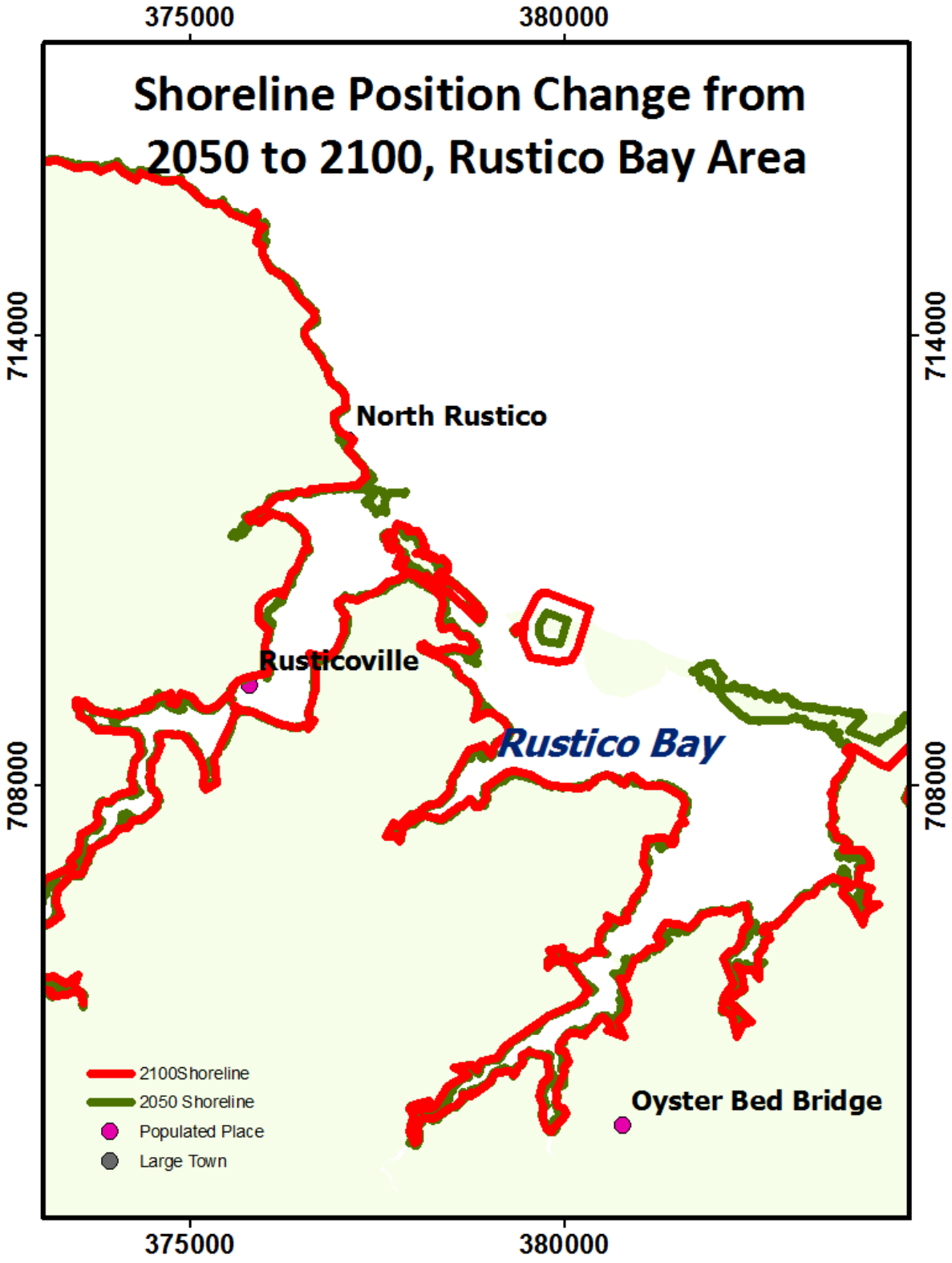

Figure 82: Map of 2050 and 2100 shorelines, Rustico Bay area

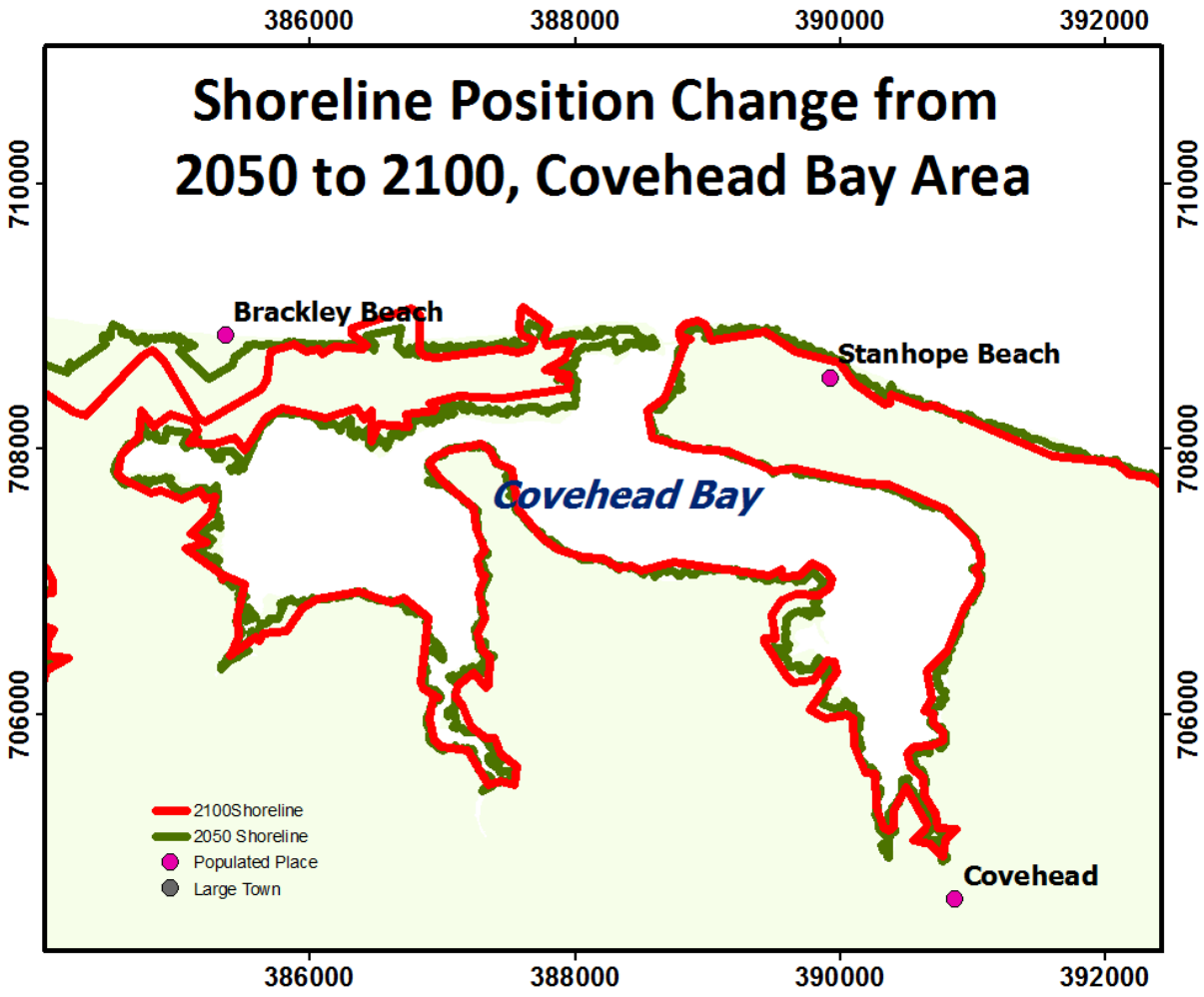

Figure 83: Map of 2050 and 2100 shorelines, Covehead Bay area

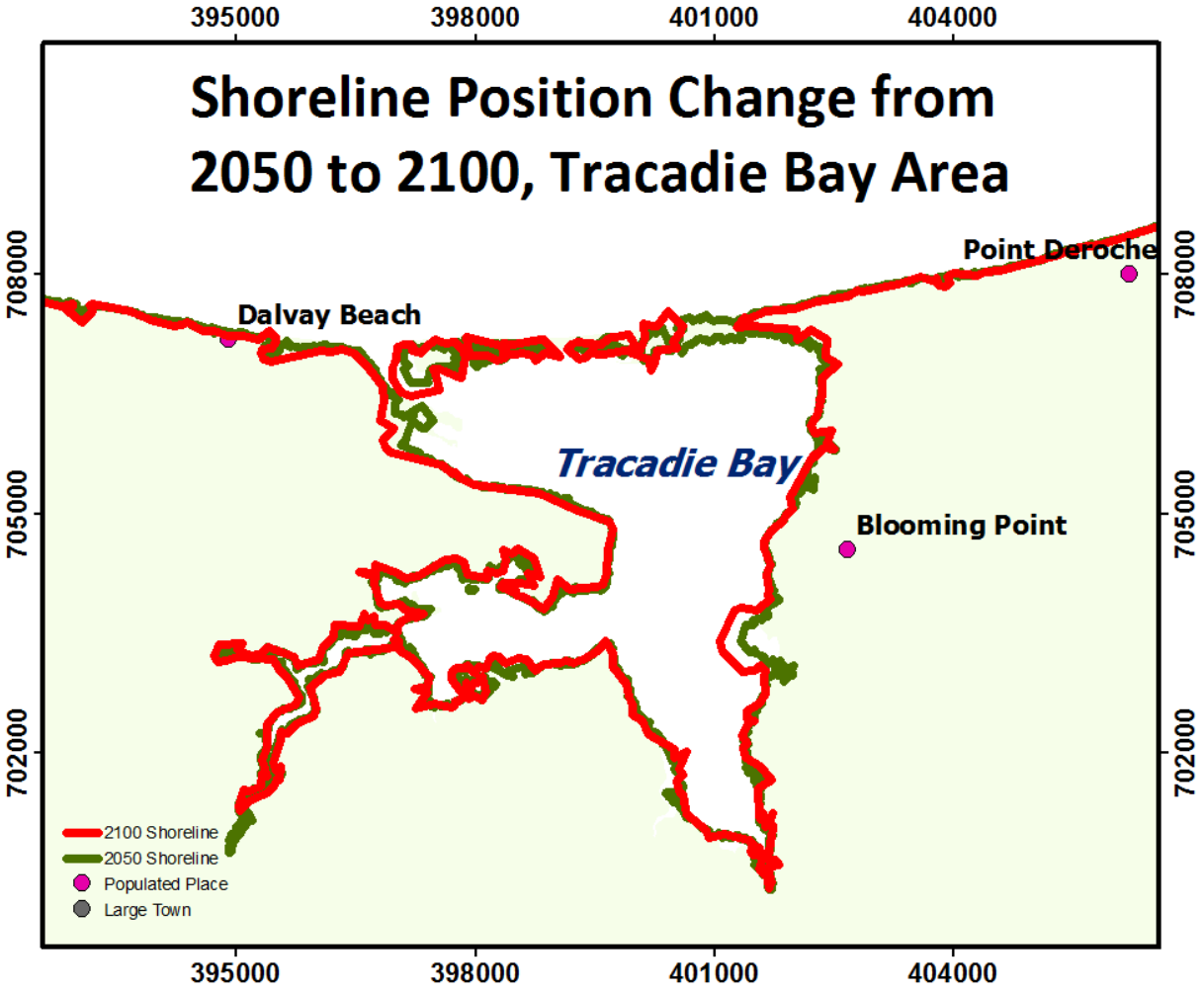

Figure 84: Map of 2050 and 2100 shorelines, Tracadie Bay area

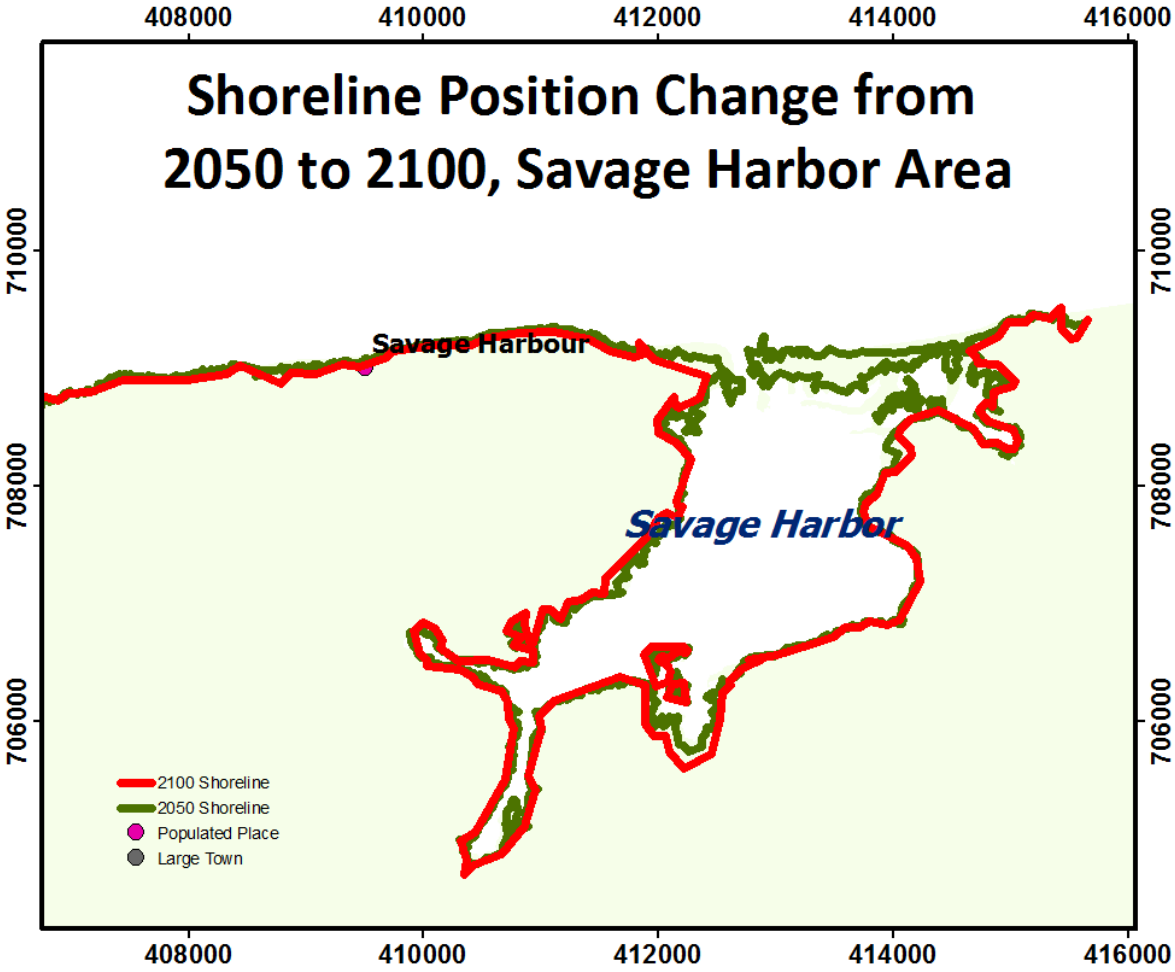

Figure 85: Map of 2050 and 2100 shorelines, Savage Harbor area

Appendix B: Regional Physical Vulnerability

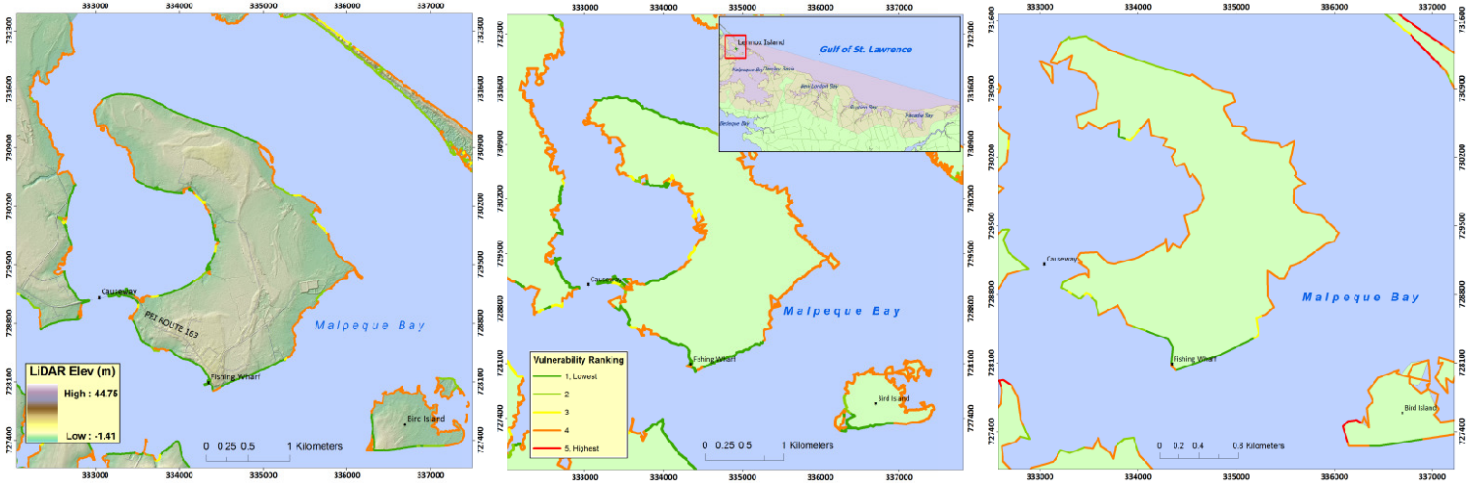

Figure 86: Relative physical vulnerability for Lennox Island in (a) 2010 (b) 2050 (c) 2100

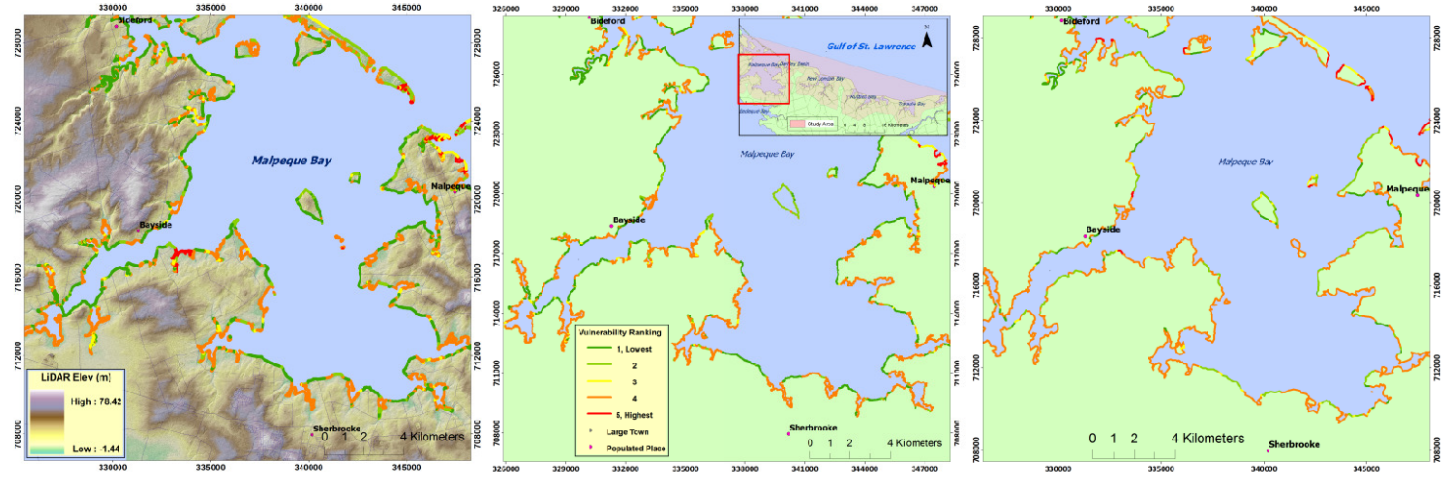

Figure 87: Relative physical vulnerability for Malpeque Bay in (a) 2010 (b) 2050 (c) 2100

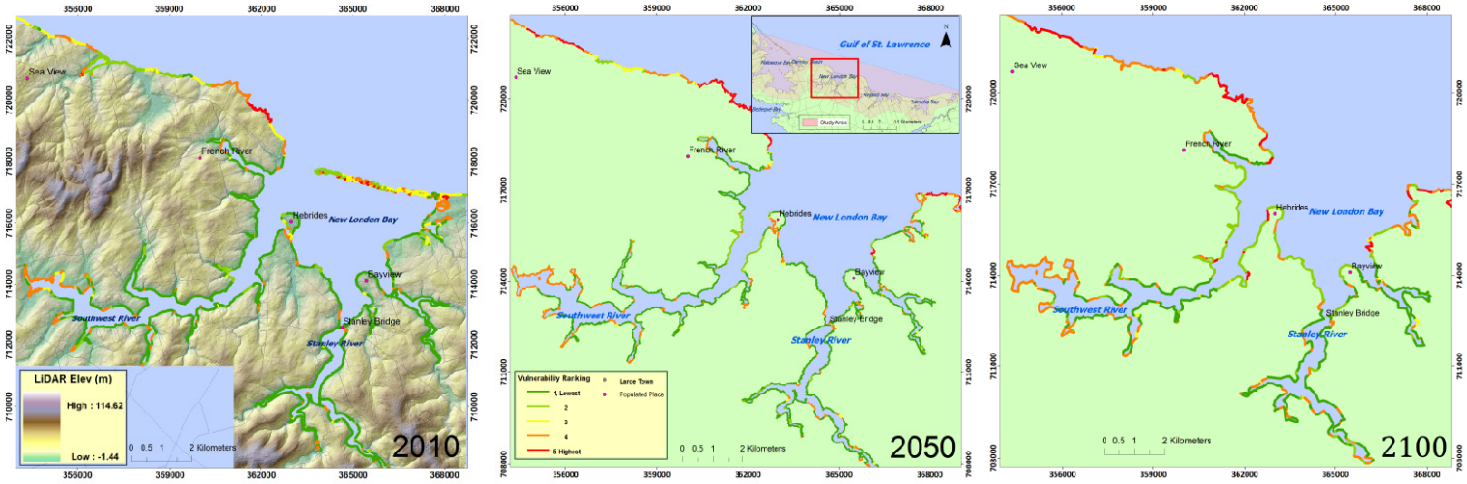

Figure 88: Relative physical vulnerability for New London Bay in (a) 2010 (b) 2050 (c) 2100

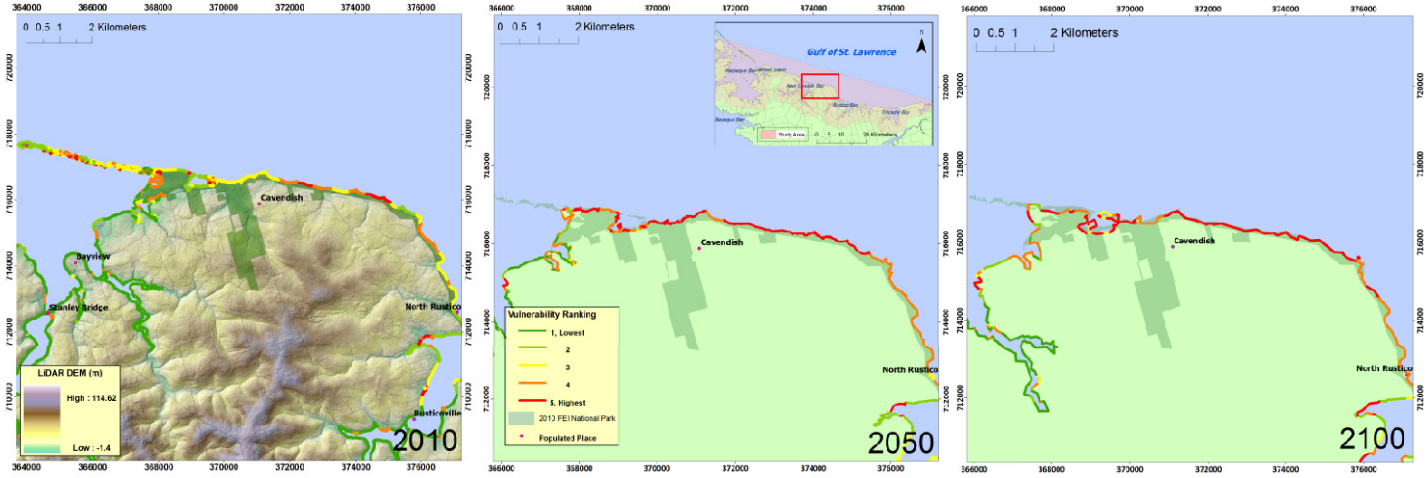

Figure 89: Relative physical vulnerability for Cavendish in (a) 2010 (b) 2050 (c) 2100

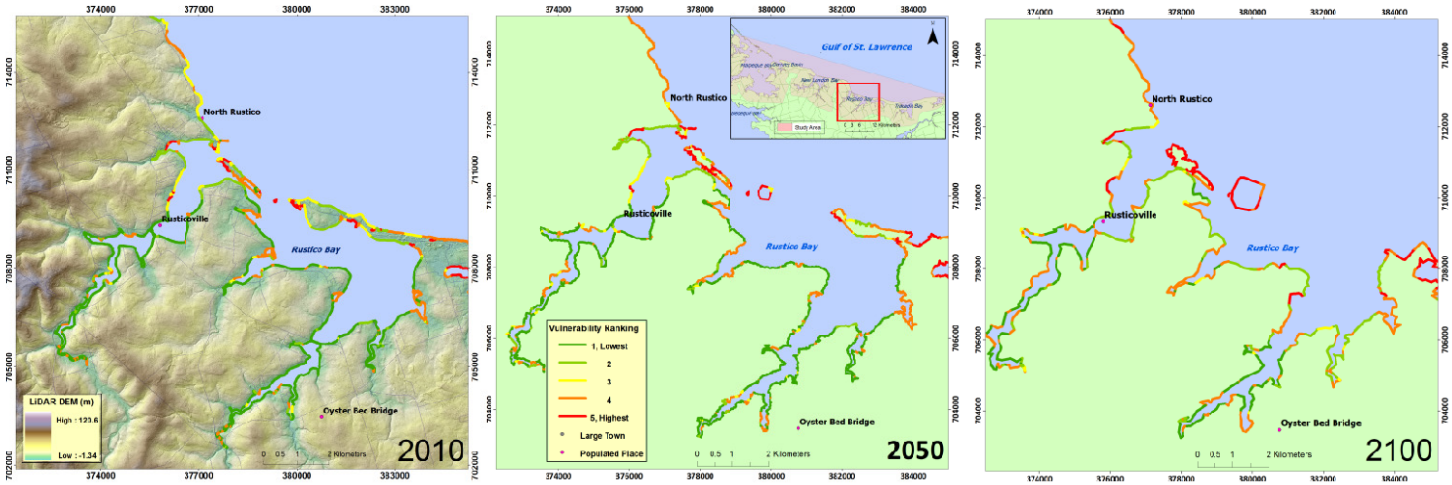

Figure 90: Relative physical vulnerability for Rustico in (a) 2010 (b) 2050 (c) 2100